1-1-1969

Analog Computer Solution of the Unsteady Flow Equations and Its Use in Modeling the Surface Runoff Process

Utah Water Research Laboratory

Utah State University

Logan, Utah 84321

PRWG38-2

Analog Computer Solution of the Unsteady Flow Equations and Its Use in Modeling the Surface Runoff Process

Utah Water Research Laboratory / College of Engineering
by Roger A. Amisial, J. Paul Riley, Kenneth G. Renard, Eugene K. Israelsen

May 1969

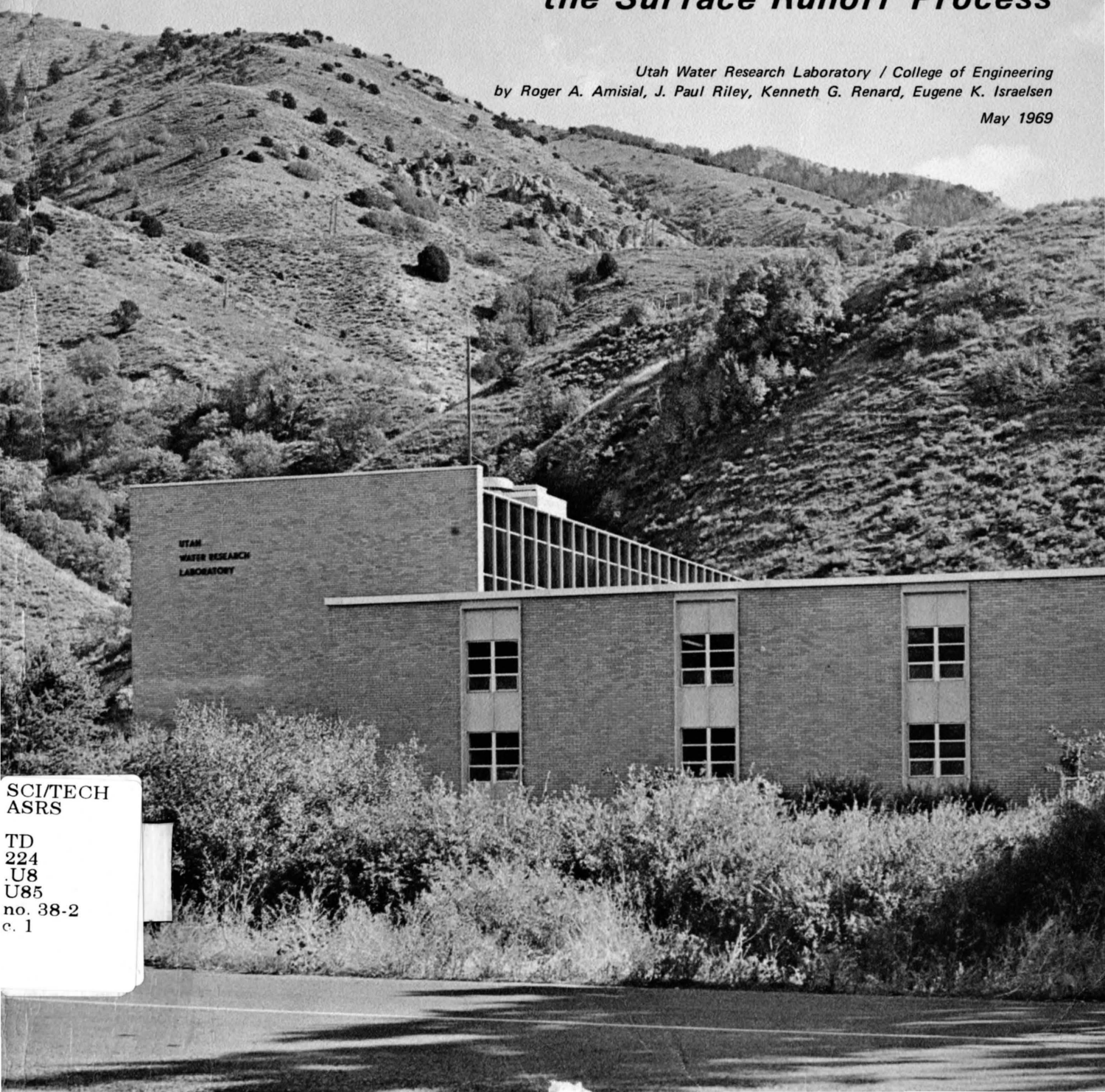

ANALOG COMPUTER SOLUTION OF THE UNSTEADY FLOW EQUATIONS AND ITS USE IN MODELING THE SURFACE RUNOFF PROCESS

by
Roger A. Amisial
J. Paul Riley
Kenneth G. Renard
Eugene K. Israelsen

The work reported by this project progress report was supported primarily with funds provided by the United States Department of Agriculture, Agricultural Research Service, Soil and Water Conservation Research Division

Utah Water Research Laboratory
College of Engineering
Utah State University
Logan, Utah

May 1969

$2.50

PRWG 38-2

ABSTRACT

Analog Computer Solution of the Unsteady Flow Equations and Its Use in Modeling The Surface Runoff Process

The flow of water on a watershed is usually unsteady and spatially varied, but can be adequately portrayed by the equations of momentum and continuity, commonly referred to as the unsteady flow equations. Because these equations are quasi-linear, hyperbolic, partial differential equations, they are not easily amenable to solution. Analog computer models of surface runoff generally have been based on simplified forms of these equations. As an improvement of those models, an analog computer solution is presented here for the unsteady flow equations. The solution involves the conversion of the partial differential equations into a differential-difference system, and a consideration of the stability of the difference approach was performed.

The analog computer solution is then used to develop a model of surface runoff generated from rainfall on a watershed. Spatial distribution of the watershed parameters is accounted for by dividing the drainage basin into a number of subzones according to its physiography and the rainfall input was made to each subzone. Both the overland and channel flow components are considered in the surface runoff process. Preliminary testing and verification of the model have been made by simulating two runoff events on a subwatershed of the Walnut Gulch experimental watershed near Tombstone, Arizona.

Amisial, Roger A.; Riley, J. Paul; Renard, Kenneth G.; Israelsen, Eugene K. ANALOG COMPUTER SOLUTION OF THE UNSTEADY FLOW EQUATIONS AND ITS USE IN MODELING THE SURFACE RUNOFF PROCESS
Research Project Progress Report to Soil and Water Conservation Research Division, Agricultural Research Service, United States Department of Agriculture, December 1969, Washington, D.C.

KEYWORDS--*surface runoff/ *hydrologic models/ *hydrologic simulation/ *electronic analog computer/ infiltration/ *runoff/ rainfall/ semiarid watershed studies/ precipitation/ convective storms/ water yields/ water yield improvement/ hydrologic relationships/ hydrologic data/ experimental watersheds/ hydrology/ research and development/ hydrologic research/ water resource planning and development.

ACKNOWLEDGMENTS

This publication represents a report on a phase of a continuing cooperative research program between Utah State University and the Soil and Water Conservation Research Division of the Agricultural Research Service, the United States Department of Agriculture. The funding for the report of this work was provided primarily by the Agricultural Research Service.

The authors acknowledge the assistance provided by the staff and facilities of both the Southwest Watershed Research Center at Tucson, Arizona,and the Utah Water Research Laboratory. This project has clearly demonstrated the many advantages to be gained from a cooperative research program of this nature.

Special thanks are extended to Dr. Jay M. Bagley, Director of the Utah Water Research Laboratory, who was closely associated with the program at its inception and has continued to lend helpful advice and encouragement.

Roger A. Amisial
J. Paul Riley
Kenneth G. Renard
Eugene K. Israelsen

TABLE OF CONTENTS

Chapter		Page
I.	INTRODUCTION	1
	Previous Work	1
	Objectives	2
II.	DERIVATION OF THE UNSTEADY FLOW EQUATIONS	3
	Assumptions	3
	Continuity Equation	3
	Momentum Equation	3
	Pressure forces	4
	Gravity forces	6
	Resistance forces	7
	Application of the Momentum and Continuity Equations to Irregular Channels	9
III.	REVIEW OF THE METHODS OF SOLUTION FOR UNSTEADY FLOW EQUATIONS	11
	Exact Methods	11
	Exact method of characteristics	11
	Linearization techniques	12
	Direct Electrical Analog	12
	Finite-Difference Methods	13
	Difference methods for the two basic equations of continuity and momentum	13
	Implicit methods	13
	Explicit methods	14
	Unstable method	14
	Diffusing method	14
	Leap-frog method	15
	Lax-Wendroff method	15
	Numerical methods of characteristics	15
	Grid of characteristics method	15
	Method of specified time intervals	15
	Explicit scheme	15
	Implicit scheme	16
	Mixed difference methods	17
	Stability study by the perturbation technique	17

TABLE OF CONTENTS (Continued)

Chapter — Page

Equations of first variation . . . 17
The von Neumann stability criteria . . . 18

General comments . . . 18

IV. THE ELECTRONIC ANALOG COMPUTER AND THE PARTIAL DIFFERENTIAL EQUATIONS OF UNSTEADY FLOW . . . 21

The Analog Computer . . . 21
Solution of Unsteady Flow Equations on the Analog Computer . . . 21

The differential-difference equations . . . 21

Stability . . . 22
Explicit schemes . . . 22

Backward difference quotient . . . 22
Forward difference quotient . . . 23

Implicit scheme . . . 23

Programming the equations . . . 23

Magnitude scaling . . . 24
Time scaling . . . 24
Effects of the time scale factor and the resistance term on the stability of the implicit differential-difference scheme . . . 24

Error analysis . . . 27

Truncation errors . . . 27
Computing errors . . . 27

Error propagation equations . . . 27
Computing stability . . . 28

V. THE SURFACE RUNOFF MODEL . . . 29

Treatment of the Watershed . . . 30
Effective Rainfall Rate . . . 30

Rainfall rate . . . 30
Retention rate . . . 30

Overland Flow . . . 32

Infiltration rate on the planes . . . 32
Initial conditions . . . 33
Upstream boundary conditions . . . 33
Downstream boundary conditions . . . 35

Channel Flow . . . 35

Seepage rate in the channels . . . 35
Initial conditions . . . 35

TABLE OF CONTENTS (Continued)

Chapter		Page
	Upstream boundary conditions	36
	Downstream boundary conditions	36
	Conditions at the junctions	36
VI.	PROCEDURES OF MODEL REGULATION AND VERIFICATION	37
	Adaptation of the Analog Solution to Flow Conditions of a Watershed	37
	Model Regulation	37
	Function parameters	38
	Plane characteristics	38
	Channel characteristics	38
	Condition parameters	38
	Retention rate	38
	Infiltration rates	38
	Roughness coefficients	38
	Procedure	39
	Methods and criteria for goodness of fit	39
	Model Verification	39
VII.	THE EXPERIMENTAL WATERSHED	41
	Geology	41
	Topography	41
	Soils and Vegetation	41
	Instrumentation	41
	Precipitation	41
	Subwatershed 11	41
	Drainage conditions	41
	Natural subzones	47
	Equivalent subzones	47
	Boundary conditions	47
	Overland flow	47
	Channel flow	47
	Runoff events	49
VIII.	RESULTS AND DISCUSSION	51
	Flow hydrographs	51
	Condition Parameters	55
	Check on Conservation of Mass Principle	55
	Distribution of the Watershed Losses	55
	Solution Speed	55
	Models Based on Simplified Unsteady Flow Equations	57
	Sensitivity Analysis	57
	Overland flow hydrograph	57
	Channel flow hydrograph	60

TABLE OF CONTENTS (Continued)

Chapter	Page
IX. CONCLUSIONS AND RECOMMENDATIONS	63
Conclusions	63
Suggestions for Further Research	64
LITERATURE CITED	65

LIST OF FIGURES

Figure		Page
2.1	Definition sketch for the derivation of the continuity equation	4
2.2	Definition sketches for the derivation of the net pressure force between two channel sections	5
2.3	Simplified representation of the force exerted on the fluid by the walls or sides of the channel	6
2.4	Simplified representation of energy in steady flow	8
3.1	Electrical circuit applied to the solution of simplified forms of the unsteady flow equations	13
3.2	Point numbering for the implicit and explicit methods applied to the two basic equations of continuity and momentum	13
3.3	Point lettering for the grid of characteristics method	15
3.4	Point numbering and lettering for the explicit method of specified time intervals	16
3.5	Point numbering and lettering for the implicit method of specified time intervals	16
4.1	Flow profile illustrating finite increment procedure adopted for the flow model	22
4.2	An elemetal computer program for the implicit differential-difference equations of unsteady flow	25
4.3	Computer program for the solution of the implicit differential-difference equations of unsteady flow at the first ten sections of a channel	26
5.1	Schematic diagram of the runoff cycle	29
5.2	Sketches showing a natural subzone and its equivalent area	30
5.3	Flow chart for the surface runoff model	31
5.4	Computer program for computing the retention capacity rate, R_{cr} , and the effective rainfall, P_e	33
5.5	Computer program for the generation of the infiltration capacity rate function, f_{cr}	34
5.6	Flow profile for the equivalent plane showing boundary conditions for overland flow	34
7.1	Walnut Gulch experimental watershed	42

LIST OF FIGURES (Continued)

Figure		Page
7.2	Soils map of the Walnut Gulch experimental watershed	43
7.3	Vegetation map of the Walnut Gulch experimental watershed	44
7.4	Map of the Walnut Gulch experimental watershed showing the location of subwatershed 11	45
7.5	Subwatershed 11 of Walnut Gulch experimental watershed, as divided in 9 subzones	46
7.6	Measuring section of flume 11 located at the outlet of subwatershed 11	48
8.1	Outflow from subwatershed 11 for the event of July 20, 1966	52
8.2	Outflow from subwatershed 11 for the event of July 29, 1966	53
8.3	Overland flow hydrographs at successive sections of the equivalent plane of subzone 2	54
8.4	Channel flow hydrographs at successive sections of the channel of subzone 2	54
8.5	Stage and velocity hydrographs at a channel section of subzone 2	54
8.6	Input and output data for the plane of subzone 2 used in the check on the conservation of mass principle	56
8.7	Overland flow hydrograph for subzone 2 as affected by changes in the retention storage capacity, R_{cs}, July 20, 1966	58
8.8	Overland flow hydrograph for subzone 2 as affected by changes in the time constant of the retention capacity rate function, k_r, July 20, 1966	58
8.9	Overland flow hydrograph for subzone 2 as affected by changes in the plane roughness coefficient, K, July 20, 1966	58
8.10	Overland flow hydrograph for subzone 2 as affected by changes in the plane minimum infiltration capacity rate, f_m, July 20, 1966	59
8.11	Overland flow hydrograph for subzone 2 as affected by changes in the plane maximum infiltration capacity rate, f_o, July 20, 1966	59
8.12	Overland flow hydrograph for subzone 2 as affected by changes in the plane time constant of the infiltration capacity rate function, k_f, July 20, 1966	59
8.13	Channel flow hydrograph for subzone 2 as affected by changes in the retention storage capacity, R_{cs}, July 20, 1966	60
8.14	Channel flow hydrograph for subzone 2 as affected by changes in the time constant of the retention capacity rate function, k_r, July 20, 1966	60

LIST OF FIGURES (Continued)

Figure		Page
8.15	Channel flow hydrograph for subzone 2 as affected by changes in the plane roughness coefficient, K, July 20, 1966	60
8.16	Channel flow hydrograph for subzone 2 as affected by changes in the plane minimum infiltration capacity rate, f_m, July 20, 1966	61
8.17	Channel flow hydrograph for subzone 2 as affected by changes in the plane maximum infiltration capacity rate, f_o, July 20, 1966	61
8.18	Channel flow hydrograph for subzone 2 as affected by changes in the plane infiltration time constant, k_f, July 20, 1966	61
8.19	Channel flow hydrograph for subzone 2 as affected by changes in the channel minimum infiltration capacity rate, f_m, July 20, 1966	61
8.20	Channel flow hydrograph for subzone 2 as affected by changes in the channel maximum infiltration capacity rate, f_o, July 20, 1966	62
8.21	Channel flow hydrograph for subzone 2 as affected by changes in the channel infiltration time constant, k_f, July 20, 1966	62
8.22	Channel flow hydrograph for subzone 2 as affected by changes in the constant applied to the computation of channel seepage, c, July 20, 1966	62
8.23	Channel flow hydrograph for subzone 2 as affected by changes in the channel roughness coefficient, K, July 20, 1966	62

LIST OF TABLES

Table		Page
3.1	Stability conditions for the implicit and explicit finite-difference methods	19
7.1	Physical characteristics of the natural subzones	47
7.2	Physical characteristics of the equivalent subzones	48
7.3	Precipitation data for event of July 20, 1966, on subwatershed 11 of the Walnut Gulch experimental watershed	49
7.4	Precipitation data for event of July 29, 1966, on subwatershed 11 of the Walnut Gulch experimental watershed	50
8.1	Selected criteria for goodness of fit	52
8.2	Principal outflow hydrograph characteristics and percent error for the event of July 20, 1966	52
8.3	Principal hydrograph characteristics and percent error for the event of July 29, 1966	53
8.4	Fitted values for the constants involved in the condition parameters for the land surfaces of subwatershed 11	55
8.5	Fitted values for the constants involved in the condition parameters for the channels of subwatershed 11	55
8.6	Check on conservation of mass principle for subzones 1 and 2 for the event of July 20, 1966	56
8.7	Distribution of watershed losses for the runoff events of July 20, and July 29, 1966, as computed from the model inputs and outputs	57

PARTIAL LIST OF SYMBOLS

Symbol		Definition
A	=	cross-section area of the flow
B	=	top width of the cross-sectional area of flow
c	=	a constant applied to the computation of the channel seepage
F_{cr}	=	channel seepage capacity rate at any time
f_{cr}	=	infiltration capacity rate at any time
f_m	=	minimum value of the infiltration capacity rate
f_o	=	maximum value of the infiltration capacity rate
f_r	=	actual infiltration rate
g	=	acceleration due to gravity
h	=	time scale factor
I	=	unit rate of lateral inflow into a channel
j	=	subscript indicating the section number
J	=	subzone number
K	=	channel roughness coefficient
k	=	a real constant
k_f	=	constant less than one in Horton equation
k_r	=	constant less than or equal to one in the retention capacity rate equation and depending upon vegetation and soil surface characteristics
m	=	mass of fluid within a control volume, also superscript indicating time interval
M	=	subscript indicating maximum expected values
n	=	subscript indicating the downstream end section of a channel
O	=	unit rate of channel loss due to seepage
P_e	=	effective rainfall rate
P_r	=	rainfall rate

PARTIAL LIST OF SYMBOLS (Continued)

Symbol		Definition
Q	=	total rate of flow at any section of a channel and at any time
Q_1	=	rate of lateral flow from a channel branch or tributary
q	=	rate of overland flow per unit width
q_{crg}	=	capacity rate of seepage loss from a unit length of channel
q_{rg}	=	rate of seepage loss from channel
R_{cr}	=	retention capacity rate
R_{cs}	=	retention storage capacity of the vegetation and land surface
R_r	=	actual rate at which rainfall is entering retention storage
R_s	=	amount of rainfall in retention storage
S_f	=	friction slope
S_o	=	channel slope
t	=	real time
V	=	average velocity of flow
x	=	distance along channel
y	=	flow depth
Z	=	total number of subzones, and also stands for the subzone containing the watershed outlet
γ	=	specific weight of fluid
ϕ	=	a variable which can be y, A, V, q, or Q
ρ	=	fluid density
τ	=	computer time

CHAPTER I

INTRODUCTION

The determination of the response of a drainage basin to water input is the core of many hydrologic problems. Some of these problems are: forecast of flood peaks in rivers, protection against flood damage, design of hydraulic structures, determination of the downstream effects of proposed structures, and development of additional water supplies for a growing population. Solutions to these problems require reliable procedures to determine, at some point on the watershed, the flows resulting from known or given distributions of water input. Such flows become quite complex when they are the response of the watershed to the history of precipitation. Any conventional procedure for the computation of flow in open channels is beset with many difficulties. The meteoric water is depleted by retention on trees and in surface depressions, evaporation, and seepage into the ground, while unsteady spatially varied flow prevails on the land surface and in the channel system.

Previous Work

The basic analytical approach to the overland and channel flow phenomena was provided by de Saint-Venant (1871) who derived the equations of continuity and momentum for unsteady, gradually-varied flow. These equations, which adequately describe the surface flow over a drainage basin, are nonlinear partial differential equations of the hyperbolic type. They are commonly referred to as the Saint-Venant equations, the unsteady flow equations, or the shallow water equations, and their integration by a direct method has been obtained for only simplified cases.

Massau (1889) transformed the Saint-Venant equations into a set of equivalent characteristic equations and presented a graphical method for their integration. His method was simplified and adapted to practical purposes by Craya (1946) who made the assumption of straight-line characteristics to solve the unsteady flow equations for problems involving flow resistance in sloping channels with changing cross-section. Nosek et al. (1947) used a modified Craya method to route the wave which resulted from the failure of the Saint Francis Dam near Los Angeles, California. They obtained good agreement with the recorded flood measurements.

Thomas (1937) was the first to outline finite-difference methods for the Saint-Venant equations in relation to the study of flood movement in rivers. However, such methods were of little practical use at the time of their development because of the extensive manual computations involved. Since then, computational difficulties have been considerably reduced by the concurrent development of electronic computers and improved numerical analysis techniques. Stoker (1953) formulated an explicit finite-difference method for the shallow water equations. Isaacson et al. (1954) solved on a UNIVAC digital computer a mathematical model of the Ohio River basin by making use of the numerical method developed by Stoker. The same model was successfully applied for flood prediction on the Ohio and Mississippi Rivers. After the pioneering work of Stoker and his co-workers, many mathematical models of channel flow based on the Saint-Venant equations have been solved by finite difference methods on digital computers. Amien (1966), Daubert et al. (1967), Preissman et al. (1967), Thirriot et al. (1967), Fletcher et al. (1967), and Baltzer et al. (1968), have used several difference methods for the solution of the Saint-Venant equations, and have successfully applied them to route flow through river networks and irregular channels.

Keulegan (1945) seems to have been the first to use the Saint-Venant equations in an analysis of overland flow. Iwagaki (1951) used those equations to compute runoff on road surfaces. Overland flow models based on the unsteady flow equations were developed at Stanford University. A well-known example of the Stanford studies is the runoff model developed by Morgali et al. (1965) in which a difference scheme somewhat similar to the one presented by Stoker was utilized. These investigators found good agreement between the computed and the measured hydrographs. Woolhiser et al. (1967) made a study of the rising hydrograph for overland flow based on the solution by finite-difference integration of the non-dimensional characteristic equations utilizing the grid of characteristics. They found that no unique dimensionless rising hydrograph exists for overland flow.

Formulation of finite-difference solutions involves consideration of the stability of the various methods. Ritchmyer (1962) made a survey of several difference

schemes applicable to unsteady flow in general, and developed the conditions under which each scheme is stable. Liggett et al. (1967) made an empirical examination of the stability of some of the difference methods used in the numerical solution of the shallow water equations. They found that a finite-difference scheme based on the method of characteristics was stable but that explicit methods were not satisfactory except for some special cases.

Because of mathematical difficulties involved in the solution of the Saint-Venant equations, a number of mathematical models of unsteady flow have been based on simplified forms of those equations. Deymie (1939) linearized the equations and solved the resulting simplified forms by the Riemann-Hadamard method. Lighthill et al. (1955) presented a solution by Laplace Transform for the Deymie linearized equations, and also developed the kinematic wave theory based on the continuity equation and a simplified form of the dynamic equation of unsteady flow. Henderson et al. (1964) and Wooding (1965, 1966) made use of the kinematic wave theory in the solution of hydrologic problems. Brakensiek (1967) replaced the natural watershed by an equivalent sloping plane and applied the simple kinematic flow equations to route the rainfall excess over the equivalent plane. He found the computation system to be feasible for predicting hydrographs. Ishihara et al. (1955), Harder et al. (1960), and Shen (1965) developed special electronic analog facilities to solve runoff models based on simplified unsteady flow equations. Riley (1967) introduced further simplifications by using the continuity equation in the form of a storage equation, and a simplified momentum equation. His model was solved on the general-purpose electronic analog computer, and the hydrographs obtained from the model showed encouraging agreement with measured hydrographs.

In the past, mathematical models of surface runoff based on the unsimplified shallow water equations have been solved exclusively on digital computers, while the analog computer has been restricted to models based on simplified forms of those equations. However, there is now growing recognition that the unsimplified equations yield improved results, and that the analog computer presents some advantages in the simulation of physical systems governed by nonlinear partial differential equations. There is, therefore, a specific need to investigate techniques for solving on the analog computer surface runoff models based on the unsimplified unsteady flow equations.

In the interest of simplicity, most of the above mentioned mathematical models of surface runoff have neglected spatial variation of hydrologic elements such as rainfall, slope, channel size, soil, and vegetation within the watershed. Also, the surface runoff process is often assumed to take place either on the land surfaces or in the channel system, overlooking the fact that both overland and channel flows occur on the watershed. Further, the equations of unsteady flow are usually adapted to route the excess rainfall over impervious surfaces, although it is well known that infiltration continues as long as water is available in detention storage. There is a definite need for improved mathematical models of surface runoff which adequately account for both time and space variation in the physical characteristics within the watershed, and the occurrence of both overland and channel flows, considering that infiltration does not necessarily cease concurrently with rainfall.

Objectives

The overall objective of the study was to investigate the possibility of improving analog computer models of surface runoff from rainfall over a watershed, with particular emphasis on the model developed by Riley (Riley, 1967, Riley et al., 1967). The specific objectives are as follows:

1. To develop appropriate expressions for the actual infiltration over the land surfaces and in the stream channels.
2. To develop the unsteady flow equations applicable to the movement of flow generated from excess rainfall over a watershed, and to transform them into a differential-difference system of equations for solution on a general-purpose electronic analog computer.
3. To adapt or develop a method to study the stability of the differential-difference system of equations.
4. To use the analog solution of the equations of flow in a program to route the rainfall excess over the land surfaces and through the channel network.
5. To test and verify the surface runoff model on a natural watershed.
6. To study the effect of neglecting certain terms of the unsteady flow equations on the flow hydrographs.

schemes applicable to unsteady flow in general, and developed the conditions under which each scheme is stable. Liggett et al. (1967) made an empirical examination of the stability of some of the difference methods used in the numerical solution of the shallow water equations. They found that a finite-difference scheme based on the method of characteristics was stable but that explicit methods were not satisfactory except for some special cases.

Because of mathematical difficulties involved in the solution of the Saint-Venant equations, a number of mathematical models of unsteady flow have been based on simplified forms of those equations. Deymie (1939) linearized the equations and solved the resulting simplified forms by the Riemann-Hadamard method. Lighthill et al. (1955) presented a solution by Laplace Transform for the Deymie linearized equations, and also developed the kinematic wave theory based on the continuity equation and a simplified form of the dynamic equation of unsteady flow. Henderson et al. (1964) and Wooding (1965, 1966) made use of the kinematic wave theory in the solution of hydrologic problems. Brakensiek (1967) replaced the natural watershed by an equivalent sloping plane and applied the simple kinematic flow equations to route the rainfall excess over the equivalent plane. He found the computation system to be feasible for predicting hydrographs. Ishihara et al. (1955), Harder et al. (1960), and Shen (1965) developed special electronic analog facilities to solve runoff models based on simplified unsteady flow equations. Riley (1967) introduced further simplifications by using the continuity equation in the form of a storage equation, and a simplified momentum equation. His model was solved on the general-purpose electronic analog computer, and the hydrographs obtained from the model showed encouraging agreement with measured hydrographs.

In the past, mathematical models of surface runoff based on the unsimplified shallow water equations have been solved exclusively on digital computers, while the analog computer has been restricted to models based on simplified forms of those equations. However, there is now growing recognition that the unsimplified equations yield improved results, and that the analog computer presents some advantages in the simulation of physical systems governed by nonlinear partial differential equations. There is, therefore, a specific need to investigate techniques for solving on the analog computer surface runoff models based on the unsimplified unsteady flow equations.

In the interest of simplicity, most of the above mentioned mathematical models of surface runoff have neglected spatial variation of hydrologic elements such as rainfall, slope, channel size, soil, and vegetation within the watershed. Also, the surface runoff process is often assumed to take place either on the land surfaces or in the channel system, overlooking the fact that both overland and channel flows occur on the watershed. Further, the equations of unsteady flow are usually adapted to route the excess rainfall over impervious surfaces, although it is well known that infiltration continues as long as water is available in detention storage. There is a definite need for improved mathematical models of surface runoff which adequately account for both time and space variation in the physical characteristics within the watershed, and the occurrence of both overland and channel flows, considering that infiltration does not necessarily cease concurrently with rainfall.

Objectives

The overall objective of the study was to investigate the possibility of improving analog computer models of surface runoff from rainfall over a watershed, with particular emphasis on the model developed by Riley (Riley, 1967, Riley et al., 1967). The specific objectives are as follows:

1. To develop appropriate expressions for the actual infiltration over the land surfaces and in the stream channels.
2. To develop the unsteady flow equations applicable to the movement of flow generated from excess rainfall over a watershed, and to transform them into a differential-difference system of equations for solution on a general-purpose electronic analog computer.
3. To adapt or develop a method to study the stability of the differential-difference system of equations.
4. To use the analog solution of the equations of flow in a program to route the rainfall excess over the land surfaces and through the channel network.
5. To test and verify the surface runoff model on a natural watershed.
6. To study the effect of neglecting certain terms of the unsteady flow equations on the flow hydrographs.

CHAPTER II

DERIVATION OF THE UNSTEADY FLOW EQUATIONS

To derive the equations which govern unsteady flow, use will be made of the conservation of mass, momentum, and energy principles (Watters, 1967).

Assumptions

In deriving the basic equations of unsteady flow the following assumptions are made:

1. The fluid is incompressible.
2. The acceleration is in the x-direction.
3. The curvature of the water is small, so that the y-component of acceleration of the water particles has a negligible effect on the pressure. Consequently, the pressure distribution is hydrostatic and there is no vertical velocity component. Also the pressure-distribution coefficient is equal to unity.
4. The shear stress, τ_o, is uniform over the perimeter of the channel for the infinitesimal distance dx.
5. Lateral inflow and outflow rates are uniform with respect to a particular channel element.
6. The momentum influx of the lateral inflow and the momentum efflux of the lateral outflow are ignored.
7. The angle of inclination of the bed with respect to the horizontal surface, θ, is so small that it is considered as:
   $\sin \theta \approx S_o$ = slope of the bed
   and
   $\cos \theta \approx 1$
8. The effects of resistance to flow in unsteady flow are the same as in steady flow.
9. The energy and momentum coefficients are assumed to be equal to unity.

Continuity Equation

The continuity equation will be derived by applying the principle of conservation of mass in an infinitesimal space between two channel sections as illustrated by Figure 2.1. With reference to Figure 2.1, the quantity of fluid entering the element per unit time, dt, is given by the expression:

$$\left(Q - \frac{1}{2}\frac{\partial Q}{\partial x}\,dx\right) dt + I\,dx\,dt$$

Similarly, the quantity of fluid leaving the element per unit time, dt, is given by:

$$\left(Q + \frac{1}{2}\frac{\partial Q}{\partial x}\,dx\right) dt + O\,dx\,dt$$

The net amount of fluid leaving the element per unit time, dt, is, therefore:

$$\left(\frac{\partial Q}{\partial x} + O - I\right) dx\,dt$$

According to the principle of conservation of mass, the net outflow is equal to the decrease in storage during the time dt. Therefore

$$\left(\frac{\partial Q}{\partial x} + O - I\right) dx\,dt = -dA\,dx$$

or

$$\frac{\partial A}{\partial t} + \frac{\partial Q}{\partial x} + O - I = 0 \quad \ldots\ldots\ldots \quad (2.1)$$

Momentum Equation

According to Newton's second law, the rate of change of momentum of the fluid within a control volume must equal the external forces maintaining the control volume in the position at which it is analyzed. This statement, when expressed as a vector equation, reads as follows:

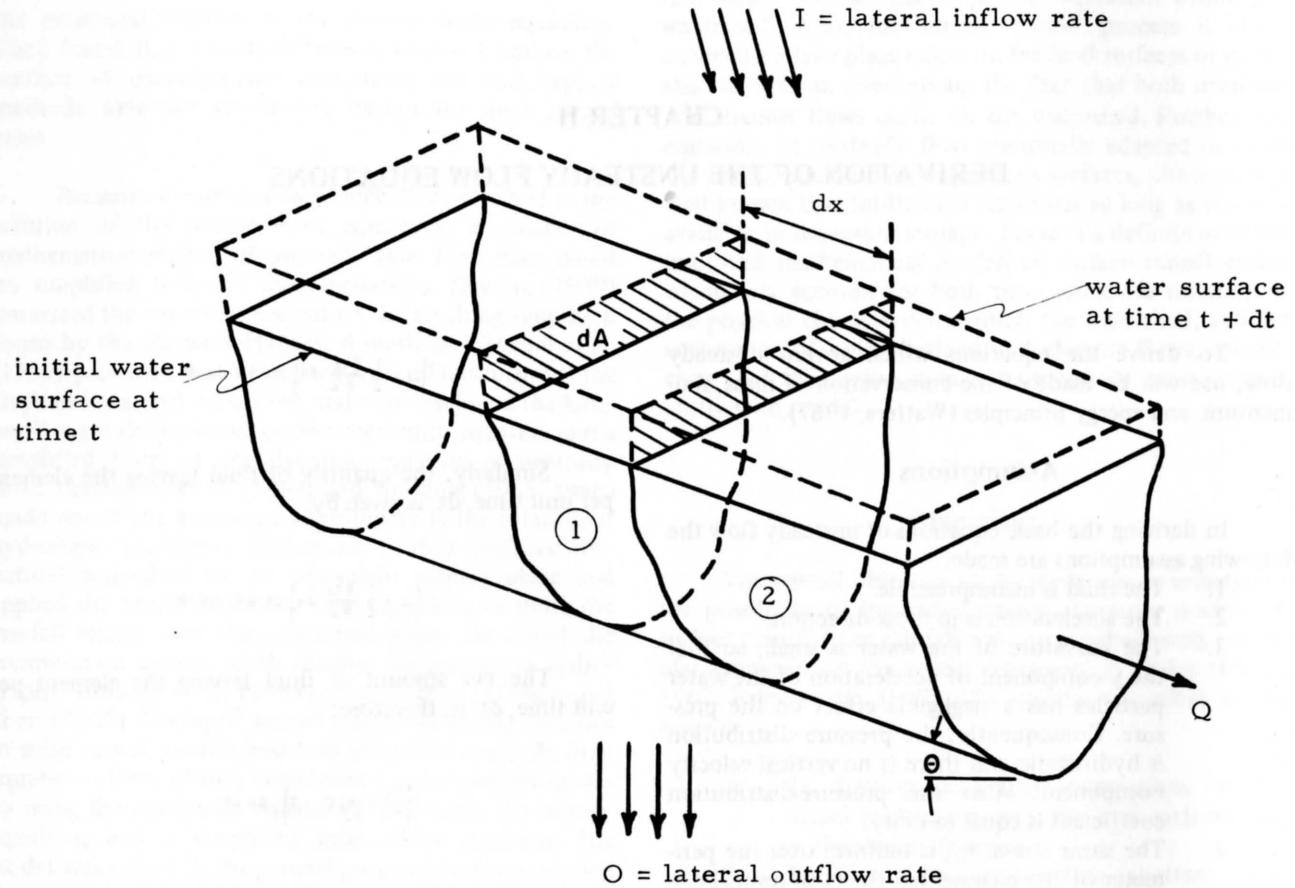

Figure 2.1. Definition sketch for the derivation of the continuity equation.

$$\Sigma \vec{F}_{external} = \frac{D}{Dt}\left[m \vec{V}\right] \quad . \quad . \quad . \quad . \quad . \quad . \quad . \quad . \quad . \quad (2.2)$$

In the x-direction the external forces are

$$\Sigma F_x = F_p + F_g + F_r$$

in which

F_p represents the pressure forces
F_g represents the gravity forces
F_r represents the resistance forces

Therefore, Equation (2.2) takes the following form in the x-direction:

$$F_p + F_g + F_r = \frac{D}{Dt}\left[m V\right] \quad . \quad . \quad . \quad . \quad . \quad . \quad . \quad . \quad (2.3)$$

Pressure forces

The net pressure force in the x-direction on the control volume shown in Figure 2.2a is

$$F_p = F_{p_1} + F_{p_2} \quad . \quad . \quad . \quad . \quad . \quad . \quad . \quad . \quad . \quad . \quad . \quad . \quad . \quad (2.4)$$

in which

F_{p_1} represents the net force between sections 1 and 2

F_{p^2} stands for the force exerted on the fluid by the walls or sides of the channel F_{p1} is obtained by the hydrostatic law of pressure distributions:

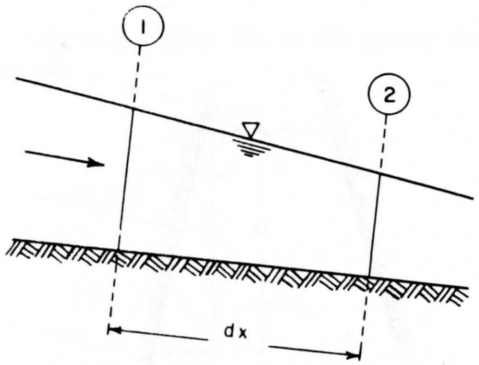

a. Flow profile showing control volume.

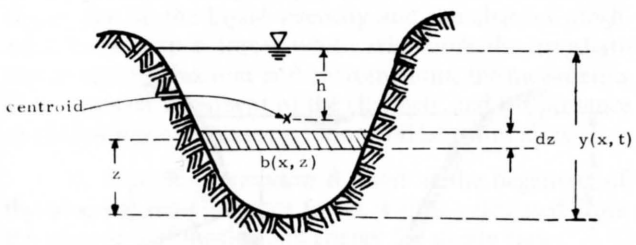

b. Cross-section of flow showing centroid and defining variables.

Figure 2.2. Definition sketches for the derivation of the net pressure force between two channel sections.

$$F_{P_1} = \beta' \left[\gamma \bar{h}_c A - \frac{dx}{2} \frac{\partial}{\partial x} \left(\gamma \bar{h}_c A \right) \right] - \beta' \left[\gamma \bar{h}_c A + \frac{dx}{2} \frac{\partial}{\partial x} \left(\gamma \bar{h}_c A \right) \right]$$

or

$$F_{P_1} = -\beta' \gamma \frac{\partial}{\partial x} \left(\bar{h}_c A \right) dx \quad . \quad . \quad . \quad . \quad (2.5)$$

in which

h_c is the distance of the centroid of the cross-sectional area A from the water surface

β' is the pressure-distribution coefficient which corrects for the curvature effect of the streamlines of the flow

The pressure-distribution coefficient is generally expressed by

$$\beta' = 1 + \frac{1}{A\bar{h}} \int_o^A c \, dA$$

The pressure head correction, c, is given by

$$c = \frac{y}{g} \frac{V^2}{r}$$

in which

r is the radius of curvature
V is the average velocity of the flow
y is the flow depth

The pressure-distribution coefficient β' is greater than 1.0 for concave flow, less than 1.0 for convex flow, and equal to 1.0 for parallel flow. By definition:

$$\bar{h}_c A = \int_o^{y(x,t)} (y-z)\, b(x, z) dz \quad . \quad . \quad . \quad . \quad (2.6)$$

in which

y(x,t), b(x,z), and z are defined as shown in Figure 2.2b Therefore:

$$\frac{\partial}{\partial x} (\bar{h}_c A) = \frac{\partial}{\partial x} \int_o^{y(x,t)} (y-z)\, b(x, z) dz$$

or applying Leibnitz's rule: [1]

$$\frac{\partial}{\partial x} (\bar{h}_c A) = \int_o^y \left[(y-z) \frac{\partial b}{\partial x} + b \frac{\partial y}{\partial x} \right] dz + (y-z)\, b\left(x, z\right) \frac{\partial y}{\partial x}\Big|_{z=y} - (y-z)\, b(x, z)\, o\Big|_{z=o}$$

or

$$\frac{\partial}{\partial x} (\bar{h}_c A) = \int_o^y (y-z) \frac{\partial b}{\partial x} dz + \frac{\partial y}{\partial x} \int_o^y b dz \quad . \quad . \quad (2.7)$$

Equation (2.7) can be written as

$$\frac{\partial}{\partial x} (\bar{h}_c A) = \int_o^y (y-z) \frac{\partial b}{\partial x} dz + A \frac{\partial y}{\partial x} \quad . \quad . \quad . \quad (2.8)$$

---

[1] According to Leibnitz's rule, if $F(t) = \int_{a(t)}^{b(t)} \phi \, (x,t)dx$ where a and b are differentiable functions of t and where $\Phi(x,t)$ and $\frac{\partial \phi (x,t)}{\partial t}$ are continuous in x and t, then

$$\frac{\partial F}{\partial t} = \int_{a(t)}^{b(t)} \frac{\partial \phi (x,t)}{\partial t} dx + \phi\left[b(t), t\right] \frac{db(t)}{dt} - \phi\left[a(t), t\right] \frac{da(t)}{dt}$$

since

$$\int_o^y b\,dz = A$$

Equations (2.5) and (2.8) yield:

$$F_{p_1} = \beta' \left[-\gamma dx \int_o^y (y-z) \frac{\partial b}{\partial x} dz - \gamma A \frac{\partial y}{\partial x} dx \right] \quad . \quad . \quad . \quad (2.9)$$

In the more general case of a non-prismatic channel (diverging or converging channel), there is the additional pressure force F_{p_2} that the fluid exerts on the sides. This force will be evaluated in Figure 2.3.

Consider an elemental area, ds dl, on the side wall of the channel. The differential force on that area is p dl ds. From Figure 2.3b it can be seen that the horizontal component of that force is p dl ds cos β, and its x-component is p dl ds cos β sin α (see Figure 2.3a). Thus:

$$dF_{p_2} = p\ dl\ ds \cos\beta \sin\alpha \quad . \quad . \quad . \quad . \quad . \quad (2.10)$$

From Figure 2.3a:

$$ds \sin\alpha = \frac{1}{2} db$$

From Figure 2.3b:

$$dl \cos\beta = dz$$

Therefore:

$$dF_{p_2} = \frac{1}{2} p\ dz\ db$$

or

$$dF_{p_2} = \frac{1}{2} p\ dz \frac{\partial b}{\partial x} dx$$

According to the hydrostatic law of pressure distribution:

$$p = \beta' \gamma (y-z)$$

Thus, for a constant length of channel dx and for both sides

$$F_{p_2} = 2 \int_o^y dF_2 = \beta' \gamma\, dx \int_o^y (y-z) \frac{\partial b}{\partial x} dz \quad . \quad . \quad . \quad (2.11)$$

When Equations (2.4), (2.9), and (2.11) are combined, the pressure forces are obtained as

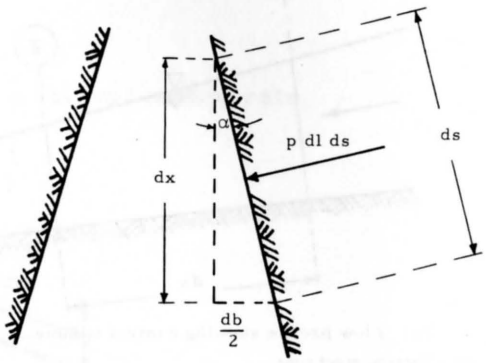

a. Plan view of channel.

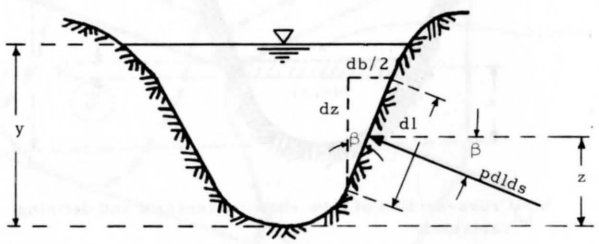

b. Channel cross-section.

Figure 2.3. Simplified representation of the force exerted on the fluid by the walls or sides of the channel.

$$F_p = -\beta' \gamma A \frac{\partial y}{\partial x} dx$$

According to assumption 3 given at the beginning of this chapter, the pressure-distribution coefficient, β', is equal to unity. Therefore:

$$F_p = -\gamma A \frac{\partial y}{\partial x} dx \quad . \quad . \quad . \quad . \quad . \quad . \quad . \quad (2.12)$$

Gravity forces

From Figure 2.1 the weight of the elemental volume of fluid is:

$$W = \gamma A\, dx \quad . \quad . \quad . \quad . \quad . \quad . \quad . \quad . \quad (2.13)$$

This weight gives rise to the gravity force in the x-direction:

$$F_g = \gamma A\, dx \sin\theta$$

or

$$F_g = \gamma A\, dx\, S_o \quad \ldots\ldots\ldots \quad (2.14)$$

Resistance forces

In the category of resistance forces are grouped those forces which oppose the movement of flow and induce losses of energy. These forces include: a) frictional forces due to the liquid viscosity and the channel roughness; b) resistance forces which arise from the irregularities in channel bottom and cross-sections, the meandering and nonlinear alignment of the channels, and the presence of obstructions such as vegetation and large boulders.

In view of assumption 8 given at the beginning of this chapter, the resistance forces will be calculated from the equations of motion and energy for steady flow.

For steady flow tne equations of continuity and motion can be written in the form:

$$A\frac{dV}{dx} + V\frac{dA}{dx} = I - 0 \quad \ldots\ldots\ldots \quad (2.15)$$

$$F_p + F_g + F_r = V\frac{d}{dx}(mV) \quad \ldots\ldots \quad (2.16a)$$

Since Equations (2.12) and (2.14) hold for steady as well as for unsteady flow, they can be combined with Equation (2.16a) to yield

$$-\gamma A\frac{dy}{dx}dx + \gamma A\, dx\, S_o + F_r = mV\frac{dV}{dx} + V^2\frac{dm}{dx} \quad . \quad (2.16b)$$

Since

$$m = \frac{\gamma}{g} A\, dx \quad \ldots\ldots\ldots \quad (2.17)$$

and for steady, one-dimensional flow x is the only independent variable. Equation (2.16b) becomes

$$-\gamma A\frac{dy}{dx}dx + \gamma A\, dx\, S_o + F_r = \frac{\gamma}{g} A\, dx V\frac{dV}{dx} + \frac{\gamma}{g} dx\, V^2\frac{dA}{dx}$$

or

$$F_r = \gamma A dx\left(\frac{dy}{dx} - S_o + \frac{V}{g}\frac{dV}{dx} + \frac{V^2}{gA}\frac{dA}{dx}\right) \quad . \quad (2.18a)$$

Combining Equation (2.18a) with (2.15)

$$F_r = \frac{\gamma}{g} A\, dx \left[g\left(\frac{dy}{dx} - S_o + \frac{V}{g}\frac{dV}{dx}\right) + (I - 0)\frac{V}{A} - V\frac{dV}{dx}\right] \quad \ldots\ldots\ldots \quad (2.18b)$$

The total energy in foot-pounds per pound of water in any streamline passing through a channel section can be expressed as the total head in feet of water, which is the sum of the elevation above a chosen datum, the pressure head, and the velocity head. According to the principle of conservation of energy, the total energy head at an upstream section should be equal to the total energy head at a downstream section plus the energy head lost between the two sections.

With reference to Figure 2.4, y and V designate respectively the flow depth and velocity at section 0 midway between sections 1 and 2. Values at sections 1 and 2 are obtained from values at section 0 by Taylor series expansion.

By the principle of conservation of energy the following expression can be written between sections 1 and 2:

$$-\frac{dx}{2}S_o + \frac{dx}{2}S_f + y + \frac{dx}{2}\frac{dy}{dx} + \frac{V^2}{2g} + \frac{dx}{2}\frac{d}{dx}\left(\frac{V^2}{2g}\right) = \frac{dx}{2}S_o - \frac{dx}{2}S_f + y - \frac{dx}{2}\frac{dy}{dx} + \frac{V^2}{2g} - \frac{dx}{2}\frac{d}{dx}\left(\frac{V^2}{2g}\right)$$

or

$$\frac{dy}{dx} - S_o + \frac{d}{dx}\left(\frac{V^2}{2g}\right) = -S_f \quad \ldots\ldots \quad (2.19)$$

Comparison of Equations (2.18b) and (2.19) gives the resistance forces as

$$F_r = \frac{\gamma}{g} Adx \left[-g\, S_f + (I - 0)\frac{V}{A} - V\frac{dV}{dx}\right] \quad . \quad (2.20a)$$

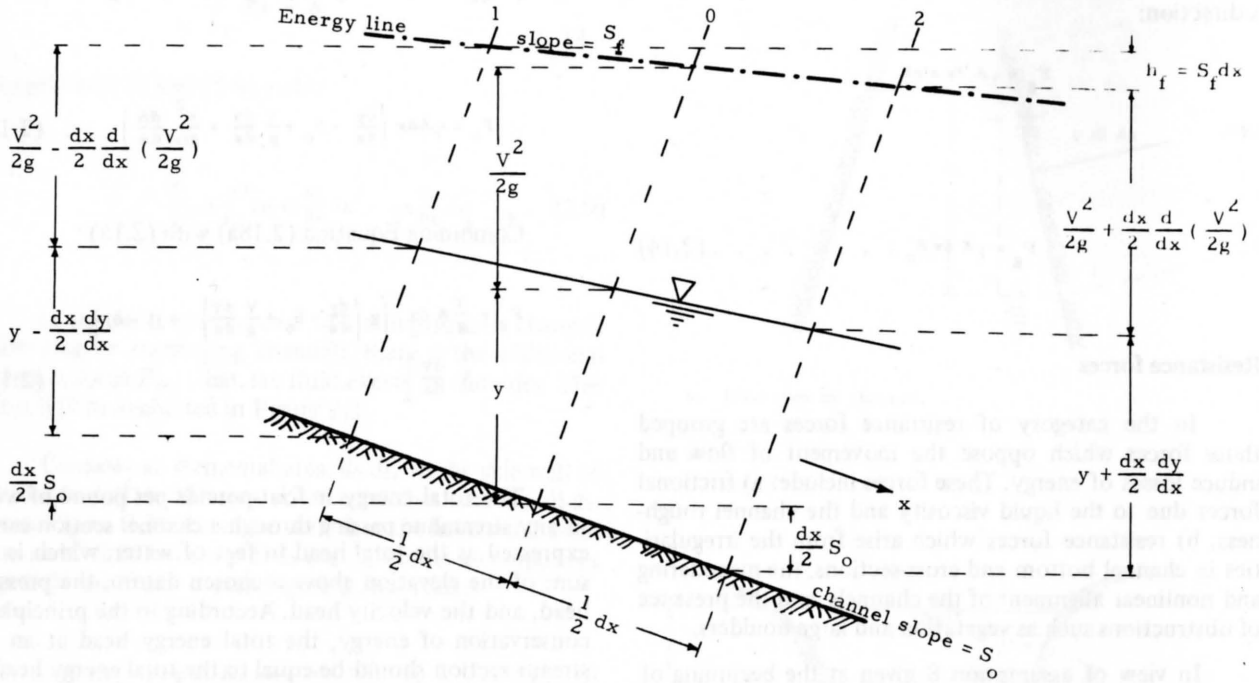

Figure 2.4. Simplified representation of energy in steady flow.

Equation (2.3) becomes

$$F_p + F_g + F_r = \frac{\gamma}{g} dx \left(A \frac{\partial V}{\partial t} + V \frac{\partial A}{\partial t} + V^2 \frac{\partial A}{\partial x} + AV \frac{\partial V}{\partial x} \right)$$

The continuity equation (Equation (2.1)) can be written as

$$V \frac{\partial A}{\partial t} + V^2 \frac{\partial A}{\partial x} + AV \frac{\partial V}{\partial x} = (I - 0) V$$

Therefore

$$F_p + F_g + F_r = \frac{\gamma}{g} A \, dx \left[\frac{\partial V}{\partial t} + (I - 0) \frac{V}{A} \right] \quad . \; . \quad (2.20b)$$

When the expressions for F_p, F_g, and F_r (Equations (2.12), (2.14) and (2.20a) respectively) are substituted in Equation (2.20b), the latter equation becomes

$$- \gamma A \frac{\partial y}{\partial x} dx + \gamma A dx \, S_o + \frac{\gamma}{g} A dx \left[- g S_f + (I - 0) \frac{V}{A} - V \frac{\partial V}{\partial x} \right]$$

$$= \frac{\gamma}{g} A dx \left[\frac{\partial V}{\partial t} + (I - 0) \frac{V}{A} \right]$$

Thus:

$$\frac{\partial V}{\partial t} + V \frac{\partial V}{\partial x} + g \frac{\partial y}{\partial x} = g (S_o - S_f) \quad . \; . \; . \; . \; (2.21)$$

Many expressions have been proposed for the computation of the energy line slope S_f. A commonly used relationship is the Manning formula which expresses S_f in terms of the hydraulic radius. In this study it was found convenient to assume that the energy line slope is proportional to the kinetic energy of the flow. Since the kinetic energy depends on the square of the flow velocity, the following general expression can be written

$$S_f = K |V| V \quad . \; . \; . \; . \; . \; . \; . \; (2.22a)$$

in which

K is the resistance coefficient, treated here as a positive constant, and defined as follows:

$$K = K_o + K_1 + K_2 + K_3 \quad . \; . \; . \; . \; . \; (2.22b)$$

in which

K_0 is the basic resistance coefficient for a straight, uniform channel in the natural materials involved

K_1 is a term added to correct for the effect of obstructions

K_2 is a term for channel irregularities

K_3 is a value added to compensate for meandering of the channel

Application of the Momentum and Continuity Equations to Irregular Channels

The cross-sectional area of the flow can be expressed in terms of the flow depth, y. The relationship between the area and the depth varies longitudinally for natural channels, so that

$$A = A(y, \Psi)$$

in which

Ψ is a shape factor which can include various parameters such as the base width or the top width, a measure of the divergence or convergence of the channel, etc.

Thus, the space derivative of A can be written as

$$\frac{\partial A}{\partial x} = \left(\frac{\partial A}{\partial y}\right)_{\psi = \text{const.}} \frac{\partial y}{\partial x} + \left(\frac{\partial A}{\partial \psi}\right)_{y = \text{const.}} \frac{\partial \psi}{\partial x} \quad . . (2.23)$$

The function $\Psi(x)$ is usually known, and for a prismatic channel is constant. Natural channels are nonprismatic and irregular in shape. However, for ease in mathematical treatment, their cross-section is usually assumed to have a regular geometric shape so that

$$\frac{\partial A}{\partial y} = B \quad . . . . . (2.24)$$

in which

B is generally a function of y

Equation (2.23) then becomes:

$$\frac{\partial A}{\partial x} = B\frac{\partial y}{\partial x} + \left(\frac{\partial A}{\partial \psi}\right)\frac{\partial \psi}{\partial x}$$

or

$$\frac{\partial y}{\partial x} = \frac{1}{B}\frac{\partial A}{\partial x} - G \quad . . . . . (2.25)$$

in which

$$G = \frac{1}{B}\left(\frac{\partial A}{\partial \psi}\right)\frac{\partial \psi}{\partial x} \quad . . . . . (2.26)$$

Equations (2.1) and (2.21) when combined with Equation (2.25) become

$$\frac{\partial A}{\partial t} + \frac{\partial Q}{\partial x} = I - O \quad . . . . . (2.27a)$$

$$\frac{\partial V}{\partial t} + \frac{1}{2}\frac{\partial V^2}{\partial x} + \frac{g}{B}\frac{\partial A}{\partial x} = g(S_o - S_f + G) \quad . . (2.27b)$$

These forms were found quite suitable for solution of the equations on the general-purpose electronic analog computer.

When Q is replaced by AV, Equations (2.27) take the form

$$\frac{\partial A}{\partial t} + A\frac{\partial V}{\partial x} + V\frac{\partial A}{\partial x} = I - O \quad . . . . . (2.28a)$$

$$\frac{\partial V}{\partial t} + V\frac{\partial V}{\partial x} + \frac{g}{B}\frac{\partial A}{\partial x} = g(S_o - S_f + G) \quad . . . . (2.28b)$$

The equations can also be expressed in terms of A and Q by replacing V by Q/A in (2.28). The substitution results in the following system of equations:

$$\frac{\partial A}{\partial t} + \frac{\partial Q}{\partial x} = I - O \quad . . . . . (2.29a)$$

$$\frac{\partial Q}{\partial t} - \frac{Q}{A}\frac{\partial A}{\partial t} + \frac{Q}{A}\frac{\partial Q}{\partial x} - \left(\frac{Q^2}{A^2} - \frac{gA}{B}\right)\frac{\partial A}{\partial x} = gA(S_o - S_f + G) \quad (2.29b)$$

Natural channels are sometimes divided into several sections, each of which is approximated by a prismatic channel. Under this hypothesis the term G is equal to zero.

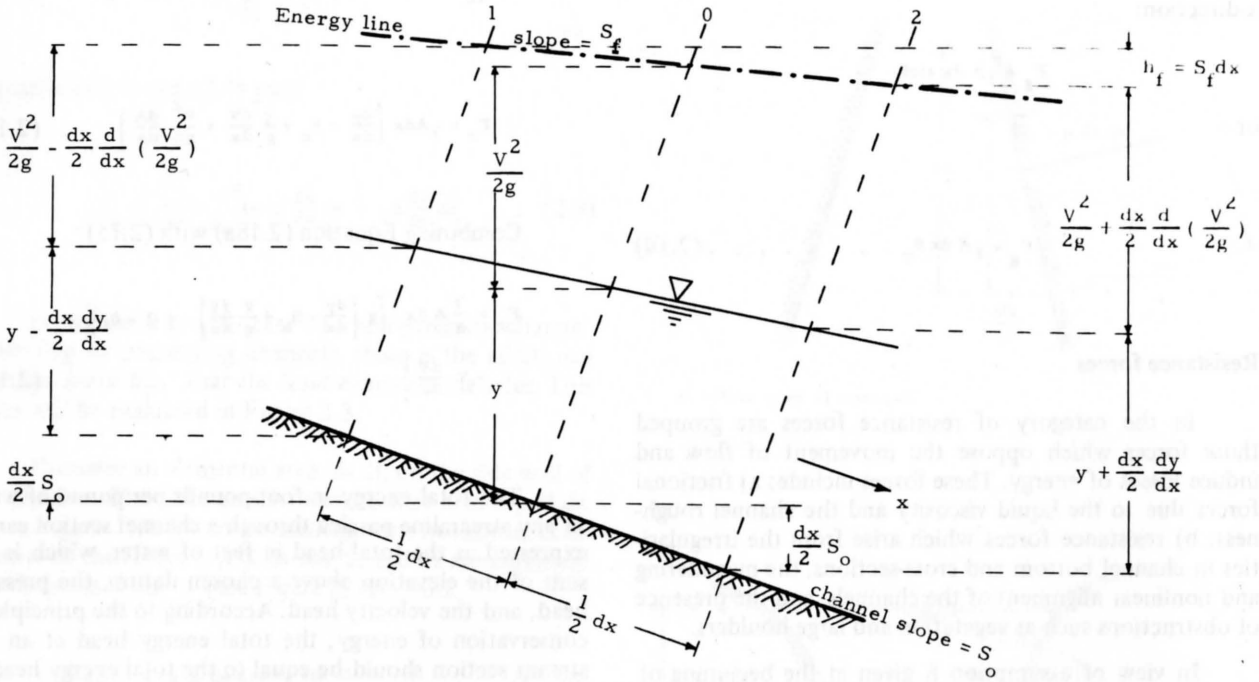

Figure 2.4. Simplified representation of energy in steady flow.

Equation (2.3) becomes

$$F_p + F_g + F_r = \frac{\gamma}{g} dx \left(A \frac{\partial V}{\partial t} + V \frac{\partial A}{\partial t} + V^2 \frac{\partial A}{\partial x} + AV \frac{\partial V}{\partial x} \right)$$

The continuity equation (Equation (2.1)) can be written as

$$V \frac{\partial A}{\partial t} + V^2 \frac{\partial A}{\partial x} + AV \frac{\partial V}{\partial x} = (I - 0) V$$

Therefore

$$F_p + F_g + F_r = \frac{\gamma}{g} A \, dx \left[\frac{\partial V}{\partial t} + (I - 0) \frac{V}{A} \right] \quad . . \quad (2.20b)$$

When the expressions for F_p, F_g, and F_r (Equations (2.12), (2.14) and (2.20a) respectively) are substituted in Equation (2.20b), the latter equation becomes

$$- \gamma A \frac{\partial y}{\partial x} dx + \gamma A dx \, S_o + \frac{\gamma}{g} A dx \left[- g S_f + (I - 0) \frac{V}{A} - V \frac{\partial V}{\partial x} \right]$$

$$= \frac{\gamma}{g} A dx \left[\frac{\partial V}{\partial t} + (I - 0) \frac{V}{A} \right]$$

Thus:

$$\frac{\partial V}{\partial t} + V \frac{\partial V}{\partial x} + g \frac{\partial y}{\partial x} = g (S_o - S_f) \quad . . . . (2.21)$$

Many expressions have been proposed for the computation of the energy line slope S_f. A commonly used relationship is the Manning formula which expresses S_f in terms of the hydraulic radius. In this study it was found convenient to assume that the energy line slope is proportional to the kinetic energy of the flow. Since the kinetic energy depends on the square of the flow velocity, the following general expression can be written

$$S_f = K |V| V \quad . . . . . (2.22a)$$

in which

K is the resistance coefficient, treated here as a positive constant, and defined as follows:

$$K = K_o + K_1 + K_2 + K_3 \quad . . . . . (2.22b)$$

in which

K_0 is the basic resistance coefficient for a straight, uniform channel in the natural materials involved

K_1 is a term added to correct for the effect of obstructions

K_2 is a term for channel irregularities

K_3 is a value added to compensate for meandering of the channel

Application of the Momentum and Continuity Equations to Irregular Channels

The cross-sectional area of the flow can be expressed in terms of the flow depth, y. The relationship between the area and the depth varies longitudinally for natural channels, so that

$$A = A(y, \psi)$$

in which

Ψ is a shape factor which can include various parameters such as the base width or the top width, a measure of the divergence or convergence of the channel, etc.

Thus, the space derivative of A can be written as

$$\frac{\partial A}{\partial x} = \left(\frac{\partial A}{\partial y}\right)_{\psi = \text{const.}} \frac{\partial y}{\partial x} + \left(\frac{\partial A}{\partial \psi}\right)_{y = \text{const.}} \frac{\partial \psi}{\partial x} \quad . . (2.23)$$

The function $\Psi(x)$ is usually known, and for a prismatic channel is constant. Natural channels are nonprismatic and irregular in shape. However, for ease in mathematical treatment, their cross-section is usually assumed to have a regular geometric shape so that

$$\frac{\partial A}{\partial y} = B \quad . . . . . (2.24)$$

in which

B is generally a function of y

Equation (2.23) then becomes:

$$\frac{\partial A}{\partial x} = B \frac{\partial y}{\partial x} + \left(\frac{\partial A}{\partial \psi}\right) \frac{\partial \psi}{\partial x}$$

or

$$\frac{\partial y}{\partial x} = \frac{1}{B} \frac{\partial A}{\partial x} - G \quad . . . . . (2.25)$$

in which

$$G = \frac{1}{B}\left(\frac{\partial A}{\partial \psi}\right) \frac{\partial \psi}{\partial x} \quad . . . . . (2.26)$$

Equations (2.1) and (2.21) when combined with Equation (2.25) become

$$\frac{\partial A}{\partial t} + \frac{\partial Q}{\partial x} = I - O \quad . . . . . (2.27a)$$

$$\frac{\partial V}{\partial t} + \frac{1}{2} \frac{\partial V^2}{\partial x} + \frac{g}{B} \frac{\partial A}{\partial x} = g(S_o - S_f + G) \quad . . (2.27b)$$

These forms were found quite suitable for solution of the equations on the general-purpose electronic analog computer.

When Q is replaced by AV, Equations (2.27) take the form

$$\frac{\partial A}{\partial t} + A \frac{\partial V}{\partial x} + V \frac{\partial A}{\partial x} = I - O \quad . . . . . (2.28a)$$

$$\frac{\partial V}{\partial t} + V \frac{\partial V}{\partial x} + \frac{g}{B} \frac{\partial A}{\partial x} = g(S_o - S_f + G) \quad . . . . (2.28b)$$

The equations can also be expressed in terms of A and Q by replacing V by Q/A in (2.28). The substitution results in the following system of equations:

$$\frac{\partial A}{\partial t} + \frac{\partial Q}{\partial x} = I - O \quad . . . . . (2.29a)$$

$$\frac{\partial Q}{\partial t} - \frac{Q}{A} \frac{\partial A}{\partial t} + \frac{Q}{A} \frac{\partial Q}{\partial x} - \left(\frac{Q^2}{A^2} - \frac{gA}{B}\right) \frac{\partial A}{\partial x} = gA(S_o - S_f + G) \quad (2.29b)$$

Natural channels are sometimes divided into several sections, each of which is approximated by a prismatic channel. Under this hypothesis the term G is equal to zero.

CHAPTER III

REVIEW OF THE METHODS OF SOLUTION FOR UNSTEADY FLOW EQUATIONS

The exact solution of the unsteady flow equations is a difficult task which thus far has been successful in only a few simplified cases. However, numerical solutions have been obtained on the digital computer by the use of finite-difference approximations. In this chapter, a number of methods which have been applied to the solution of the unsteady flow equations are presented. A technique for determining the restrictions to be imposed on some of the finite-difference methods as a result of the approximations underlying them is also included.

Exact Methods

The Saint-Venant equations are quasi-linear hyperbolic partial differential equations which are not easily amenable to solution. Attempts at their integration by direct analytical methods include the exact method of characteristics and the linearization techniques.

Exact method of characteristics

Under the method of characteristics the two partial differential equations of unsteady flow are transformed into a system of four ordinary differential equations by the following manipulations.

The equations of momentum and continuity (2.28) are identified as L_1 and L_2 respectively.

$$L_1 = \frac{\partial V}{\partial t} + V\frac{\partial V}{\partial x} + \frac{g}{B}\frac{\partial A}{\partial x} - g(S_o - S_f + G) = 0 \quad . \quad . \quad (3.1a)$$

$$L_2 = \frac{\partial A}{\partial t} + A\frac{\partial V}{\partial x} + V\frac{\partial A}{\partial x} - I + O = 0 \quad . \quad . \quad . \quad (3.1b)$$

A linear combination of the two equations is performed using an unknown multiplier λ:

$$L_1 + \lambda L_2 = \left[\frac{\partial V}{\partial t} + \frac{\partial V}{\partial x}(V + \lambda A)\right] + \left[\frac{\partial A}{\partial x}\left(\frac{g}{B} + \lambda V\right) + \lambda\frac{\partial A}{\partial t}\right]$$
$$- g(S_o - S_f + G) - \lambda(I - O) = 0 \quad . \quad . \quad . \quad . \quad (3.2)$$

The unknown λ should be chosen such that Equation (3.2) can be transformed into a system of two total differential equations. The expression in the first pair of brackets is the total derivative dV/dt if

$$\frac{dx}{dt} = V + \lambda A \quad . \quad . \quad . \quad . \quad . \quad . \quad . \quad (3.3)$$

For the expression in the second pair of brackets to be equal to the total derivative dA/dt the following expression must hold:

$$\frac{dx}{dt} = V + \frac{g}{B\lambda} \quad . \quad . \quad . \quad . \quad . \quad . \quad (3.4)$$

By comparing Equations (3.3) and (3.4) the values of λ are obtained as:

$$\lambda = \pm\sqrt{\frac{g}{AB}} \quad . \quad . \quad . \quad . \quad . \quad . \quad . \quad (3.5)$$

When those values of λ are substituted into Equations (3.2) to (3.4) the following system of characteristic equations is obtained

$$\frac{dx}{dt} = V + \sqrt{g\frac{A}{B}} \quad . \quad . \quad . \quad . \quad . \quad . \quad (3.6a)$$

$$\frac{dV}{dt} + \sqrt{\frac{g}{AB}}\frac{dA}{dt} - g(S_o - S_f + G) - \sqrt{\frac{g}{AB}}(I - O) = 0 \quad . \quad . \quad (3.6b)$$

$$\frac{dx}{dt} = V - \sqrt{g\frac{A}{B}} \quad . \quad . \quad . \quad . \quad . \quad . \quad . \quad (3.6c)$$

$$\frac{dV}{dt} - \sqrt{\frac{g}{AB}}\frac{dA}{dt} - g(S_o - S_f + G) + \sqrt{\frac{g}{AB}}(I - O) = 0 \quad . (3.6d)$$

The lines in the (x,t)-plane defined by Equation (3.6a) are called the α-characteristic lines or α-characteristics, and those defined by Equation (3.6c) are called the β-characteristic lines or β-characteristics. Equation (3.6b) holds only along the α-characteristics while Equation (3.6d) is valid only along the β-characteristics.

The system of partial differential Equations (2.28) has been converted into the equivalent system of ordinary differential Equations (3.6). This change is desirable if solution of the system is facilitated by the transformation. However, the system of Equations (3.6) is also nonlinear and still cannot be solved by direct methods of integration.

Linearization techniques

Solutions by direct integration have been obtained for simplified forms of the unsteady flow equations. In general, such simplifications involve the linearization of the equations. The usual way of obtaining the linear equations is by substituting $Q = Q_o + q$, $A = A_o + a$ in Equations (2.29), and retaining only first order terms in q and a. Equations (2.29) thus become:

$$\frac{\partial a}{\partial t} + \frac{\partial q}{\partial x} = I - O \quad . . . . . (3.7a)$$

$$\frac{\partial q}{\partial t} - v_o\frac{\partial a}{\partial t} + v_o\frac{\partial q}{\partial x} - (v_o^2 - gy_o)\frac{\partial a}{\partial x} = g(A_o + a)(S_o - S_f + G) \quad . . . . . (3.7b)$$

where v_o y_o A_o and Q_o are respectively the velocity, depth, flow cross-sectional area, and discharge rate during the initial steady uniform regime, while q and a are respectively the increments in the discharge rate and the flow area under the unsteady regime.

A single linearized equation is obtained by eliminating the incremental area, a, between Equations (3.7a) and (3.7b).

$$\frac{\partial^2 q}{\partial t^2} + 2v_o\frac{\partial^2 q}{\partial x \partial t} + \left(v_o^2 - gy_o\right)\frac{\partial^2 q}{\partial x^2} = g\lambda(I - O) \quad . (3.8)$$

in which

$$\lambda = S_o - S_f + G$$

Solutions for the linearized Equation (3.8) have been obtained by the Riemann-Adamard method (Deymie, 1939), by conformal mapping (Masse, 1939), and by Laplace transform (Lighthill et al., 1955). However, because the approximations introduced by linearization are quite severe, the method is not very accurate and should be used only for rough computations. Furthermore, linearization requires an initial finite value for the base flow. The technique is, therefore, not applicable to the conditions of ephemeral streams and overland flow where base flow values are usually zero. This same condition also makes difficult the use of the general method of characteristics for the solution of this problem.

Direct Electrical Analog

A direct electrical analog can be applied to the solution of simplified forms of the unsteady flow equations. A useful application of this method is illustrated below in which the unsteady flow equations are expressed in the following simplified form:

$$\frac{\partial q}{\partial x} + B\frac{\partial y}{\partial t} = I - O \quad . . . . . (3.9a)$$

$$\frac{\partial y}{\partial x} + \frac{1}{gA}\frac{\partial q}{\partial t} + S_f = S_o \quad . . . . . (3.9b)$$

The segment of electrical transmission shown in Figure 3.1 yields the following set of equations

$$\frac{\partial i}{\partial x} + C\frac{\partial e}{\partial t} = i' \quad . . . . . (3.10a)$$

$$\frac{\partial e}{\partial x} + L\frac{\partial i}{\partial t} + Ri = E_o \quad . . . . (3.10b)$$

When the sets of Equations (3.9) and (3.10) are compared, it can be seen that the following variables are equivalent:

Electrical Variables	Hydraulic Variables
voltage (e)	water depth (y)
current (i)	discharge (q)
inductance (L)	inertia coefficient (1/gA)
capacitance (c)	surface width (B)
constant voltage (E_o)	channel slope (S_o)
resistance term (Ri)	friction slope (S_f)
current gradient (i')	excess lateral inflow (I - O)

Use has also been made of other direct electrical analog techniques which, in general, introduce further simplifications in the unsteady flow equations.

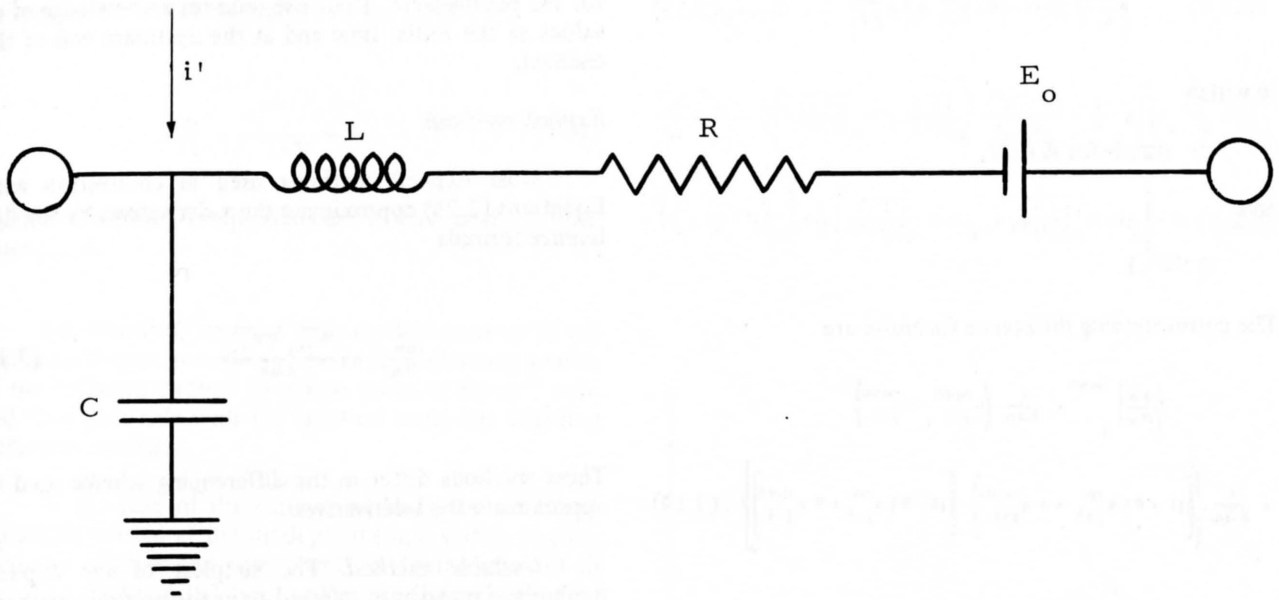

Figure 3.1. Electrical circuit applied to the solution of simplified forms of the unsteady flow equations.

Finite-Difference Methods

Several methods have been adapted for the numerical integration of the Saint-Venant equations on the digital computer. Those methods include:

1. The explicit and implicit finite-difference methods for the two basic equations of continuity and momentum.
2. The numerical integration of the characteristic equations.
3. The mixed difference method.

Difference methods for the two basic equations of continuity and momentum

Those methods use a grid of points in the (x,t)-plane, consisting of vertices of rectangles of sides Δx and Δt formed by the system of lines.

$$x = j\Delta x \qquad j = 0, 1, 2, 3, \ldots \qquad (3.11)$$

$$t = m\Delta t \qquad m = 0, 1, 2, 3, \ldots \qquad (3.12)$$

Values of the dependent variables are computed at the grid points. With reference to Figure 3.2, the values at time $(m+1)\,\Delta t$ can be calculated if the solution at time $m\Delta t$ is known. The difference scheme is said to be an implicit scheme if the finite-difference formula used for the evaluation of the x-derivatives contains unknown values of the m + 1 row, otherwise the solution is said to be explicit in nature.

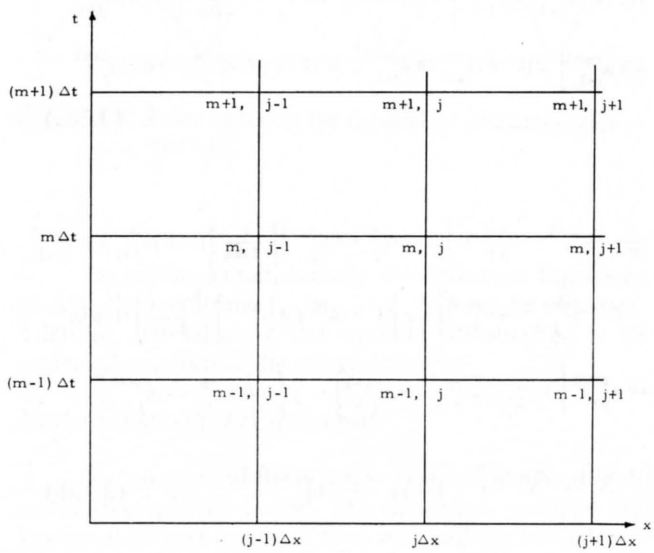

Figure 3.2. Point numbering for the implicit and explicit methods applied to the two basic equations of continuity and momentum.

Implicit methods

In these methods the difference equations are usually written at some intermediate point where values of the variables are determined by linear interpolation, that is,

$$\phi_j^{m+\theta} = (1-\theta)\,\phi_j^m + \theta\,\phi_j^{m+1} \quad \ldots\ldots (3.13)$$

in which

Φ stands for A or V,

and

$0 < \theta < 1$

The corresponding difference formulae are

$$\left(\frac{\partial \phi}{\partial x}\right)_j^{m+\theta} = \frac{1}{2\Delta x}\left(\phi_{j+1}^{m+\theta} - \phi_{j-1}^{m+\theta}\right)$$

$$= \frac{1}{2\Delta x}\left\{\left[(1-\theta)\,\phi_{j+1}^m + \theta\,\phi_{j+1}^{m+1}\right] - \left[(1-\theta)\,\phi_{j-1}^m + \theta\,\phi_{j-1}^{m+1}\right]\right\} \quad (3.14)$$

$$\left(\frac{\partial \phi}{\partial t}\right)_j^{m+\theta} = \frac{1}{\Delta t}\left(\phi_j^{m+1} - \phi_j^m\right) \quad \ldots\ldots (3.15)$$

Equations (2.28) take the following difference form

$$\frac{1}{\Delta t}\left(A_j^{m+1} - A_j^m\right) + \left[(1-\theta)A_j^m + \theta\,A_j^{m+1}\right]\frac{1}{2\Delta x}\left[(1-\theta)V_{j+1}^m + \theta\,V_{j+1}^{m+1}\right.$$

$$\left. - (1-\theta)V_{j-1}^m - \theta\,V_{j-1}^{m+1}\right] + \left[(1-\theta)V_j^m + \theta\,V_j^{m+1}\right]\frac{1}{2\Delta x}\left[(1-\theta)A_{j+1}^m\right.$$

$$\left. + \theta\,A_{j+1}^{m+1} - (1-\theta)A_{j-1}^m - \theta\,A_{j-1}^{m+1}\right] = (1-\theta)\,(I-O)_j^m + \theta\,(I-O)_j^{m+1}$$

$\ldots\ldots\ldots$ (3.16a)

$$\frac{1}{\Delta t}\left(V_j^{m+1} - V_j^m\right) + \left[(1-\theta)V_j^m + \theta\,V_j^{m+1}\right]\frac{1}{2\Delta x}\left[(1-\theta)V_{j+1}^m + \theta\,V_{j+1}^{m+1}\right.$$

$$\left. - (1-\theta)V_{j-1}^m - \theta\,V_{j-1}^{m+1}\right] + g\left[(1-\theta)B_j^m + \theta\,B_j^{m+1}\right]^{-1}\frac{1}{2\Delta x}\left[(1-\theta)A_{j+1}^m\right.$$

$$\left. + \theta\,A_{j+1}^{m+1} - (1-\theta)A_{j-1}^m - \theta\,A_{j-1}^{m+1}\right] = g\left[(1-\theta)A_j^m + \theta\,A_j^{m+1}\right]$$

$$\left[(1-\theta)\left(S_o - S_f + G\right)_j^m + \theta\left(S_o - S_f + G\right)_j^{m+1}\right]. \quad \ldots\ldots (3.16b)$$

The difference equations for all the grid points of the row m + 1 must be solved simultaneously. However, the iterative solution is time consuming. A procedure developed by Ritchmyer (1956) simplifies the computations to a large extent by first determining a recurrence formula and then calculating the values at the entire row in reverse order. Implicit methods differ mainly by the value chosen for the parameter θ. Their use requires a knowledge of all values at the initial time and at the upstream end of the channel.

Explicit methods

Most explicit methods used in connection with Equations (2.28) approximate the x-derivatives by the difference formula

$$\frac{\partial \phi}{\partial x} = \frac{\phi_{j+1}^m - \phi_{j-1}^m}{2\Delta x} \quad \ldots\ldots (3.17)$$

These methods differ in the differencing scheme used to approximate the t-derivatives.

Unstable method. The simplest of the explicit methods is sometimes referred to as the unstable method. This method approximates the t-derivatives by the difference formula

$$\frac{\partial \phi}{\partial t} = \frac{\phi_j^{m+1} - \phi_j^m}{\Delta t} \quad \ldots\ldots (3.18)$$

Equations (2.28), written in finite difference form at point (m, j), take the form

$$A_j^{m+1} - A_j^m + \frac{\Delta t}{2\Delta x}\left[A_j^m\left(V_{j+1}^m - V_{j-1}^m\right) + V_j^m\left(A_{j+1}^m - A_{j-1}^m\right)\right]$$

$$- \Delta t(I-O)_j^m = 0 \quad \ldots\ldots (3.19a)$$

$$V_j^{m+1} - V_j^m + \frac{\Delta t}{2\Delta x}V_j^m\left(V_{j+1}^m - V_{j-1}^m\right) + \frac{g\Delta t}{2B\Delta x}\left(A_{j+1}^m - A_{j-1}^m\right)$$

$$- g\Delta t\left(S_o - S_f + G\right)_j^m = 0 \quad \ldots\ldots (3.19b)$$

Diffusing method. The difference scheme for the t-derivatives is:

$$\frac{\partial \phi}{\partial t} = \frac{\phi_j^{m+1} - \frac{1}{2}\left(\phi_{j+1}^m + \phi_{j-1}^m\right)}{\Delta t} \quad \ldots\ldots (3.20)$$

The difference equations are evaluated at the central point (m, j).

Leap-frog method. This method uses an approximation formula for the t-derivatives of the form

$$\frac{\partial \phi}{\partial t} = \frac{\phi_j^{m+1} - \phi_j^{m-1}}{2\Delta t} \quad \ldots\ldots (3.21)$$

Again the difference equations are written at the central point (m, j).

Lax-Wendroff method. This method assumes all values to be known at row m - 1, uses the difference scheme of the diffusing method to obtain values at the m^{th} row, and then proceeds with the solution using the leap-frog difference formula.

In the case of the explicit methods, the difference equations written at the mesh point (m, j) suffice to compute the values at the point (m+1, j). Again, values of all variables at the initial time and at the channel upstream end are required.

Numerical methods of characteristics

Various types of difference schemes are available for solving the system of characteristic Equations (3.6) numerically. In general, numerical solutions are obtained by making use of a grid of characteristics, or by the method of specified time intervals.

Grid of characteristics method

The basic computational step under the grid of characteristics method consists of advancing the solution from a curve on which the variables are known. In general, the values at the initial time are given so that the values are known on the line t = 0.

In Figure 3.3, P is the intersection of the α-characteristic through C and the β-characteristic through D. All variables are known at points C and D, and the problem is to determine the coordinates x_P , t_P of P as well as the values of A_P and V_P at this point.

With reference to Figure 3.3, Equations (3.6) can be written in the following finite-difference form:

$$\frac{x_P - x_C}{t_P - t_C} = \frac{1}{2}\left[\left(V + \sqrt{g\frac{A}{B}}\right)_P + \left(V + \sqrt{g\frac{A}{B}}\right)_C\right] \quad . \quad (3.22a)$$

$$\frac{V_P - V_C}{t_P - t_C} + \frac{1}{2}\left[\sqrt{g\left(\frac{1}{AB}\right)_P} + \sqrt{g\left(\frac{1}{AB}\right)_C}\right]\frac{A_P - A_C}{t_P - t_C} - \frac{1}{2}g\left[\left(S_o - S_f + G\right)_P + \left(S_o - S_f + G\right)_C\right] - \frac{1}{2}\left[\sqrt{g\left(\frac{1}{AB}\right)_P}(I-O)_P + \sqrt{g\left(\frac{1}{AB}\right)_C}(I-O)_C\right] = 0 \quad (3.22b)$$

$$\frac{x_P - x_D}{t_P - t_D} = \frac{1}{2}\left[\left(V - \sqrt{g\frac{A}{B}}\right)_P + \left(V - \sqrt{g\frac{A}{B}}\right)_D\right] \quad . \quad (3.22c)$$

$$\frac{V_P - V_D}{t_P - t_D} - \frac{1}{2}\left[\sqrt{g\left(\frac{1}{AB}\right)_P} + \sqrt{g\left(\frac{1}{AB}\right)_D}\right]\frac{A_P - A_D}{t_P - t_D} - \frac{1}{2}g\left[\left(S_o - S_f + G\right)_P + \left(S_o - S_f + G\right)_D\right] + \frac{1}{2}\left[\sqrt{g\left(\frac{1}{AB}\right)_P}(I-O)_P + \sqrt{g\left(\frac{1}{AB}\right)_D}(I-O)_D\right] = 0 \quad (3.22d)$$

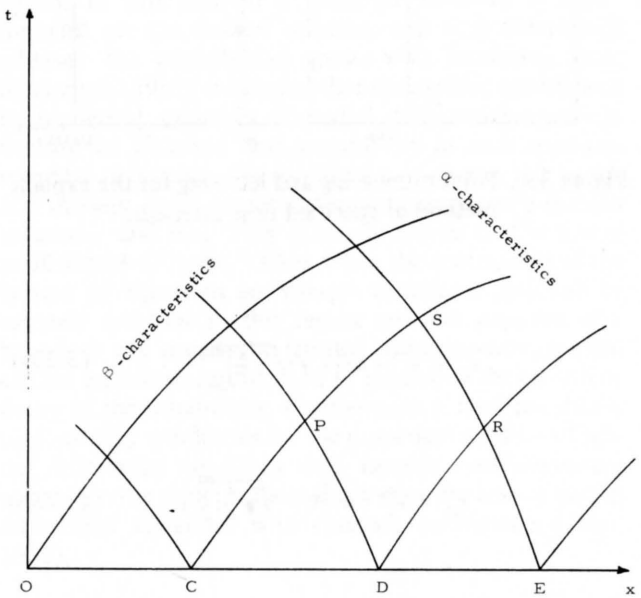

Figure 3.3. Point lettering for the grid of characteristics method.

By solving simultaneously the difference Equations (3.22), the unknowns t_P , x_P , A_P , V_P can be obtained. Likewise, the values of the variables are obtained at all intersection points in the solution region.

Method of specified time intervals

In this method the solution region is replaced by a rectangular grid of points. The dependent variables are known at all grid points at time $m\Delta t$ and are to be determined at time $(m+1)\,\Delta t$. The computations can be carried out by using either an explicit or an implicit scheme.

Explicit scheme. With reference to Figure 3.4, the values of A and V are to be calculated at the grid point (m+1, j). The x-coordinates of C and D, the intersections of the α- and β-characteristics through point (m+1, j) with the line $t = m\Delta t$, can be obtained from Equations (3.6a) and (3.6c) as

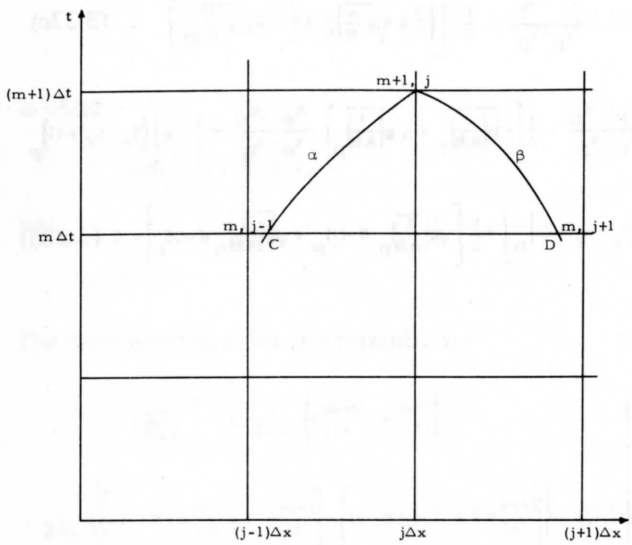

Figure 3.4. Point numbering and lettering for the explicit method of specified time intervals.

$$x_C = x_j^m - \Delta t \left(V + \sqrt{g \frac{A}{B}}\right)_j^m \quad . \quad . \quad . \quad . \quad (3.23a)$$

$$x_D = x_j^m + \Delta t \left(V - \sqrt{g \frac{A}{B}}\right)_j^m \quad . \quad . \quad . \quad . \quad (3.23b)$$

The values of the dependent variables at points C and D are obtained by linear interpolation between known values at points (m, j-1), (m, j), and (m, j+1).

$$\phi_C = \phi_j^m - \frac{\Delta t}{\Delta x} \left(\phi_j^m - \phi_{j-1}^m\right) \left(V + \sqrt{g \frac{A}{B}}\right)_j^m \quad . \quad . \quad (3.24a)$$

$$\phi_D = \phi_j^m + \frac{\Delta t}{\Delta x} \left(\phi_j^m - \phi_{j-1}^m\right) \left(V - \sqrt{g \frac{A}{B}}\right)_j^m \quad . \quad . \quad (3.24b)$$

Equations (3.6b) and (3.6d) become

$$V_j^{m+1} - V_C + \frac{1}{2}\left[\left(\sqrt{g \frac{1}{AB}}\right)_j^{m+1} + \left(\sqrt{g \frac{1}{AB}}\right)_C\right]\left(A_j^{m+1} - A_C\right)$$

$$- \frac{\Delta t}{2} g \left[\left(S_o - S_f + G\right)_j^{m+1} + \left(S_o - S_f + G\right)_C\right]$$

$$- \frac{\Delta t}{4}\left[\left(\sqrt{g \frac{1}{AB}}\right)_j^{m+1} + \left(\sqrt{g \frac{1}{AB}}\right)_C\right]\left[(I-O)_j^{m+1} + (I-O)_C\right] = 0 \quad . \quad (3.25a)$$

$$V_j^{m+1} - V_D - \frac{1}{2}\left[\left(\sqrt{g \frac{1}{AB}}\right)_j^{m+1} + \left(\sqrt{g \frac{1}{AB}}\right)_D\right]\left(A_j^{m+1} - A_D\right)$$

$$- \frac{\Delta t}{2} g \left[\left(S_o - S_f + G\right)_j^{m+1} + \left(S_o - S_f + G\right)_D\right]$$

$$+ \frac{\Delta t}{4}\left[\left(\sqrt{g \frac{1}{AB}}\right)_j^{m+1} + \left(\sqrt{g \frac{1}{AB}}\right)_D\right]\left[(I-O)_j^{m+1} + (I-O)_D\right] = 0 \quad . \quad (3.25b)$$

The unknowns V_j^{m+1} and A_j^{m+1} are obtained by solving simultaneously the system of Equations (3.24) and (3.25).

Implicit scheme. In Figure 3.5, a point P[t = $(m+\theta_t)\,\Delta t$, x = $(j+\theta_x)\,\Delta x$] is chosen. Values of the functions at point P are evaluated by the following interpolation formula:

$$\phi_P = \phi_{j+\theta_x}^{m+\theta_t} = (1-\theta_t)\left[(1-\theta_x)\,\phi_j^m + \theta_x\,\phi_{j+1}^m\right] + \theta_t\left[(1-\theta_x)\,\phi_j^{m+1} + \theta_x\,\phi_{j+1}^{m+1}\right] \quad . \quad . \quad . \quad . \quad . \quad . \quad . \quad . \quad (3.26)$$

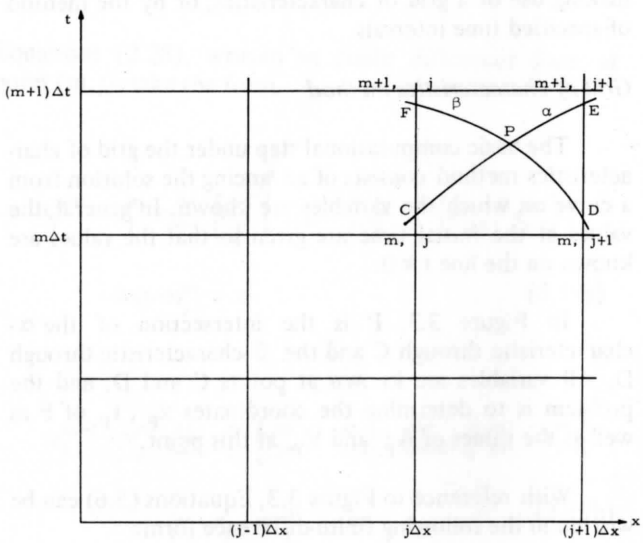

Figure 3.5. Point numbering and lettering for the implicit method of specified time intervals.

The α-and β-characteristics intersect line x = jΔx at C and F, and line x = (j+1) Δx at E and D. The t-coordinates of those points are obtained by writing Equations (3.6a) and (3.6c) in difference form along the α- and β-lines. Values of the variables at those points are then approxi-

mated by linear interpolation between adjacent grid points. When the values thus established are substituted into Equations (3.6b) and (3.6d) written in difference form along lines CE and FD, the resulting difference system is:

$$\theta_x\left[\frac{V_j^{m+1}-V_j^m}{\Delta t}+\sqrt{g\left(\frac{1}{AB}\right)}_P\frac{A_j^{m+1}-A_j^m}{\Delta t}\right]+(1-\theta_x)\left[\frac{V_{j+1}^{m+1}-V_{j+1}^m}{\Delta t}+\sqrt{g\left(\frac{1}{AB}\right)}_P\frac{A_{j+1}^{m+1}-A_{j+1}^m}{\Delta t}\right]+\theta_t\left(V+\sqrt{g\frac{A}{B}}\right)_P\left[\frac{V_{j+1}^{m+1}-V_j^{m+1}}{\Delta x}+\sqrt{g\left(\frac{1}{AB}\right)}_P\frac{A_{j+1}^{m+1}-V_j^{m+1}}{\Delta x}\right]+(1-\theta_t)\left(V+\sqrt{g\frac{A}{B}}\right)_P\left[\frac{V_{j+1}^m-V_j^m}{\Delta x}+\sqrt{g\left(\frac{1}{AB}\right)}_P\frac{A_{j+1}^m-A_j^m}{\Delta x}\right]-g\left(S_o-S_f+G\right)_P-\sqrt{g\left(\frac{1}{AB}\right)}_P(I-O)_P=0 \quad \ldots\ldots\ldots\ldots \quad (3.27a)$$

$$\theta_x\left[\frac{V_j^{m+1}-V_j^m}{\Delta t}-\sqrt{g\left(\frac{1}{AB}\right)}_P\frac{A_j^{m+1}-A_j^m}{\Delta t}\right]+(1-\theta_x)\left[\frac{V_{j+1}^{m+1}-V_{j+1}^m}{\Delta t}-\sqrt{g\left(\frac{1}{AB}\right)}_P\frac{A_{j+1}^{m+1}-A_{j+1}^m}{\Delta t}\right]-\theta_t\left(V-\sqrt{g\frac{A}{B}}\right)_P\left[\frac{V_{j+1}^{m+1}-V_j^{m+1}}{\Delta x}-\sqrt{g\left(\frac{1}{AB}\right)}_P\frac{A_{j+1}^{m+1}-A_j^{m+1}}{\Delta x}\right]-(1-\theta_t)\left(V-\sqrt{g\frac{A}{B}}\right)_P\left[\frac{V_{j+1}^m-V_j^m}{\Delta x}-\sqrt{g\left(\frac{1}{AB}\right)}_P\frac{A_{j+1}^m-A_j^m}{\Delta x}\right]+g\left(S_o-S_f+G\right)_P+\sqrt{g\left(\frac{1}{AB}\right)}_P(I-O)_P=0 \quad \ldots\ldots\ldots\ldots \quad (3.27b)$$

Simultaneous equations of the form of Equations (3.26) and (3.27) are written for all grid points along row m + 1, and the resulting system solved for values of A and V at all the grid points in that row.

Mixed difference methods

The finite-difference approximations presented so far involve the replacement of the derivatives by a difference quotient, and are crude when compared with numerical methods available for the integration of ordinary differential equations. Nevertheless, some of the latter methods can be adapted to such hyperbolic systems as the unsteady flow equations. When the x-derivatives are replaced by a difference quotient, Equations (2.28) written as $x = j\Delta x$ become:

$$\frac{dA_j}{dt}+A_j\Delta V_j+V_j\Delta A_j=(I-O)_j \quad \ldots \quad (3.28a)$$

$$\frac{dV_j}{dt}+V_j\Delta V_j+\frac{g}{B_j}\Delta A_j=g\left(S_o-S_f+G\right)_j \quad \ldots \quad (3.28b)$$

Equations (3.28) form a set of ordinary differential equations in the variable, t, and numerical methods, such as the Euler method, the Adams' method, and the Runge-Kutta method, can be used for their integration.

Stability study by the perturbation technique

The perturbation method has been found to be useful in determining the stability of a differential or a difference system of equations (von Neumann and Ritchmyer, 1950). In this method a small perturbation is superimposed on the desired solution, and it is determined whether the perturbation grows with increasing time. Ritchmyer (1962) concluded that the method applies well to numerical solutions of partial differential equations because he observed that instabilities in such solutions manifest themselves "as oscillations of short wave length and initially small amplitude superimposed on a smooth solution," and that "they generally appear first in a very small region of space." Thus, when the coefficients of the system of equations are smooth functions, they can be assumed constant in this region and the presence of a boundary can usually be ignored. Consequently, the linearized equations can be used in predicting the growth or decay of the instabilities. Furthermore, it has been shown that stability conditions for the numerical solution of partial differential equations with variable coefficients are essentially the same as those known for the case of partial differential equations with constant coefficients (John, 1952).

The procedure of the perturbation method involves replacing the dependent variables of the system of partial differential equations by the perturbed solution. This leads to a system of linear partial differential equations in the disturbances called the equations of first variation. Those equations are used to predict the behavior of the disturbances.

Equations of first variation

When the perturbed solutions $A + \delta A$ and $V + \delta V$ are substituted for A and V in Equations (2.28), in view of the above assumptions, the following system is obtained:

$$\frac{\partial}{\partial t}\delta A+V\frac{\partial}{\partial x}\delta A+A\frac{\partial}{\partial x}\delta V=0 \quad \ldots \quad (3.29a)$$

$$\frac{\partial}{\partial t}\delta V+V\frac{\partial}{\partial x}\delta V+\frac{g}{B}\frac{\partial}{\partial x}\delta A=0 \quad \ldots \quad (3.29b)$$

Equations (3.29) are the linear equations of first variation for the basic equations of unsteady flow. They can be used to study the stability of the various difference methods.

The von Neumann stability criteria

The exact solution of Equations (3.29), which would give information concerning the behavior of the disturbances δA and δV, cannot be found by direct integration. The usual procedure is to assume a solution at some time and to determine whether or not the disturbances grow without bounds at a later time. Under the assumption of constant coefficients, the stability of the difference system can be explored by making use of the fact that an initial exponential function remains exponential. Thus, if the following are assumed as initial values for δA and δV:

$$\delta A(x,o) = \delta A_o e^{ikx} \quad . \quad . \quad . \quad . \quad . \quad (3.30a)$$

$$\delta V(x,o) = \delta V_o e^{ikx} \quad . \quad . \quad . \quad . \quad . \quad (3.30b)$$

in which

A_o, V_o, k are constant and k is real, then the solution of Equations (3.29) at time t can be assumed to take the form:

$$\delta A(x,t) = \delta A_o e^{ikx + \alpha t} \quad . \quad . \quad . \quad . \quad (3.31a)$$

$$\delta V(x,t) = \delta V_o e^{ikx + \alpha t} \quad . \quad . \quad . \quad . \quad (3.31b)$$

At the grid point (j, m) $x = j\Delta x$ and $t = m\Delta t$. Equations (3.31) thus become:

$$\delta A_j^m = \delta A_o \zeta^j \xi^m \quad . \quad . \quad . \quad . \quad (3.32a)$$

$$\delta V_j^m = \delta V_o \zeta^j \xi^m \quad . \quad . \quad . \quad . \quad (3.32b)$$

in which

$$\zeta = e^{ik\Delta x} \quad . \quad . \quad . \quad . \quad . \quad . \quad (3.33a)$$

$$\xi = e^{\alpha \Delta t} \quad . \quad . \quad . \quad . \quad . \quad . \quad (3.33b)$$

The disturbances will not grow without bounds with increasing time if $|\xi| \leq 1$ for all real k. In other words, all values of ξ must fall on the unit circle of the complex plane. This criteria was first used by von Neumann and Ritchmyer (1950) to study the stability of differential and difference equations of unsteady flow, and is generally known as the von Neumann stability condition. Ritchmyer (1957, 1962) has proved that, in the case of the equations of unsteady flow, the von Neumann condition is necessary and sufficient for stability.

Using the procedure described above, stability studies were carried out for the explicit and implicit finite-difference methods applied to the two partial differential equations of unsteady flow. The results of these studies are summarized in Table 1. The stability condition which the explicit methods have to satisfy is usually referred to as the Courant-Friedrichs-Lewy condition in honor of the investigators who first discovered it (Courant et al., 1928).

The results shown in Table 1 agree with those obtained by Ritchmyer (1962) who used a somewhat different approach restricted to those difference methods in which both the time and space variables are differenced. The chief advantage of the perturbation technique presented here is that it can be applied to the study of the stability of difference, differential, as well as mixed differential-difference hyperbolic systems.

General comments

The method using the grid of characteristics does not present stability problems and is considered the most accurate of the numerical methods for digital computers. However, this method presents the disadvantage of finding the solution at odd points in the (x, t)-plane, and it would be difficult if not impossible to organize the computations so that the intersections of the characteristics occurred at the grid points of a rectangular mesh in the (x, t)-plane. When the time distribution of the dependent variables is needed at some fixed points of the x-coordinate, as is the case in runoff studies, then tedious two-dimensional interpolations in the characteristic grid are required. This operation can be carried out only on a computer having a memory sufficiently large to contain all data points.

The methods of specified time intervals, although less accurate, involve only one-dimensional interpolation, and the values of the variables on a line x = constant can be obtained at different times. However, these methods share the disadvantages inherent to the explicit and implicit methods.

Table 3.1. Stability conditions for the implicit and explicit finite-difference methods.

Method	ξ	When stable
Implicit	$\dfrac{1-i\dfrac{\Delta t}{\Delta x}\left(V\pm\sqrt{g\dfrac{A}{B}}\right)\left(1-\theta\right)\sin k\Delta x}{1+i\dfrac{\Delta t}{\Delta x}\left(V\pm\sqrt{g\dfrac{A}{B}}\right)\sin k\Delta x}$	always
Unstable	$1-i\dfrac{\Delta t}{\Delta t}\left(V\pm\sqrt{g\dfrac{A}{B}}\right)\sin k\Delta x$	never
Diffusing	$\cos k\Delta x-i\dfrac{\Delta t}{\Delta x}\left(V\pm\sqrt{g\dfrac{A}{B}}\right)\sin k\Delta x$	$\left\lvert\dfrac{\Delta t}{\Delta x}\left(V\pm\sqrt{g\dfrac{A}{B}}\right)\right\rvert<1$
Leap-frog	$-1\dfrac{\Delta t}{\Delta x}\left(V\pm\sqrt{g\dfrac{A}{B}}\right)\sin k\Delta x$ $\pm\sqrt{1-\left[\dfrac{\Delta t}{\Delta x}\left(V\pm\sqrt{g\dfrac{A}{B}}\right)\sin k\Delta x\right.}$	$\left\lvert\dfrac{\Delta t}{\Delta x}\left(V\pm\sqrt{g\dfrac{A}{B}}\right)\right\rvert<1$
Lax-Wendrof	Same as the diffusing and leap-frog methods.	$\left\lvert\dfrac{\Delta t}{\Delta x}\left(V\pm\sqrt{g\dfrac{A}{B}}\right)\right\rvert<1$

The main advantages of the implicit methods are that they can be made unconditionally stable, and the calculations are well organized on the rectangular grid of points. Although it is generally believed that the implicit methods are most suitable for river problems, some investigators (Liggett et al., 1967) have reported instances in which they were forced to abandon an implicit method which would not give the desired accuracy.

The explicit methods have the advantages of simplicity, and their use involved somewhat less labor. Their chief disadvantage is that they are required to satisfy the Courant-Friedrichs-Lewy condition in order to be stable, as shown in Table 1. This condition places severe limitations on the size of the steps Δx and Δt. In the case of an initially dry channel the stability condition may lead to ridiculously small values of the steps x and t. This situation makes prohibitive the use of explicit methods when dealing with a natural watershed where the channel is generally several miles long and where the duration of the event may be several hours.

Some investigators (Thirriot et al., 1967) have reported that in the mixed difference method the computation is reduced when compared to other difference methods. In addition, for an initial steady state, the steps Δx and Δt can be chosen much larger than those of the explicit methods. The Courant-Friedrichs-Lewy condition, however, still imposes serious limitations for an initially dry channel. Furthermore, the method requires that the derivatives of the variables be known at the initial time.

CHAPTER IV

THE ELECTRONIC ANALOG COMPUTER AND THE PARTIAL DIFFERENTIAL EQUATIONS OF UNSTEADY FLOW

The Analog Computer

The basic equations of unsteady flow were solved using an electronic analog computer at the Utah Water Research Laboratory. This electronic analog computer is a general-purpose machine which can perform operations such as addition, subtraction, multiplication, division, integration, and function generation.

The electronic analog computer is particularly adaptable for use in the solution of ordinary differential equations both linear and nonlinear, because it can perform directly such sophisticated operations as integration and differentiation on a continuous basis. In addition, because all operations take place in parallel on the computer, the "turn-around" time is short. This advantage and the ease with which modifications can be introduced into a problem or its solution enable the analog computer to handle particularly well the problem of model regulation where it is necessary to resort to "trial and error" explorations by altering various parameters within the mathematical model of the system under study. The operator is therefore able to quickly investigate the effects of a parameter change on the solution, and thus is provided with increased insight into the nature of the problem under consideration. The analog computer is able to output a continuous solution with respect to only one independent variable. For partial differential equations, a solution in terms of the remaining independent variables is achieved by a difference technique.

Solution of Unsteady Flow Equations on the Analog Computer

The differential-difference equations

The analog computer handles only ordinary differential equations directly. In order to use it in the solution of partial differential equations, the equations must be replaced by a set of equivalent ordinary differential equations. Conversion of the partial differential Equations (2.28) into ordinary differential equations involves treating one of the independent variables by finite-difference techniques (Johnson, 1963; Jackson, 1960; Mackay et al., 1962). This procedure is accomplished by dividing the range of the independent variable selected into a number of finite intervals. Either one of the two independent variables can be differenced. However, because runoff data are often given in the form of an outflow hydrograph at the watershed outlet, it is convenient to treat time as a continuous variable and to divide the channel length into N equal intervals of length Δx, as illustrated in Figure 4.1. The differential operator $D_x = \partial / \partial x$ is then replaced by the approximating difference operator Δ_x and the unsteady flow Equations (2.27) written at section $x = j\Delta x$ become:

$$\frac{dA_j}{dt} = I - O - \Delta_x Q_j \quad . \quad . \quad . \quad . \quad . \quad . \quad . \quad (4.1a)$$

$$\frac{dV_j}{dt} = gS_o + gG - gS_f - \frac{g}{B}\Delta_x A_j - \frac{1}{2}\Delta_x V_j^2 \quad . \quad . \quad (4.1b)$$

$$Q_j = A_j V_j \quad . \quad . \quad . \quad . \quad . \quad . \quad . \quad . \quad . \quad (4.1c)$$

in which

$$\Delta_x \varphi_j = a_1 \varphi_1 + a_2 \varphi_2 + a_3 \varphi_3 + \cdots \quad . \quad . \quad . \quad (4.2)$$

and not all a's are zero.

According to the difference quotient used for the x-derivative, the system of differential-difference Equations (4.1) will be either explicit or implicit. A backward or forward difference formula will yield an explicit system, while an implicit system is obtained when a centered difference quotient is used. The stability of the system of Equations (4.1) is closely related to the difference quotient used.

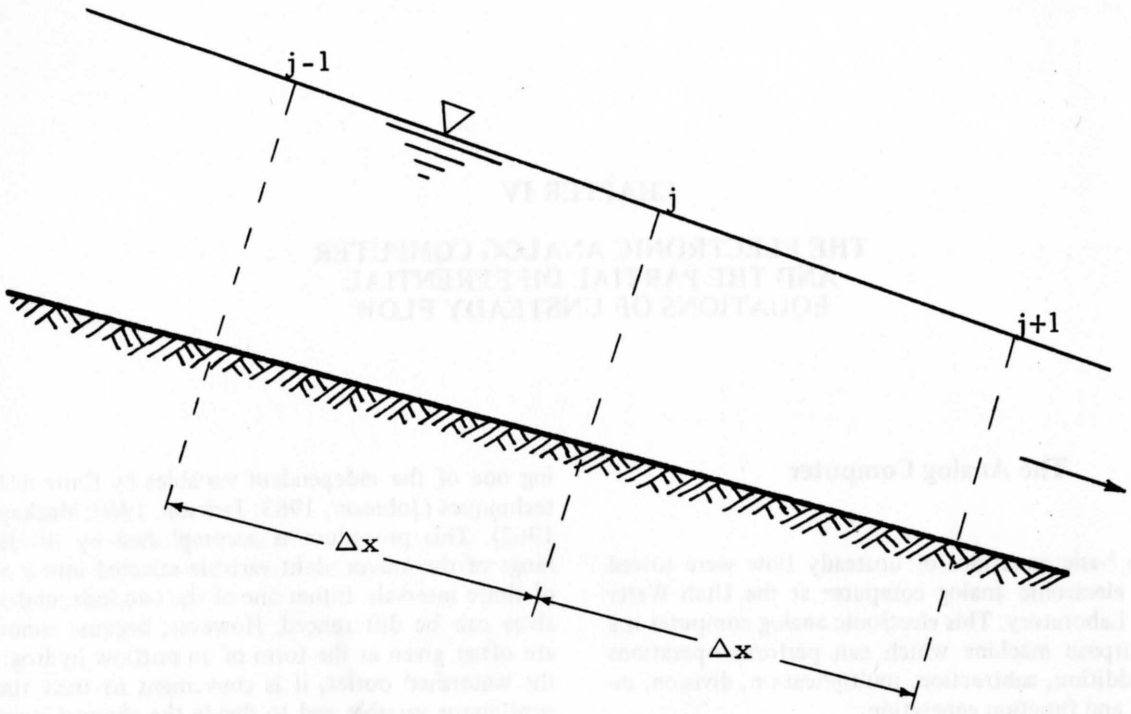

Figure 4.1. Flow profile illustrating finite increment procedure adopted for the flow model.

Stability

The equations of first variation (3.29) derived in Chapter III will be used to study the stability of the differential-difference equations. When the space derivatives are differenced, Equations (3.29) become:

$$\frac{d}{dt}\delta A + A\Delta_x \delta V + V\Delta_x \delta A = 0 \quad . \quad . \quad . \quad . \quad (4.3a)$$

$$\frac{d}{dt}\delta V + V\Delta_x \delta V + \frac{g}{B}\Delta_x \delta A = 0 \quad . \quad . \quad . \quad . \quad (4.3b)$$

A typical Fourier series solution is

$$\delta A = \delta A_o e^{ikj\Delta x + \alpha t} \quad . \quad . \quad . \quad . \quad (4.4a)$$

$$\delta V = \delta V_o e^{ikj\Delta x + \alpha t} \quad . \quad . \quad . \quad . \quad (4.4b)$$

or

$$\delta A = \delta A_o \zeta^j \xi \quad . \quad . \quad . \quad . \quad . \quad . \quad . \quad (4.5a)$$

$$\delta V = \delta V_o \zeta^j \xi \quad . \quad . \quad . \quad . \quad . \quad . \quad . \quad (4.5b)$$

Again, for stability all values of ξ should map in the unit circle of the complex plane.

Explicit schemes

Backward difference quotient. A typical backward difference formula is

$$\Delta_x \phi_j = \frac{\phi_j - \phi_{j-1}}{\Delta x} \quad . \quad . \quad . \quad . \quad . \quad . \quad . \quad (4.6)$$

When Equations (4.5) and (4.6) are combined with Equations (4.3), the equations of first variation become:

$$\alpha \delta A_o \zeta^j \xi + \frac{A\delta V_o}{\Delta x}(\zeta^j \xi - \zeta^{j-1}\xi) + \frac{V\delta A_o}{\Delta x}(\zeta^j \xi - \zeta^{j-1}\xi) = 0$$

$$. \quad . \quad . \quad . \quad . \quad . \quad . \quad . \quad . \quad . \quad . \quad . \quad (4.7a)$$

$$\alpha \delta V_o \zeta^j \xi + \frac{A\delta V_o}{\Delta x}(\zeta^j \xi - \zeta^{j-1}\xi) + \frac{g\delta A_o}{B\Delta x}(\zeta^j \xi - \zeta^{j-1}\xi) = 0$$

$$. \quad . \quad . \quad . \quad . \quad . \quad . \quad . \quad . \quad . \quad . \quad . \quad (4.7b)$$

From Equations (4.7), α is obtained as:

$$\alpha = \frac{1}{\Delta x}(\cos k\Delta x - 1 - i \sin k\Delta x)(V \pm \sqrt{g\frac{A}{B}}) \quad . \quad . \quad (4.8)$$

Therefore

$$\xi = \exp\left[\frac{\cos k\Delta x - 1}{\Delta x}(V \pm \sqrt{g\frac{A}{B}})t - i\,\frac{\sin k\Delta x}{\Delta x}(V \pm \sqrt{g\frac{A}{B}})t\right] \quad . \quad . \quad . \quad . \quad . \quad . \quad . \quad . \quad . \quad . \quad (4.9)$$

ξ will map in the unit circle of the complex plane if

$$|\xi| = \exp\left[\frac{\cos k\Delta x - 1}{\Delta x}(V \pm \sqrt{g\frac{A}{B}})t\right] \leq 1 \quad . \quad . \quad . \quad (4.10)$$

Since $t \geq 0$, condition (4.10) is met for all real k if

$$V \pm \sqrt{g\frac{A}{B}} \geq 0 \quad . \quad . \quad . \quad . \quad . \quad . \quad . \quad . \quad (4.11)$$

In other words, the backward difference formula can be used only if waves or disturbances are stationary or travel downstream. Therefore, this scheme applies to critical and supercritical flows only.

Forward difference quotient. In this case, the common form of the difference operator is:

$$\Delta_x \phi_j = \frac{\phi_{j+1} - \phi_j}{\Delta x} \quad . \quad . \quad . \quad . \quad . \quad . \quad . \quad (4.12)$$

The corresponding value of ξ is:

$$\xi = \exp\left[\frac{1 - \cos k\Delta x}{\Delta x}(V \pm \sqrt{g\frac{A}{B}})t - i\,\frac{\sin k\Delta x}{\Delta x}(V \pm \sqrt{g\frac{A}{B}})t\right] \quad . \quad . \quad . \quad . \quad . \quad . \quad . \quad . \quad . \quad . \quad (4.13)$$

The absolute values of ξ are less than one if

$$V \pm \sqrt{g\frac{A}{B}} \leq 0 \quad . \quad . \quad . \quad . \quad . \quad . \quad . \quad . \quad (4.14)$$

Condition (4.14) requires that the waves or disturbances be stationary or that they propagate in the upstream direction with a celerity larger than the flow velocity. This scheme can then be used in connection with critical flow and with subcritical flow with backwater effects due to some obstacle at the downstream end.

Implicit scheme

When use is made of a centered difference formula of the form

$$\Delta_x \phi_j = \frac{\phi_{j+1} - \phi_{j-1}}{2\Delta x} \quad . \quad . \quad . \quad . \quad . \quad (4.15)$$

ξ takes on the following values:

$$\xi = \exp\left[-i\,\frac{\sin k\Delta x}{\Delta x}(V \pm \sqrt{g\frac{A}{B}})t\right] \quad . \quad . \quad . \quad . \quad (4.16)$$

Since $|\xi| = 1$, while its argument is $(\sin k\Delta x)/\Delta x\,(V \pm \sqrt{g(A/B)})\,t$, ξ maps on the circumference of the unit circle in the complex plane for all real k. Therefore, the implicit differential-difference system is always stable, and is applicable to any regime of flow.

Programming the equations

Since the implicit differential-difference system is unconditionally stable, it will be used throughout this study. When Equation (4.15) is combined with Equations (4.1) and (2.20) the following system of differential-difference equations is obtained:

$$\frac{dA_j}{dt} = I - O - \frac{Q_{j+1}}{2\Delta x} + \frac{Q_{j-1}}{2\Delta x} \quad . \quad . \quad . \quad (4.17a)$$

$$\frac{dV_j}{dt} = gS_o + gG - gKV_j^2 - \frac{g}{2B\Delta x}A_{j+1} + \frac{g}{2B\Delta x}A_{j+1} - \frac{1}{4\Delta x}\left(V_{j+1}^2 - V_{j-1}^2\right) \quad . \quad . \quad . \quad . \quad . \quad . \quad . \quad . \quad . \quad . \quad (4.17b)$$

$$Q_j = A_j V_j \quad . \quad . \quad . \quad . \quad . \quad . \quad . \quad . \quad (4.17c)$$

in which the slope of the energy line is taken as KV^2 instead of $K|V|V$, because the flow velocity is always positive.

Magnitude scaling

Equations (4.17) should be scaled with respect to magnitude in order to utilize the full voltage range of the computer elements, and to permit a ready interpretation of voltages read from the computer directly in terms of the units of the problem. When magnitude-scaled Equations (4.17) can be written in the following form:

$$\left(\frac{100A_j}{|A_j|_M}\right) = \int_o^t \left[\frac{I_M}{|A_j|_M}\left(\frac{100\,I}{I_M}\right) - \frac{O_M}{|A_j|_M}\left(\frac{100\,O}{O_M}\right) - \frac{|Q_{j+1}|_M}{2\Delta x|A_j|_M}\left(\frac{100Q_{j+1}}{|Q_{j+1}|_M}\right) + \frac{|Q_{j-1}|_M}{2\Delta x|A_j|_M}\left(\frac{100Q_{j-1}}{|Q_{j-1}|_M}\right)\right] dt \quad . \quad . \quad . \quad (4.18a)$$

$$\left(\frac{100V_j}{|V_j|_M}\right) = \int_o^t \left[\frac{100gS_o}{|V_j|_M} - gK|V_i|_M\left(\frac{100V_j^2}{|V_j^2|_M}\right) - \frac{g|A_{j+1}|_M}{2B\Delta x|V_j|_M}\left(\frac{100A_{j+1}}{|A_{j+1}|_M}\right) + \frac{gG_M}{|V_j|_M}\left(\frac{100G}{G_M}\right) + \frac{g|A_{j-1}|_M}{2B\Delta x|V_j|_M}\left(\frac{100A_{j-1}}{|A_{j-1}|_M}\right) - \frac{|V_{j+1}^2|_M}{4\Delta x|V_j|_M}\left(\frac{100V_{j+1}^2}{|V_{j+1}^2|_M}\right) + \frac{|V_{j-1}^2|_M}{4\Delta x|V_j|_M}\left(\frac{100V_{j-1}^2}{|V_{j+1}^2|_M}\right)\right] dt \quad . \quad (4.18b)$$

$$\left(\frac{100Q_j}{|Q_j|_M}\right) = \frac{|A_j|_M|V_j|_M}{|Q_j|_M}\left(\frac{100A_j}{|A_j|_M}\right)\left(\frac{100V_j}{|V_j|_M}\right) \quad . \quad . \quad (4.18c)$$

in which the subscript M indicates the maximum expected values of the physical variables.

Time scaling

The speed of the computer solution can be altered by choosing a time scale factor h such that

$$h = \frac{\tau}{t} \quad . \quad . \quad . \quad . \quad . \quad . \quad . \quad . \quad (4.19a)$$

or

$$dt = \frac{1}{h}\,d\tau \quad . \quad . \quad . \quad . \quad . \quad . \quad . \quad . \quad (4.19b)$$

in which

- t represents time in the physical system under investigation
- τ represents computer time

Equations (4.18) scaled with respect to time appear as:

$$\left(\frac{100A_j}{|A_j|_M}\right) = \int_o^\tau \left[\frac{I_M}{h|A_j|_M}\left(\frac{100\,I}{I_M}\right) - \frac{O_M}{h|A_j|_M}\left(\frac{100\,O}{O_M}\right) - \frac{|Q_{j+1}|_M}{2h\Delta x|A_j|_M}\left(\frac{100Q_{j+1}}{|Q_{j+1}|_M}\right) + \frac{|Q_{j-1}|_M}{2h\Delta x|A_j|_M}\left(\frac{100Q_{j-1}}{|Q_{j-1}|_M}\right)\right] d\tau \quad . \quad . \quad (4.20a)$$

$$\left(\frac{100V_j}{|V_j|_M}\right) = \int_o^\tau \left[\frac{100gS_o}{h|V_j|_M} - \frac{gK|V_j|_M}{h}\left(\frac{100V_j^2}{|V_j^2|_M}\right) - \frac{g|A_{j+1}|_M}{2hB\Delta x|V_j|_M}\left(\frac{100A_{j+1}}{|A_{j+1}|_M}\right) + \frac{gG_M}{h|V_j|_M}\left(\frac{100G}{G_M}\right) + \frac{g|A_{j-1}|_M}{2hB\Delta x|V_j|_M}\left(\frac{100A_{j-1}}{|A_{j-1}|_M}\right) - \frac{|V_{j+1}^2|_M}{4h\Delta x|V_j|_M}\left(\frac{100V_{j+1}^2}{|V_{j+1}^2|_M}\right) + \frac{|V_{j-1}^2|_M}{4h\Delta x|V_j|_M}\left(\frac{100V_{j-1}^2}{|V_{j+1}^2|_M}\right)\right] d\tau \quad . \quad . \quad (4.20b)$$

$$\left(\frac{100Q_j}{|Q_j|_M}\right) = \frac{|A_j|_M|V_j|_M}{|Q_j|_M}\left(\frac{100A_j}{|A_j|_M}\right)\left(\frac{100V_j}{|V_j|_M}\right) \quad . \quad . \quad . \quad (4.20c)$$

In this study the computer solution was speeded up by choosing a time scale factor smaller than unity.

A computer program for Equations (4.20) is shown in Figure 4.2. However, because of their implicit nature, these equations applied to a particular section, j, and are not sufficient to calculate the variables at that section. Therefore, equations similar to (4.20) are written at each channel section, and the resulting system solved simultaneously. Figure 4.3 shows the computer program for the equations written at the first ten sections of the channel.

Effects of the time scale factor and the resistance term on the stability of the implicit differential-difference scheme

With the introduction of the time scale factor h and the resistance term KV^2 the equations of first variation take the following form for the implicit scheme.

$$\frac{d}{d\tau}\delta A_j + \frac{A}{2h\Delta x}\left(\delta V_{j+1} - \delta V_{j-1}\right) + \frac{V}{2h\Delta x}\left(\delta A_{j+1} - \delta A_{j-1}\right) = 0 \quad . \quad . \quad . \quad . \quad . \quad . \quad . \quad . \quad . \quad (4.21a)$$

$$\frac{d}{d\tau}\delta V_j + \frac{gKV}{h}\delta V_j + \frac{V}{2h\Delta x}\left(\delta V_{j+1} - \delta V_{j-1}\right) + \frac{g}{2hB\Delta x}\left(\delta A_{j+1} - \delta A_{j-1}\right) = 0 \quad . \quad . \quad . \quad . \quad (4.21b)$$

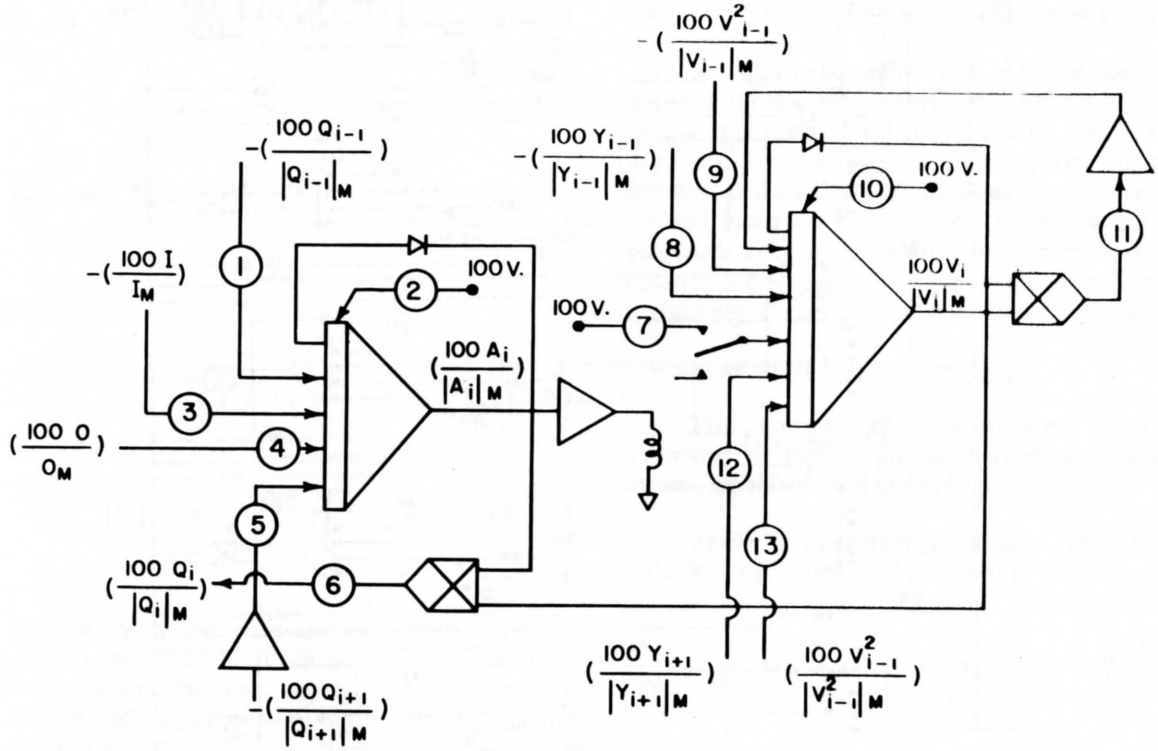

POT NO.	SETTING	POT NO.	SETTING	POT NO.	SETTING
1	$\frac{\lvert Q_{i-1}\rvert_M}{2h\Delta x\lvert A_i\rvert_M}$	6	$\frac{\lvert A_i\rvert_M\lvert V_i\rvert_M}{\lvert Q_i\rvert_M}$	11	$\frac{gK\lvert V_i^2\rvert_M}{h\lvert V_i\rvert_M}$
2	$\frac{A_i\,(0)}{\lvert A_i\rvert_M}$	7	$\frac{gS_o}{h\lvert V_i\rvert_M}$	12	$\frac{g\lvert y_{i+1}\rvert_M}{2h\Delta x\lvert V_i\rvert_M}$
3	$\frac{I_M}{h\lvert A_i\rvert_M}$	8	$\frac{g\lvert y_{i-1}\rvert_M}{2h\Delta x\lvert V_i\rvert_M}$	13	$\frac{\lvert V^2_{i+1}\rvert_M}{4h\Delta x\lvert V_i\rvert_M}$
4	$\frac{O_M}{h\lvert A_i\rvert_M}$	9	$\frac{\lvert V^2_{i-1}\rvert_M}{4h\Delta x\lvert V_i\rvert_M}$		
5	$\frac{\lvert Q_{i+1}\rvert_M}{2h\Delta x\lvert A_i\rvert_M}$	10	$\frac{V_i(0)}{\lvert V_i\rvert_M}$		

Figure 4.2. An elemental computer program for the implicit differential-difference equations of unsteady flow.

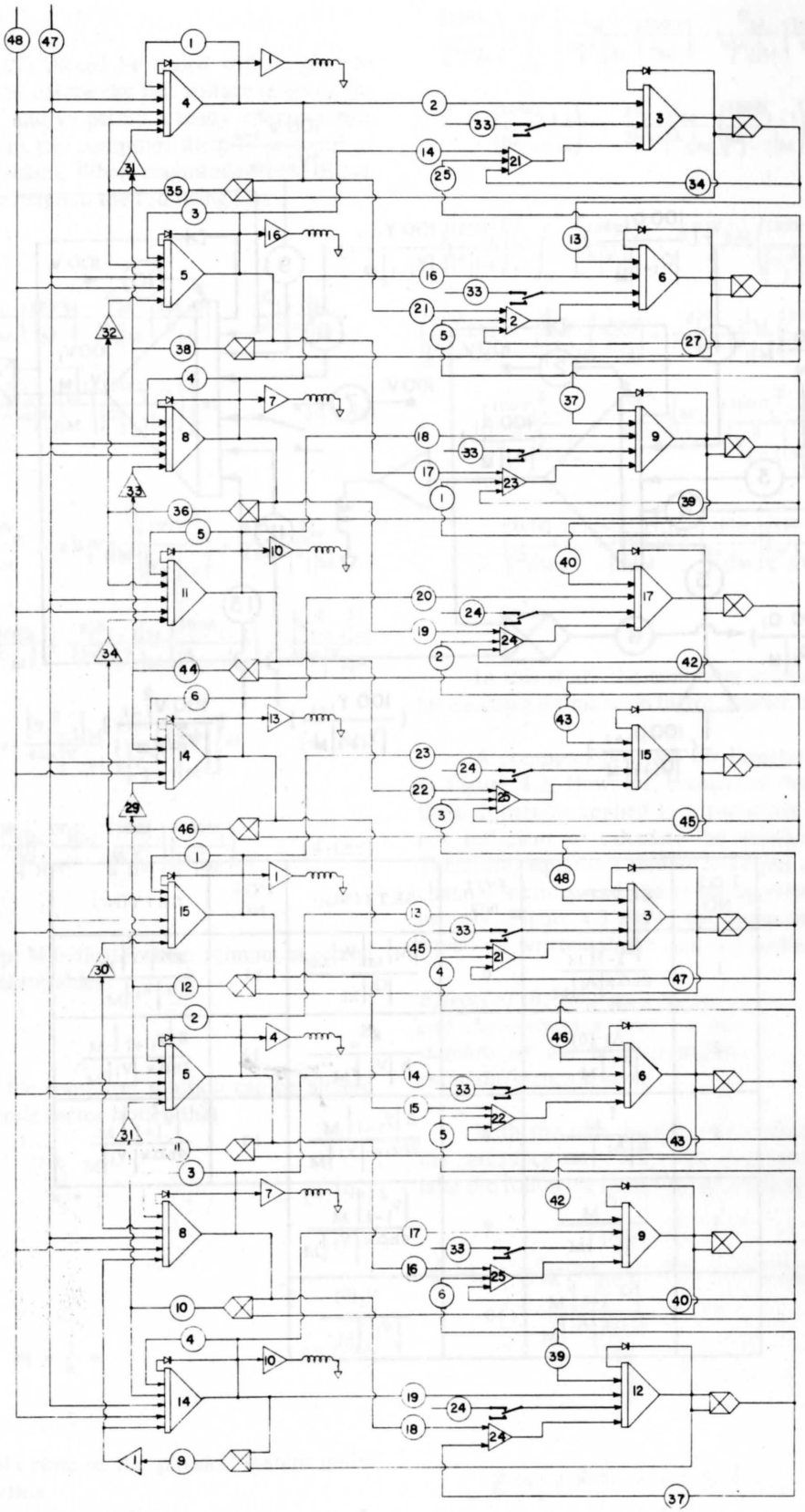

Figure 4.3. Computer program for the solution of the implicit differential-difference equations of unsteady flow at the first ten sections of a channel.

The corresponding values of ξ are

$$\xi_1 = \exp\left[-i \frac{\sin k\Delta x}{h\Delta x} \left(V + A \frac{\delta V_o}{\delta A_o}\right) \tau\right] \quad . \quad . \quad . \quad (4.22a)$$

$$\xi_2 = \exp\left[- \frac{gKV}{h} \tau - i \frac{\sin k\Delta x}{h\Delta x} \left(V + \frac{g\delta A_o}{B\delta V_o}\right) \tau\right] . \quad (4.22b)$$

Therefore

$$|\xi_1| = 1 . . . . . \quad (4.23a)$$

$$|\xi_2| = \exp\left(- \frac{gKV}{h} \tau\right) . . . . . \quad (4.23b)$$

Since K, V, h and τ are always positive, $\xi_2 < 1$, the system is always stable. It can then be concluded that the introduction of the time scale factor h and the term KV^2 does not affect the stability of the implicit differential-difference system.

Error analysis

Two types of error can be distinguished in the analog solution of the partial differential equations of unsteady flow:

1. The truncation errors which are mathematical in origin.
2. The computing errors which are due to the imperfections of the computing machine.

Truncation errors

The truncation errors are introduced by the use of finite difference approximations for the x-derivatives. It can be shown that the explicit difference scheme approximates the differential operator to the order Δx, while the implicit scheme introduces a truncation error of the order Δx^2.

Because there exists no known exact solution to general shallow water equations, evaluation of those errors is not possible. Nevertheless, the truncation errors can be regulated by the choice of the step Δx. For example, a reduction of Δx decreases truncation error. However, this procedure requires the use of additional computing components and consequently, increases the computing errors. Further, it has been shown that inherent instability in the analog solution of partial differential equations sometimes increases as the interval is reduced (Mackay and Fisher, 1962). The h^2-extrapolation method has been proposed to compensate for the truncation errors (Hartree, 1949, Miura and Iwata, 1966), but the use of this method also results in an increase of the computing errors.

An alternative method of reducing the truncation errors is the use of a higher-order difference approximation (Fisher, 1956, Mackay and Fisher, 1962). This technique avoids the increase in the computing elements, but involves increased complication in the circuitry. Another method based on the truncated Fourier series has been proposed to make correction for the truncation errors (Dieters and Nomura, 1968), but this procedure is meaningful only if used in connection with a hybrid computer.

Computing errors

The computing errors originate from the inaccuracies of the computing elements such as potentiometers, amplifiers, and multipliers.

Error propagation equations. The differential-difference equations can be written as

$$\frac{dA_j}{dt} = f_{2j-1}(A_1, A_2, \ldots, V_1, V_2, \ldots, I, O) \quad . \quad . \quad (4.24a)$$

$$\frac{dV_j}{dt} = f_{2j}(A_1, A_2, \ldots, V_1, V_2, \ldots, S_o) \quad . \quad . \quad (4.24b)$$

The solution of this system on the analog computer involves the generation of the function f_j and their integration to produce A_j and V_j. In those processes, errors are introduced due to amplifier drift, multiplier noise, potentiometer loading, discretization of the input functions, and variation in input voltages. Consequently, the exact operations

$$A_j = \int_o^\tau f_{2j-1}(A_{j-1}, A_{j+1}, V_{j-1}, V_{j+1}, I, O)d\tau \quad . \quad (4.25a)$$

$$V_j = \int_o^\tau f_{2j}(A_{j-1}, A_{j+1}, V_{j-1}, V_j, V_{j+1}, S_o)d\tau \quad . \quad (4.25b)$$

are implemented on the electronic analog computer as

$$A_j^* = \int_o^\tau \left[f_{2j-1}(A_{j-1}^*, A_{j+1}^*, V_{j-1}^*, V_{j+1}^*, I, O) + E_{2j-1}\right]d\tau$$

. . . . . (4.26a)

$$V_j^* = \int_o^\tau \left[f_{2j}(A_{j-1}^*, A_{j+1}^*, V_{j-1}^*, V_j^*, V_{j+1}^*, S_o) + E_{2j}\right]d\tau$$

. . . . . (4.26b)

The computing errors are the differences between the computer solutions and the exact solutions, or

$$\delta A_j = A_j^* - A_j \quad . \quad . \quad . \quad . \quad . \quad . \quad . \quad (4.27a)$$

$$\delta V_j = V_j^* - V_j \quad . \quad . \quad . \quad . \quad . \quad . \quad . \quad (4.27b)$$

Making use of the Taylor series expansion and neglecting terms of order higher than one, the following relationships can be derived:

$$f_{2j-1}(A_{j-1}^*, A_{j+1}^*, V_{j-1}^*, V_{j+1}^*, I, O)$$

$$= f_{2j-1}(A_{j-1}, A_{j+1}, V_{j-1}, V_{j+1}, I, O)$$

$$+ \sum_{k=j-1}^{j+1} \left(\frac{\partial f_{2j-1}}{\partial A_k} \delta A_k + \frac{\partial f_{2j-1}}{\partial V_k} \delta V_k \right) \quad . \quad . \quad . \quad (4.28a)$$

$$f_{2j}(A_{j-1}^*, A_{j+1}^*, V_{j-1}^*, V_j^*, V_{j+1}^*, S_o)$$

$$= f_{2j}(A_{j-1}, A_{j+1}, V_{j-1}, V_j, V_{j+1}, S_o)$$

$$+ \sum_{k=j-1}^{j+1} \left(\frac{\partial f_{2j}}{\partial A_k} \delta A_k + \frac{\partial f_{2j}}{\partial V_k} \delta V_k \right) \quad . \quad . \quad . \quad . \quad . \quad (4.28b)$$

By combining Equations (4.25), (4.26), (4.27), and (4.28) the computing error propagation equations are obtained as:

$$\frac{d}{d\tau} \delta A_j = \sum_{k=j-1}^{j+1} \frac{\partial f_{2j-1}}{\partial A_k} \delta A_k + \frac{\partial f_{2j-1}}{\partial V_k} \delta V_k + E_{2j-1} \quad (4.29a)$$

$$\frac{d}{d\tau} \delta V_j = \sum_{k=j-1}^{j+1} \frac{\partial f_{2j}}{\partial A_k} \delta A_k + \frac{\partial f_{2j}}{\partial V_k} \delta V_k + E_{2j} \quad . \quad (4.29b)$$

or

$$\frac{d}{d\tau} \delta A_j = \frac{A_{j-1}}{2h\Delta x} \delta V_{j-1} + \frac{V_{j-1}}{2h\Delta x} \delta A_{j-1} - \frac{A_{j+1}}{2h\Delta x} \delta V_{j+1}$$

$$- \frac{V_{j+1}}{2h\Delta x} \delta A_{j+1} + E_{2j-1} \quad . \quad . \quad . \quad . \quad . \quad . \quad . \quad . \quad (4.30a)$$

$$\frac{d}{d\tau} \delta V_j = \frac{g}{2hB\Delta x} \delta A_{j-1} + \frac{V_{j-1}}{2h\Delta x} \delta V_{j-1} - \frac{gKV_j}{h} \delta V_j$$

$$- \frac{g}{2hB\Delta x} \delta A_{j+1} - \frac{V_{j+1}}{2h\Delta x} \delta V_{j+1} + E_{2j} \quad . \quad . \quad . \quad (4.30b)$$

The forcing functions E_j are composed of a number of primary errors of the individual computer elements, and their systematic determination is beset with many difficulties. Further, the error propagation equations are nonlinear and cannot be solved by direct methods of integration. To facilitate the analysis of the errors, the nonlinear system (4.30) is replaced by the following linear system

$$\frac{d}{d\tau} \delta A_j = \frac{A}{2h\Delta x} \delta V_{j-1} + \frac{V}{2h\Delta x} \delta A_{j-1} - \frac{A}{2h\Delta x} \delta V_{j+1}$$

$$- \frac{V}{2h\Delta x} \delta A_{j+1} + E_{2j-1} \quad . \quad . \quad . \quad . \quad . \quad . \quad . \quad . \quad (4.31a)$$

$$\frac{d}{d\tau} \delta V_j = \frac{g}{2hB\Delta x} \delta A_{j-1} + \frac{V}{2h\Delta x} \delta V_{j-1} - \frac{gKV}{h} \delta V_j$$

$$- \frac{g}{2hB\Delta x} \delta A_{j+1} - \frac{V}{2h\Delta x} \delta V_{j+1} + E_{2j} \quad . \quad . \quad . \quad (4.31b)$$

in which A and V are assumed to be constant.

Computing stability. The difference between the error propagation Equations (4.31) and the equations of first variation (4.21) is the addition of the forcing functions E_{2j-1} and E_{2j} in Equations (4.31). Since the error propagation equations are nonhomogeneous, the condition for stability of those equations is more restrictive than that of system (4.21). The error-propagation equations will be said stable if, for all finite E, the disturbances δA and δV remain finite for all τ. This condition will be met if the solution of the homogeneous equations remains finite for all τ and goes to zero faster than $1/\tau$ (Vichnevetsky, 1967). A Fourier series solution of the homogeneous system was obtained as:

$$\delta A_j = \delta A_o \exp\left[-KV\frac{\tau}{h} - i\left\{ \frac{\sin kx}{\Delta x} \left(V + A\frac{\delta V_o}{\delta A_o} \right) \frac{\tau}{h} - k\Delta x \right\} \right]$$

$$. \quad . \quad . \quad . \quad . \quad . \quad . \quad . \quad . \quad . \quad . \quad (4.32a)$$

$$\delta V_j = \delta V_o \exp\left[-KV\frac{\tau}{h} - i\left\{ \frac{\sin kx}{\Delta x} \left(V + A\frac{\delta V_o}{\delta A_o} \right) \frac{\tau}{h} - k\Delta x \right\} \right].$$

$$. \quad . \quad . \quad . \quad . \quad . \quad . \quad . \quad . \quad . \quad . \quad (4.32b)$$

Because the values δA_j and δV_j as given by Equations (4.32) remain finite for all τ and go to zero faster than $1/\tau$ when $\tau \to \infty$, the error propagation can be said to be stable.

Note that δA_j and δV_j will go to zero faster if the time scale factor h is less than one. Therefore, a value of h smaller than unity strengthens the stability of the error propagation while a value of h larger than one weakens it.

CHAPTER V

THE SURFACE RUNOFF MODEL

The flow process considered here is that generated from rainfall on the surface of a drainage basin. It includes only that portion of the runoff cycle shown inside the dotted line in Figure 5.1. As a consequence, the surface model described here is restricted to the following situations:

1. Short-time duration runoff events in which interflow and groundwater flow play no part.
2. Watersheds in which infiltration and seepage water does not reappear as surface flow within the watersheds.
3. Runoff events for which interflow and groundwater flow rates, if any, have been calculated separately and are known at any point of the drainage basin.

When rainfall occurs over a watershed, only part of the rainfall appears at the outlet of the basin. The remaining portion of the rainfall is accounted for as losses on the watershed. Some of the rain which falls in the early part of the storm is both intercepted by the vegetal cover and stored in depressions in the soil surface, from where it eventually either evaporates or infiltrates to the upper soil layers. The remaining part of the rainfall is the effective rainfall which gives rise to overland and channel flows while being depleted by infiltration and channel seepage. Thus, the model discerns three phases in the surface runoff process. First, the phase in which an effective rainfall is produced. Second, the overland phase in which water flows over the land surfaces toward an established channel. Third, the channel phase whereby water flows through the channel system, and ultimately results in an outflow hydrograph at the outlet of the watershed.

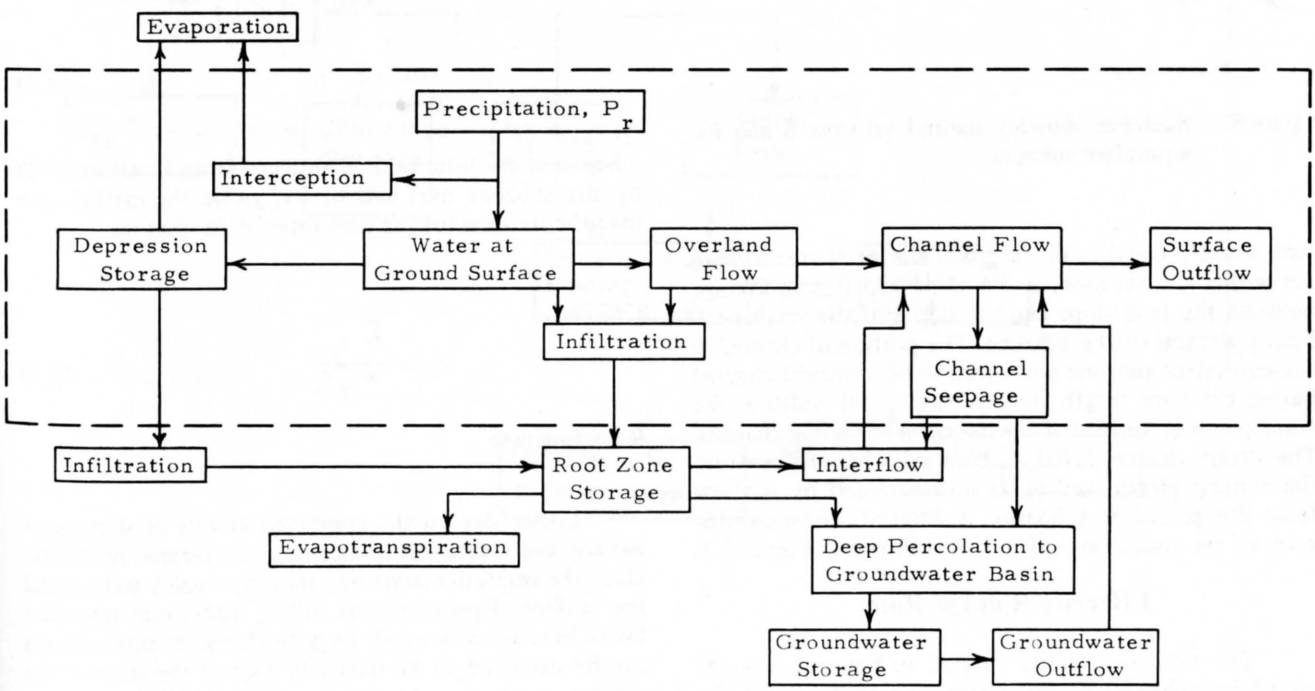

Figure 5.1. Schematic diagram of the runoff cycle.

Treatment of the Watershed

The watershed is divided into Z subzones on the basis of its physiography. Each subzone, which is in fact a small drainage basin containing only one main stream channel, is replaced by an equivalent subbasin having the same surface area as the subzone, and composed of two identical rectangular sloping planes transected by the main channel as illustrated in Figure 5.2. The rectangular planes which constitute the field of motion of the overland flow,

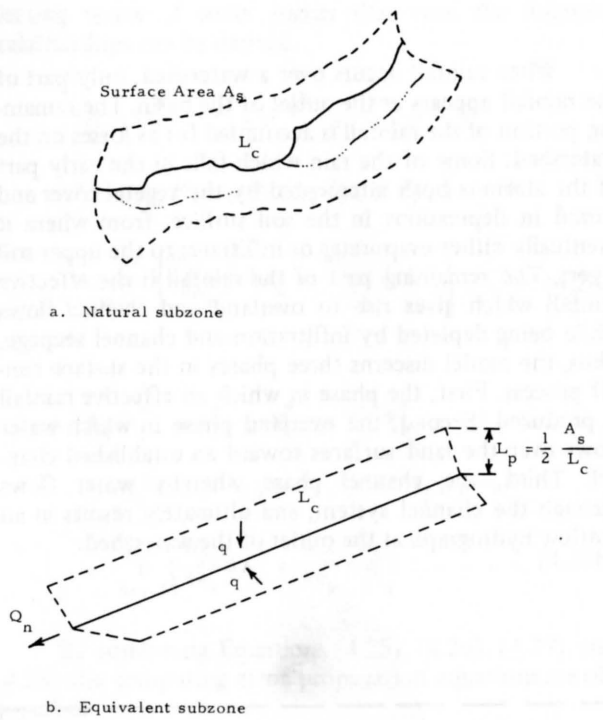

Figure 5.2. Sketches showing natural subzone 3 and its equivalent subzone.

have a width equal to the length of the main stream channel within the subzone, and a slope which is an average between the land slope and the slopes of the smaller tributary streams of the subzone. The portion of channel in the equivalent subzone is assumed to be a straight channel having the same length, average slope, and width as the corresponding segment of the natural meandering channel. The stream channel is fed on both sides by outflow from the sloping planes, and at its upstream end by outflow from the preceding subbasin. A detailed schematic diagram of the surface runoff model is shown in Figure 5.3.

Effective Rainfall Rate

The rate of effective rainfall in Figure 5.3 is obtained by substracting the retention rate R_r from the rainfall rate P_r.

Rainfall rate

A digital computer program has been written to integrate point precipitation measurements in terms of both time and space (Kwan et al., 1968). The program involves the use of interpolation techniques to determine isohyetal lines over a watershed for a given interval of time Δt. The points at which each line crosses the subzone boundary are located, and the elemental areas bounded by two adjacent isohyetal lines and the subzone boundary are calculated. Elemental rainfall volumes are then computed according to the formula

$$v_i = a_i \frac{p_i + p_{i+1}}{2} \quad \ldots\ldots\ldots \quad (5.1)$$

in which

a_i is the elemental area

p_i and p_{i+1} are the depths of rainfall on two adjacent isohyetal lines.

If the elemental area is bounded by one isohyetal line and a portion of the subzone boundary, rainfall values are determined by interpolation at several points along the portion of the boundary; then the rainfall depth over the area is computed as the average between the value on the isohyetal line and the average of the values at the chosen points along the boundary.

The rainfall volume over the subzone during the period of time Δt is computed by summing the volumes over all elemental areas comprised in the subzone, or

$$VOL = \sum_i v_i \quad \ldots\ldots\ldots \quad (5.2)$$

ıvision of the total volume obtained from Equation (5.2) by the subzone area and by Δt, yields the rainfall rate over the subzone for the time interval Δt, that is,

$$P_r = \frac{\sum_i v_i}{\Delta t \sum_i a_i} \quad \ldots\ldots\ldots \quad (5.3)$$

Retention rate

Losses due to the combined effects of depression storage and vegetation interception are termed retention. Once the vegetative cover becomes thoroughly wetted and the surface depressions are filled, additional retention losses become very small. In general, the retention losses can be expected to be relatively high at the start of the storm event and to become negligible as the event progresses. An exception is the case of an initially wet water-

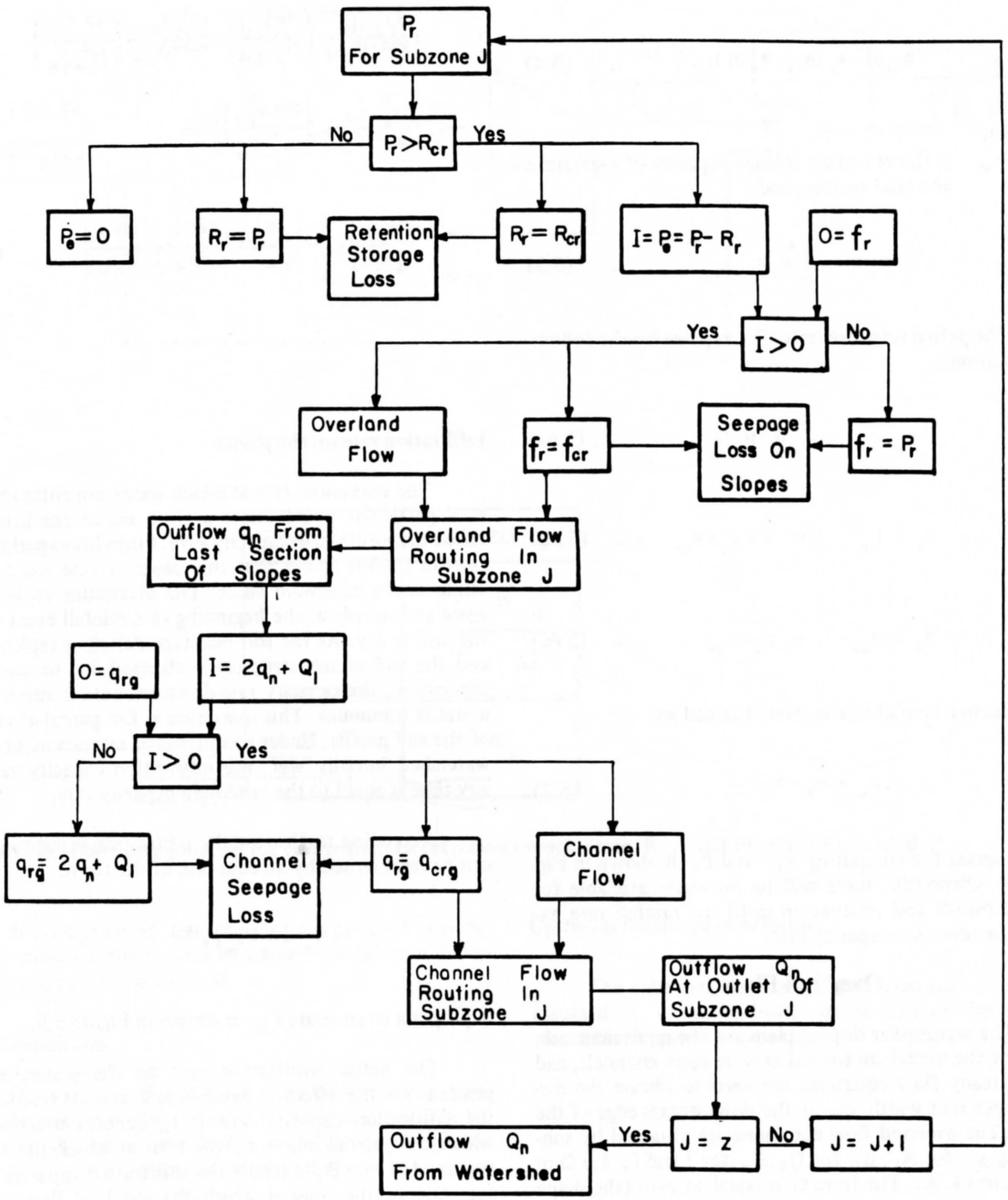

Figure 5.3. Flow chart for the surface runoff model.

shed where the retention losses can be assumed to be equal to zero. It is assumed that the maximum rate at which rainfall is lost to retention storage is given by the following expression (Riley, 1967):

$$R_{cr}(t) = k_r (R_{cs} - R_s(t)) \quad \ldots\ldots (5.4)$$

in which

R_{cs} is the retention storage capacity of vegetation and land surface, and

$$R_s(t) = \int_o^t R_r dt \quad \ldots\ldots (5.5)$$

The actual retention rate, R_r, is given by the following equations:

$$R_r = 0 \quad , \text{ if } P_r = 0 \quad \ldots\ldots (5.6a)$$

$$R_r = P_r \quad , \text{ if } 0 < P_r < R_{cr} \quad \ldots\ldots (5.6b)$$

$$R_r = R_{cr} \quad , \text{ if } P_r \geq R_{cr} \quad \ldots\ldots (5.6c)$$

The effective rainfall rate is then obtained as

$$P_e = P_r - R_r \quad \ldots\ldots (5.7)$$

The program for computing R_{cr} and P_e is shown in Figure 5.4. Obviously, there will be no water available for surface runoff and infiltration until the rainfall rate exceeds the retention capacity rate.

Overland Flow

The rectangular sloping planes of the equivalent subzones of the model are treated as wide open channels, and the unsteady flow equations are used to obtain the discharge per unit width, q_n, at the downstream edge of the planes. The overland flow equations are obtained by substituting y_j for A_j, q_j for Q_j, P_e for I and f_r for O in Equations (4.20). The term G is equal to zero (the shape factor α is constant in Equation (2.26) and Equations (4.20) become:

$$\left(\frac{100\, y_j}{|y_j|_M}\right) = \int_o^\tau \left[\frac{|P_e|_M}{h|y_j|_M}\left(\frac{100 P_e}{|P_e|_M}\right) - \frac{|f_r|_M}{h|y_j|_M}\left(\frac{100\, f_r}{|f_r|_M}\right)\right.$$

$$\left. - \frac{|q_{j+1}|_M}{2h\Delta x|y_j|_M}\left(\frac{100\, q_{j+1}}{|q_{j+1}|_M}\right) + \frac{|q_{j-1}|_M}{2h\Delta x|y_j|_M}\left(\frac{100\, q_{j-1}}{|q_{j-1}|_M}\right)\right] d\tau \quad \ldots\ldots (5.8a)$$

$$\left(\frac{100\, V_j}{|V_j|_M}\right) = \int_o^\tau \left[\frac{100\, gS_o}{h|V_j|_M} - \frac{gK|V_j|_M}{h}\left(\frac{100\, V_j^2}{|V_j^2|_M}\right) - \frac{g|y_{j+1}|_M}{2h\Delta x|V_j|_M}\left(\frac{100\, y_{j+1}}{|y_{j+1}|_M}\right)\right.$$

$$+ \frac{g|y_{j-1}|_M}{2h\Delta x|V_j|_M}\left(\frac{100\, y_{j-1}}{|y_{j-1}|_M}\right) - \frac{|V_{j+1}^2|_M}{4h\Delta x|V_j|_M}\left(\frac{100\, V_{j+1}^2}{|V_{j+1}^2|_M}\right)$$

$$\left. + \frac{|V_{j-1}^2|_M}{4h\Delta x|V_j|_M}\left(\frac{100\, V_{j-1}^2}{|V_{j-1}^2|_M}\right)\right] d\tau \quad \ldots\ldots (5.8b)$$

$$\left(\frac{100\, q_j}{|q_j|_M}\right) = \frac{|y_j|_M|V_j|_M}{|q_j|_M}\left(\frac{100\, y_j}{|y_j|_M}\right)\left(\frac{100\, V_j}{|V_j|_M}\right) \quad \ldots\ldots (5.8c)$$

Infiltration rate on the planes

The maximum rate at which water can enter the soil at a particular point under a given set of conditions is called the infiltration capacity rate. From his experiments, Horton (1933) found that this capacity rate has a maximum and a minimum value. The maximum value for a given soil occurs at the beginning of a rainfall event when the soil is dry. As the soil moisture deficit is replenished and the soil crumb structure is changed due to moisture absorption, the capacity rate decreases until it approaches a stable minimum. This minimum is the percolation rate of the soil profile. Under conditions of saturation, or for a watershed initially wet, the infiltration capacity rate at any time is equal to the minimum capacity rate.

According to Horton, the infiltration capacity curve can be represented by an equation of the form:

$$f_{cr} = f_m + (f_o - f_m) e^{-k_f t} \quad \ldots\ldots (5.9)$$

A program to generate f_{cr} is shown in Figure 5.5.

The actual infiltration rate on the planes is dependent on the effective rainfall rate and its relation to the infiltration capacity rate. If t_o denotes the time at which the rainfall starts, t_e the time at which the effective rainfall rate P_e exceeds the infiltration capacity rate f_{cr}, and t_s the time at which the overland flow stops, then the actual infiltration rate per unit area can be defined by the expressions:

$$t_o < t < t_e \quad , \quad f_r = P_e \quad \ldots (5.10a)$$

$$t_e < t < t_s \quad , \quad f_r = f_{cr} \quad \ldots (5.10b)$$

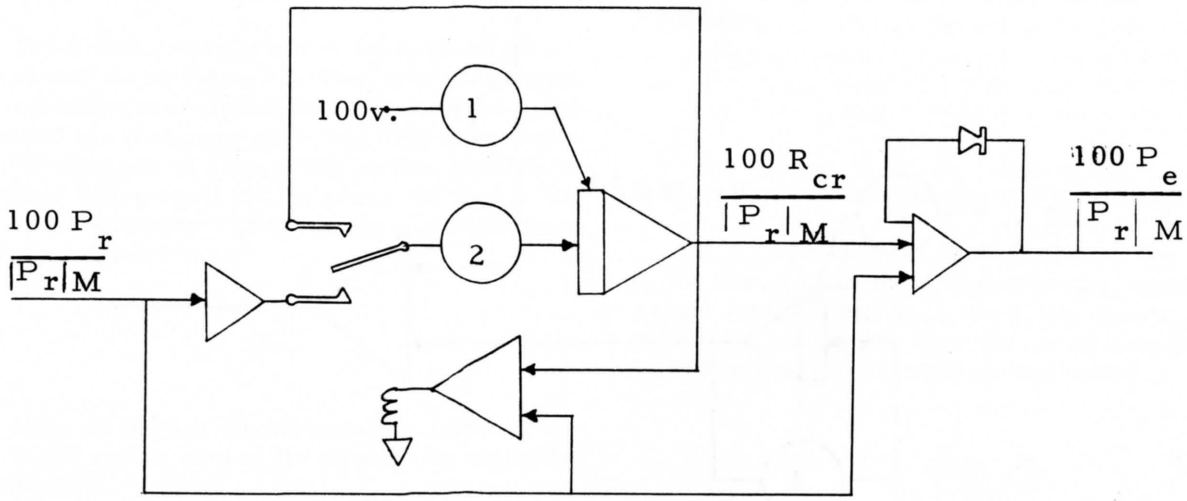

Pot No.	Setting
1	$\frac{k_r R_{cs}}{P_r M}$
2	k_r

Figure 5.4. Computer program for computing the retention capacity rate, R_{cr}, and the effective rainfall, P_e.

It is emphasized that infiltration is assumed to occur at the capacity rate as long as water is available in detention storage on the watershed.

Initial conditions

The solution of Equations (5.8) on the analog computer requires that the values of V and y at all sections be known at the initial time. In this model the sloping planes are treated as initially dry channels so that

$$t = 0 \quad , y(0) = 0 \quad , \text{ and } V_j(0) = 0 \quad . \quad . \quad . \quad (5.11,$$

Other conditions could be used if the calculations were to start at a time different from that at which the rainfall started.

Upstream boundary conditions

The subzones were established such that no flow is assumed to cross the upstream section of the sloping planes (see Figure 5.6), that is,

$$q_1 = 0 \quad . \quad . \quad . \quad . \quad . \quad . \quad . \quad . \quad . \quad . \quad (5.12a)$$

$$V_1 = 0 \quad . \quad . \quad . \quad . \quad . \quad . \quad . \quad . \quad . \quad . \quad (5.12b)$$

If it is further assumed that

$$y_1 = y_2 \quad . \quad . \quad . \quad . \quad . \quad . \quad . \quad . \quad . \quad . \quad (5.12c)$$

then all variables are known at section 1, and computation can start at section 2.

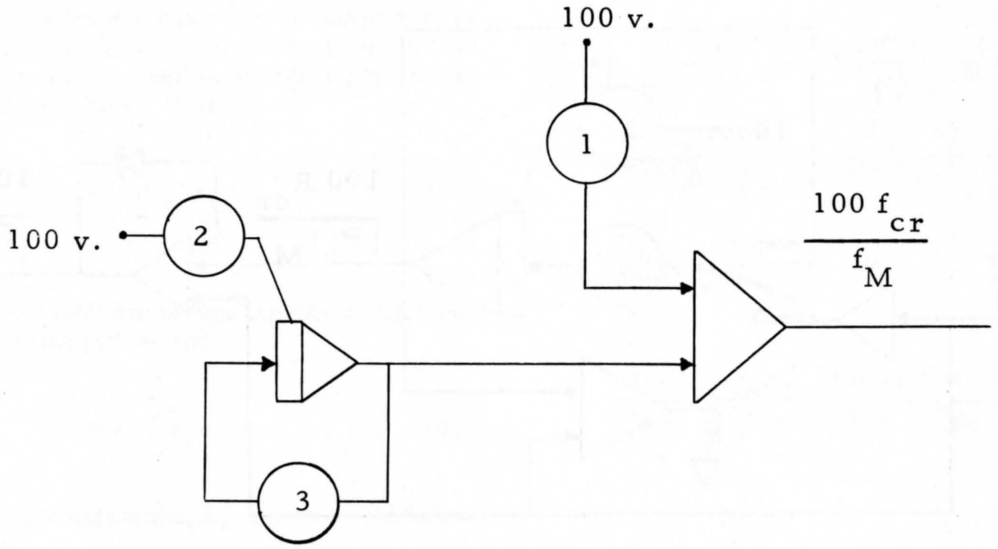

Pot No.	Setting
1	$\frac{f_m}{f_M}$
2	$\frac{f_o - f_m}{f_M}$
3	k_f

Figure 5.5. Computer program for the generation of the infiltration capacity rate function, f_{cr} .

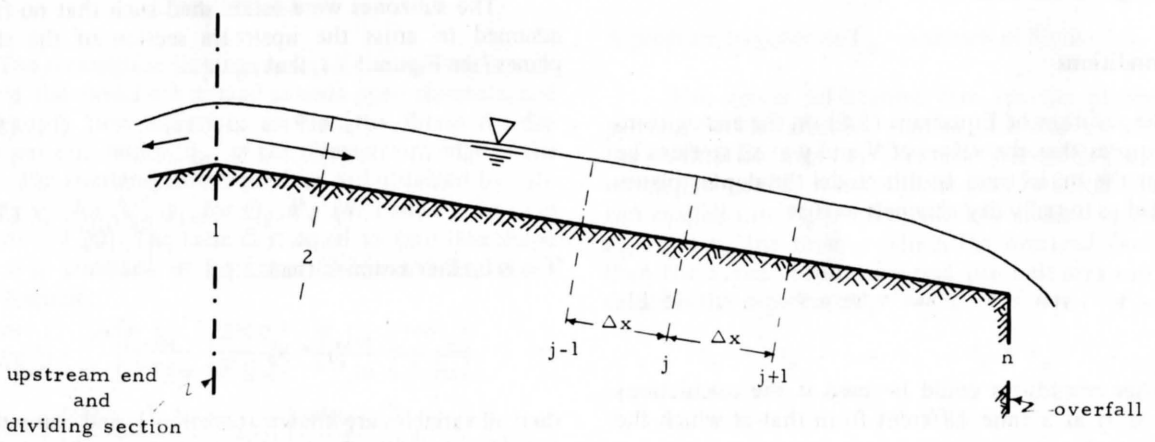

Figure 5.6. Flow profile for the equivalent plane showing boundary conditions for overland flow.

Downstream boundary conditions

The downstream edge of the sloping planes is treated as an overfall (see Figure 5.6). Thus, when the overland flow is critical or supercritical, the downstream end can be considered as a continuing plane, and there is no need to alter the equations of flow at that section. However, if subcritical flow prevails on the planes, the flow at the downstream section is critical, and the momentum equation is then replaced by:

$$V_n = \sqrt{gy_n} \quad \ldots\ldots\ldots (5.13)$$

When the implicit scheme is used the difference formula (4.15) can be used at the downstream section by assuming that

$$\phi_{n+1} = \phi_n \quad \ldots\ldots\ldots (5.14)$$

Channel Flow

The channel system is fed on both sides by the flow from the downstream end of the sloping planes, so that the term I in Equations (4.20) is replaced by $2q_n$.

Seepage rate in the channels

From his experiments on seepage, Darcy (1856) found that the rate of seepage through a column of soil increases with the depth of water over the soil surface. The infiltration capacity rate should, therefore, be expected to be higher with higher depth of water. In the case of overland flow, the depth was small so that its influence on the infiltration rate was assumed negligible. The infiltration capacity curve given by Equation (5.9) can be looked upon as the seepage capacity rate curve under conditions of insignificant depth. But with a significant depth, as is the case for channel flow, the seepage capacity rate F_{cr} can be assumed to be

$$F_{cr} = f_{cr} + cy \quad \ldots\ldots\ldots (5.15)$$

in which

- f_{cr} is given by Equation (5.9)
- y is the depth of channel flow
- c is a constant which depends on the soil permeability and the distance of the water table from the ground surface

Equation (5.15) is somewhat similar to Darcy's law (Amisial et al., 1968).

The seepage capacity rate per unit length of channel is given by:

$$q_{crg} = BF_{cr} \quad \ldots\ldots\ldots (5.16)$$

in which B represents the average width of channel.

If t_o represents the starting time of the storm, t_a the time at which the channel inflow $2q_n$ exceeds the seepage capacity rate q_{crg}, and t_s the time at which channel runoff ceases, then the actual seepage rate q_{rg} per unit length of channel can be obtained as

$$t_o < t < t_a \qquad q_{rg} = 2q_n \quad \ldots\ldots (5.17a)$$

$$t_a < t < t_s \qquad q_{rg} = q_{crg} \quad \ldots\ldots (5.17b)$$

Again attention should be called to the fact that seepage will continue at capacity rate until water is no longer available in the channel.

For channel flow the programming Equations (4.20) become:

$$\left(\frac{100\,A_j}{|A_j|_M}\right) = \int_o^\tau \left[\frac{2|q_n|_M}{h|A_j|_M}\left(\frac{100\,q_n}{|q_n|_M}\right) - \frac{|q_{rg}|_M}{h|A_j|_M}\left(\frac{100\,q_{rg}}{|q_{rg}|_M}\right)\right.$$

$$\left. - \frac{|Q_{j+1}|_M}{2h\Delta x|A_j|_M}\left(\frac{100\,Q_{j+1}}{|Q_{j+1}|_M}\right) + \frac{|Q_{j-1}|_M}{2h\Delta x|A_j|_M}\left(\frac{100\,Q_{j-1}}{|Q_{j-1}|_M}\right)\right] d\tau \quad (5.18a)$$

$$\left(\frac{100\,V_j}{|V_j|_M}\right) = \int_o^\tau \left[\frac{100\,gS_o}{h|V_j|_M} - \frac{g\,K|V_j|_M}{h}\left(\frac{100\,V_j^2}{|V_j^2|_M}\right) - \frac{g|A_{j+1}|_M}{2hB\Delta x|V_j|_M}\right.$$

$$\left(\frac{100\,A_{j+1}}{|A_{j+1}|_M}\right) + \frac{g\,G_M}{h|V_j|_M}\left(\frac{100G}{G_M}\right) + \frac{g|A_{j-1}|_M}{2hB\Delta x|V_j|_M}\left(\frac{100\,A_{j-1}}{|A_{j-1}|_M}\right)$$

$$\left. - \frac{|V_{j+1}^2|_M}{4h\Delta x|V_j|_M}\left(\frac{100\,V_{j+1}^2}{|V_{j+1}^2|_M}\right) + \frac{|V_{j-1}^2|_M}{4h\Delta x|V_j|_M}\left(\frac{100\,V_{j-1}^2}{|V_{j-1}^2|_M}\right)\right] d\tau \quad (5.18b)$$

$$\left(\frac{100\,Q_j}{|Q_j|_M}\right) = \frac{|A_j|_M|V_j|_M}{|Q_j|_M}\left(\frac{100\,A_j}{|A_j|_M}\right)\left(\frac{100\,V_j}{|V_j|_M}\right) \quad \ldots (5.18c)$$

Initial conditions

Values of the variables A and V at all sections must be known at the starting time of computation. In the case

of an initially dry channel those values will be equal to zero.

Upstream boundary conditions

Either one of two conditions can prevail at the upstream end of a channel depending upon whether or not the drainage basin under consideration receives the flow from a preceding basin.

1. If the watershed receives no flow from a preceding watershed then

$$Q_1 = V_1 = 0$$

If it is further assumed that $A_1 = A_2$ or else $y_1 = y_2$, then computation can start at section 2.

2. If, however, the upstream section of a channel coincides with the outlet of a preceding watershed, then the outflow and stage hydrographs will be known at that section. The difference formula (4.15) can be used at that section by assuming

$$\phi_{-1} = \phi_1$$

Downstream boundary conditions

In general a relationship between discharge and depth is available at the outlet of a watershed. If such an expression is not available, a relationship between the depth of the cross-sectional area, the velocity and the discharge can be developed on the basis of the geometry of the outlet section.

Conditions at the junctions

At a junction the flow in each branch is routed separately, and the resultant outflows are combined by addition to yield the flow at the junction.

CHAPTER VI

PROCEDURES OF MODEL REGULATION AND VERIFICATION

The analog program shown in Figure 4.3 provides the solution to the shallow water equations for the general case of unsteady flow. It is necessary that the program be adapted to the particular flow conditions found on a watershed. Also, some unknown parameters are included in the runoff model presented in Chapter V. The model must be fitted to a particular watershed by determining numerical values for those parameters applicable to the watershed. These fitted values are then checked by a verification procedure.

Adaptation of the Analog Solution to Flow Conditions of a Watershed

In order to adapt the solution program to a particular watershed, it is necessary to adjust the sign and the value of the dependent variables in terms of actual conditions and the physical layout of the space coordinate system. Surface runoff consists primarily of gravity flow. Consequently, by choosing the x-axis in the direction of the slope of the channel the flow will be in the direction of increasing x, and therefore always will be positive. Further, if the x-axis coincides with the center line of the channel bottom, the flow depth will be either zero or positive. Under these conditions neither the flow depth nor the flow velocity can be negative. This is implemented in the analog program by the introduction of two diode limiters which limit the values of the flow velocity and depth to positive values only.

Because of the losses to retention storage and infiltration, surface runoff does not start at the same time as precipitation. The model assumes the flow to be zero until the precipitation rate exceeds the retention and infiltration rates. This condition is easily met for the flow depth and area, since these quantities are primarily the result of the integration of the difference between the precipitation rate on one hand and the retention and infiltration rates on the other. However, with the presence of the constant slope term in the momentum equation, the velocity can assume values irrespective of the flow depth and the precipitation. This difficulty is overcome by the use of a set of comparators which prevent the computation of the flow velocity from starting until the flow depth reaches a specified value. In the absence of obstructions or structures, the velocity computation can be allowed to start as soon as the flow depth exceeds zero, unless field observations indicate that there should be a greater amount of water in detention storage before the occurrence of flow. If such is the case, the depth for incipient motion should be measured and then be specified in the model to induce the calculation of the flow velocity.

The provision of the comparators allows the program to be used for cases in which a reservoir or a pond is present in the channel system. In this case the reservoir is replaced by an equivalent reservoir or channel having the same length, storage capacity, outlet section, and average width and slope as the reservoir. The velocity computation at all sections upstream from the outlet can be allowed to start when the flow depth at those sections exceeds zero. At the outlet section the velocity is kept at zero. In other words, there will be no flow until the depth has built up to the level of the spillway inlet. At an overfall spillway the flow will be kept at zero until the reservoir is full, and conditions similar to those derived in Chapter V for the downstream boundary of the overland flow, will be used at the overfall. For conduit spillways such as chute and tunnel spillways, the flow computation will be allowed to start when the water surface reaches the level of the conduit inlet. The unsteady flow equations for channel flow can be used as long as free surface flow prevails in the conduit. However, once pressure flow is established, the flow depth will have to be replaced by the instantaneous piezometric head in the unsteady flow equations in order to compute the flow through the conduit. The piezometric head at the conduit entrance is the difference between the depth of water in the reservoir and the level of that entrance.

Model Regulation

The surface runoff model includes a number of parameters which can be divided into two types, namely, the function parameters and the condition parameters.

Function parameters

The function parameters are those watershed characteristics which are constant with respect to time, such as length, width, and slope of the planes and channels. Generally speaking, these quantities are subject to direct measurement by established methods. Function parameters vary with respect to space, but average values are usually established for each subzone of the watershed. The equivalent subzone concept discussed in Chapter V is a spatial integration technique for function parameters.

Plane characteristics

The function parameters pertaining to the plane are the width, length, and slope of the plane. The width of the plane is equal to the length of the segment of channel in a subzone. Upon measuring the surface area of the natural subzone, the length of the half-plane is obtained by dividing the subzone area by twice the length of the portion of channel in that subzone. This is illustrated in Figure 5.2. The plane slope is an average of the slopes of the land surfaces and the tributaries within a natural subzone. Aerial photographs or field surveys are required for the determination of the land slopes.

Channel characteristics

The channel dimensions and slope are also considered as function parameters. The length of the segment of channel in each equivalent subzone is the meandering length of the corresponding portion of the natural channel. This length, which is equal to the plane width, can be measured directly from a topographic map. The cross-sectional dimensions of the channel must also be measured. When the assumption is made of a rectangular channel, the width and depth for each channel reach Δx are sufficient to define the cross-section. From aerial photographs, the width and depth can be obtained respectively as the averages of the widths and of the depths in the corresponding natural channel reach. If another channel shape is assumed, a special field survey may be required for the measurement of the channel cross-sectional dimensions. For the sake of simplicity, it is desirable that each section Δx of the natural channel be replaced by an equivalent prismatic channel. The slope of a channel reach is the weighted average of the slopes within the corresponding natural channel reach. It is obtained from a topographic map or from aerial photographs of the watershed.

Condition parameters

The condition parameters are those parameters which vary with time within a given watershed and usually cannot be obtained by direct measurement. They are generally dependent upon surface and moisture conditions of the watershed. Even though these quantities are not readily available or measurable for inclusion in a model, numerical values are required and must be estimated for each subzone of the watershed. Condition parameters include the retention and infiltration rates, and the roughness coefficients.

Retention rate

The retention rate accounts for losses due to interception and depression storage. Its dependency on factors such as vegetative cover, soil surface condition, and watershed moisture status, explains the impossibility of obtaining it by direct measurement. This situation makes it compulsory to resort to some indirect method, such as model fitting, for the determination of the constants involved in the retention rate equations. The retention rate for a watershed is determined when the constants R_{cs} and k_r of Equation (5.4), the rainfall rate, and the watershed moisture condition are known.

Infiltration rates

The model distinguishes an infiltration value for the plane and another for the channel within a subzone. This distinction is substantiated by the fact that the channel bed material is often more permeable than that of the land surfaces. The model also provides for different values of the infiltration capacity rate for each subzone of a watershed.

The determination of the rate of infiltration is rendered difficult by the fact that this rate is a function of the rate of effective rainfall, the infiltration capacity rate, the depth of water above the ground surface, and the soil moisture conditions. Direct measurements of infiltration are made in situ using artificial sprinkling devices or small surface runoff plots. Such measurements, however, approach point measures of infiltration which may vary considerably from the average, and are frequently not representative of the whole watershed. Furthermore, in situ and plot measurements are not often available. Therefore, in most cases, it is necessary to use an indirect method for determining the constants of the infiltration capacity rate equation. According to Equations (5.9) and (5.15), the constants to be determined are the maximum infiltration capacity rate f_o, the minimum infiltration capacity rate f_m, the time constant k_f, and the constant c applied in the computation of channel seepage loss.

Roughness coefficients

Within the analog computer program a different roughness coefficient may be used for each plane and channel section, depending upon the conditions of the soil surface such as irregularities and vegetative cover and the meanderings and irregularities of the channels. Usually,

the channel bed has less vegetation cover than the surrounding land surfaces, and higher roughness coefficient values therefore generally can be expected in the case of overland flow. Values of the roughness coefficients for the planes and the channels can be obtained by the indirect method of model fitting.

Procedure

The mathematical model of the surface runoff process is not complete for a particular watershed unless the condition parameters are known for that watershed. The model must be fitted or regulated. That is, the condition parameters must be adapted to each watershed. Model regulation, therefore, implies the determination of a set of values for the constants involved in the condition parameters such that they fit the watershed under study.

The model is regulated by the method of data adjustment. This method involves the fitting of the condition parameters to a set of data under a particular set of criteria. A runoff event for which good data are available is used to develop estimates of the condition parameters that fit the general model to the given watershed. It is necessary that precipitation and runoff data be reliable, or that their accuracy be known. Antecedent precipitation and runoff can be used as an index to the watershed moisture status. Data concerning the topography of the watershed are needed in order to obtain the function parameters.

The next procedural step is to assume numerical values for the adjustable constants of the condition parameters. With those assumed values, the rainfall can be routed over the land and through the channel system to produce the outflow hydrograph at the outlet of the watershed. A good agreement will seldom be obtained on the first trial between the computed and the measured runoff hydrographs; therefore, the values of the condition parameters are adjusted in subsequent trials until a good fit is achieved. The set of values of the condition parameters for the watershed is adopted for which a good fit is obtained under the selected set of criteria.

Methods and criteria for goodness of fit

Obviously the computations cannot start unless some beginning numerical values are assigned to the condition parameters. The initial selection of those values is based upon available data about those parameters and the processes they represent, the antecedent moisture condition of the watershed, and, if available, upon previous studies and measurements made on the watershed.

The adjustment or fitting of the condition parameter values is performed through a trial and error procedure. The values assumed in the first approximation are changed or adjusted and the computations are carried with the modified set of condition parameter values. The procedure is repeated until a close fit is obtained between the computed and measured hydrographs. At the end of each trial it is necessary to decide which condition parameters will be modified and the degree of change for the subsequent trial. This decision is governed primarily by the closeness of fit in the previous trial, the operator's knowledge of the runoff process, and also the experience he has gained with the mathematical model and its response to changes in the condition parameters. Familiarity with the model and its response to parameter changes can be acquired by making a sensitivity analysis prior to the regulation phase of the study.

Taking for granted that the fit between the computed and the measured hydrographs should be close, some measure of closeness should be used in order to decide whether or not a particular agreement is satisfactory. In other words, the data fitting technique requires the selection of a set of criteria for goodness of fit. These criteria depend on the accuracy of the data, the objectives of the study, and the order of priority given to the hydrograph characteristics. In this study, efforts were made to match the principal characteristics of the computed and measured hydrographs in the following order of priority:

1. hydrograph peak
2. time to peak
3. volume of flow

The criteria for goodness of fit are expressed as tolerance limits or errors which are permitted on the principal characteristics of the watershed outflow hydrograph.

Model Verification

The numerical values of all the model parameters are known for a given watershed once the model has been regulated for that watershed. In the verification phase of a study the accuracy of the fitted parameters and of the model is checked. This is done by selecting other rainfall events associated with good data. The regulated model is then used to predict the watershed outflow hydrograph, and the criteria for goodness of fit are applied to assess the closeness of fit between the predicted and the measured outflow hydrographs.

CHAPTER VII

THE EXPERIMENTAL WATERSHED

A subbasin of the Walnut Gulch experimental watershed was selected to test and verify the surface runoff model developed in the preceding chapter. Walnut Gulch is a 58-square-mile watershed located at Tombstone in southeastern Arizona (see Figure 7.1). It is an ephemeral tributary of the San Pedro River which receives the outflow from Walnut Gulch at Fairbanks, Arizona. Intensive study of this basin has been undertaken by the agricultural Research Service of the U.S. Department of Agriculture which has established an intensive network of hydrologic instrumentation on the watershed.

Geology

A layer of coarse-grained Late Pleistocene sediments, varying in depth from 0 to 100 feet, constitutes the top strata of the valley fill of the region within which Walnut Gulch lies. This layer is underlain by a deposit of calcium carbonate and a layer of fine-grained early to middle Pleistocene sediments. The sediments originate mainly from granitic rocks. The regional groundwater table is situated at a depth of approximately 400 feet beneath the land surface.

Topography

Elevations vary from 4,200 feet above mean sea level at the western end of the watershed to over 6,000 feet at the eastern portions of the basin. Consequently, gradients are steep and stream channel slopes average approximately 1 percent.

Soils and Vegetation

The soils of Walnut Gulch can be grouped into six major associations (Figure 7.2) and strongly reflect the influence of parent rocks and the temperatures prevailing during wet seasons. Most of the soils are either gravelly or stony and medium-textured to bedrock. The climax vegetation of the area is Desert Plains Grassland. Today, much of the country originally described as grass-covered is predominantly brush (Figure 7.3). Black grama and curly mesquite grasses prevail in most of the eastern portion of the area with the brush areas dominated by whitethorn, creosotebush, tarbush and sand paper bush.

Instrumentation

A network of 91 recording gages is used to measure precipitation on the watershed. Runoff is measured at the outlet of the watershed and also at the outlets of 11 subwatersheds within the Walnut Gulch drainage basin.

Precipitation

Annual precipitation on Walnut Gulch averages about 14 inches. Thirty percent of the annual precipitation occurs as low-intensity rain or snow during winter, and generates no runoff over the watershed. The remaining 70 percent consists of convective, runoff-producing storms, and occurs as short-duration, high-intensity rain during the July to September period.

Subwatershed 11

The subunit of the Walnut Gulch experimental watershed which was selected for simulation is subwatershed 11 (see Figure 7.4). This subbasin, with a drainage area of 2,035 acres, is situated in the northeastern portion of Walnut Gulch. The soil is the Hathaway-Bernardino-Sonoita association with small areas of Camoro soil in the alluvial swales. The vegetation is composed of black grama and curly mesquite grasses with limited amounts of brush primarily along the channels (Figure 7.2 and 7.3).

Drainage conditions

The channel system of subwatershed 11 comprises three main branches as shown in Figure 7.5. The middle channel traverses the entire length of the subwatershed and is 4.40 miles long with an average slope of 1.98 percent. The north channel with a length of about 2 miles and an average slope of 1.98 percent, enters the middle channel some 3,000 feet upstream from measuring flume 11. The south channel is 3.6 miles long and has an average slope of 2.03 percent; its junction with the middle channel is located one thousand feet upstream from flume 11. The channel bed material, made of unconsolidated sand and gravel, comprises particles exhibiting a logarithmic normal distribution with a geometric mean particles size of 2.3 mm. Fifty-four percent of the total material lies in

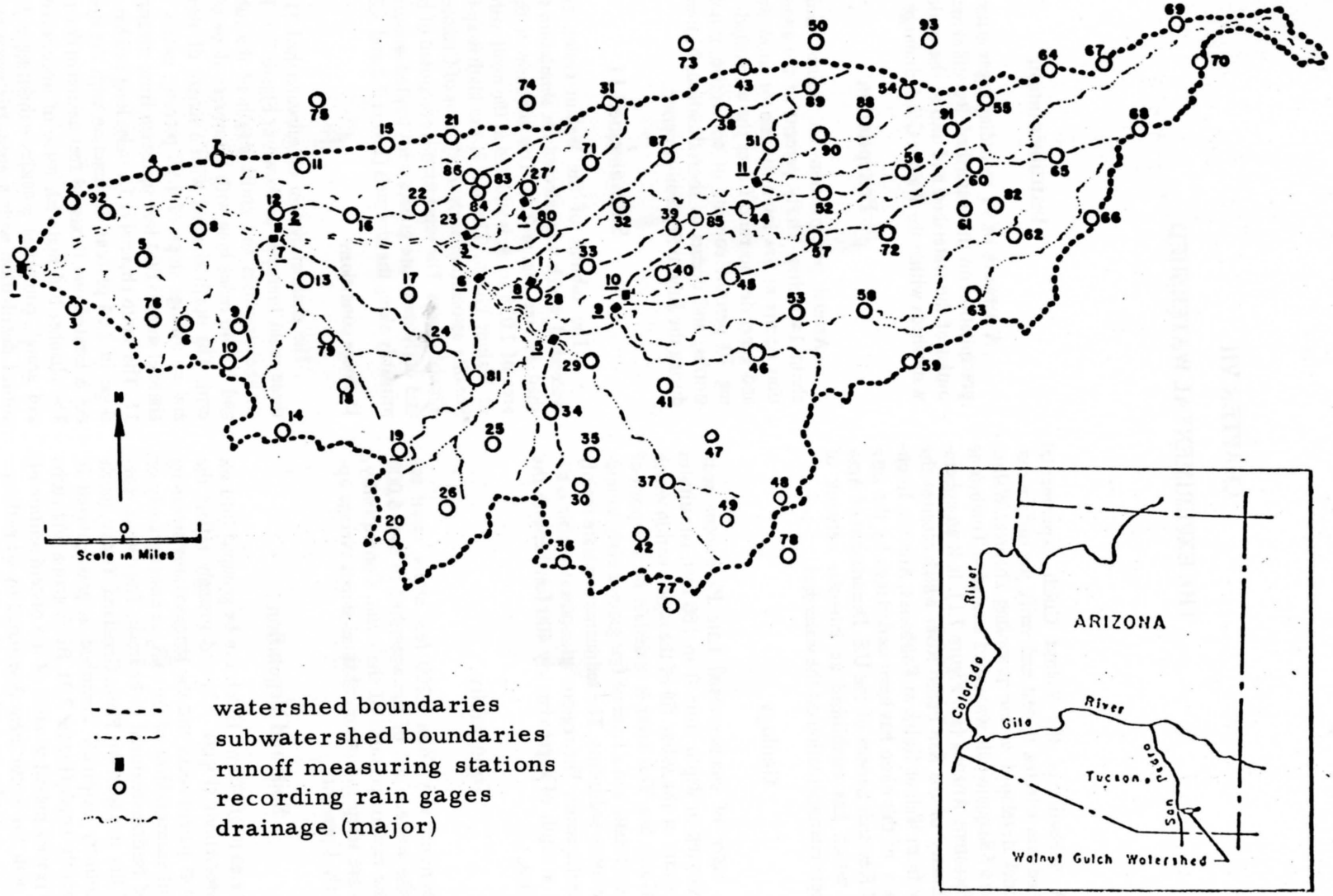

Figure 7.1. Walnut Gulch experimental watershed.

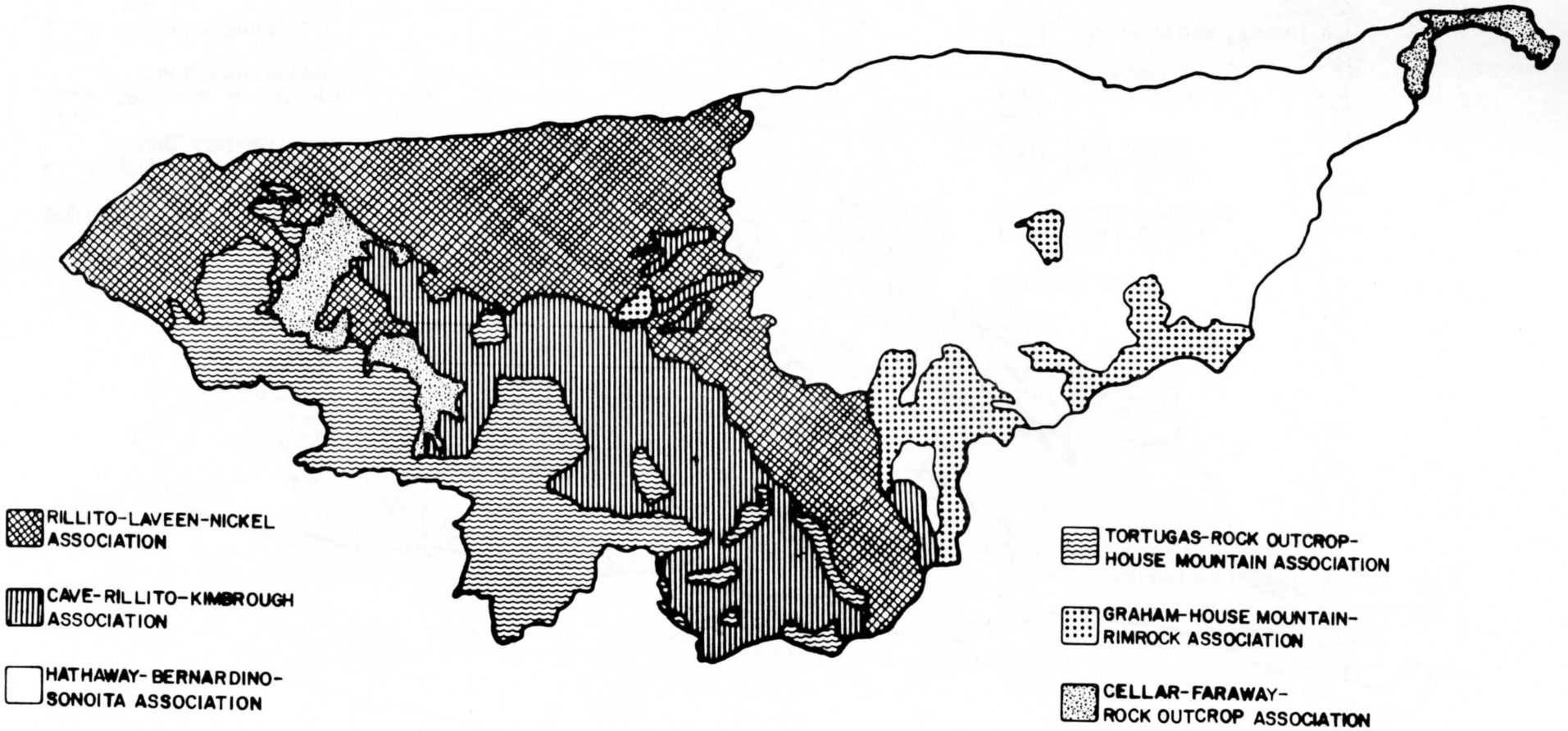

Figure 7.2. Soils map of the Walnut Gulch experimental watershed.

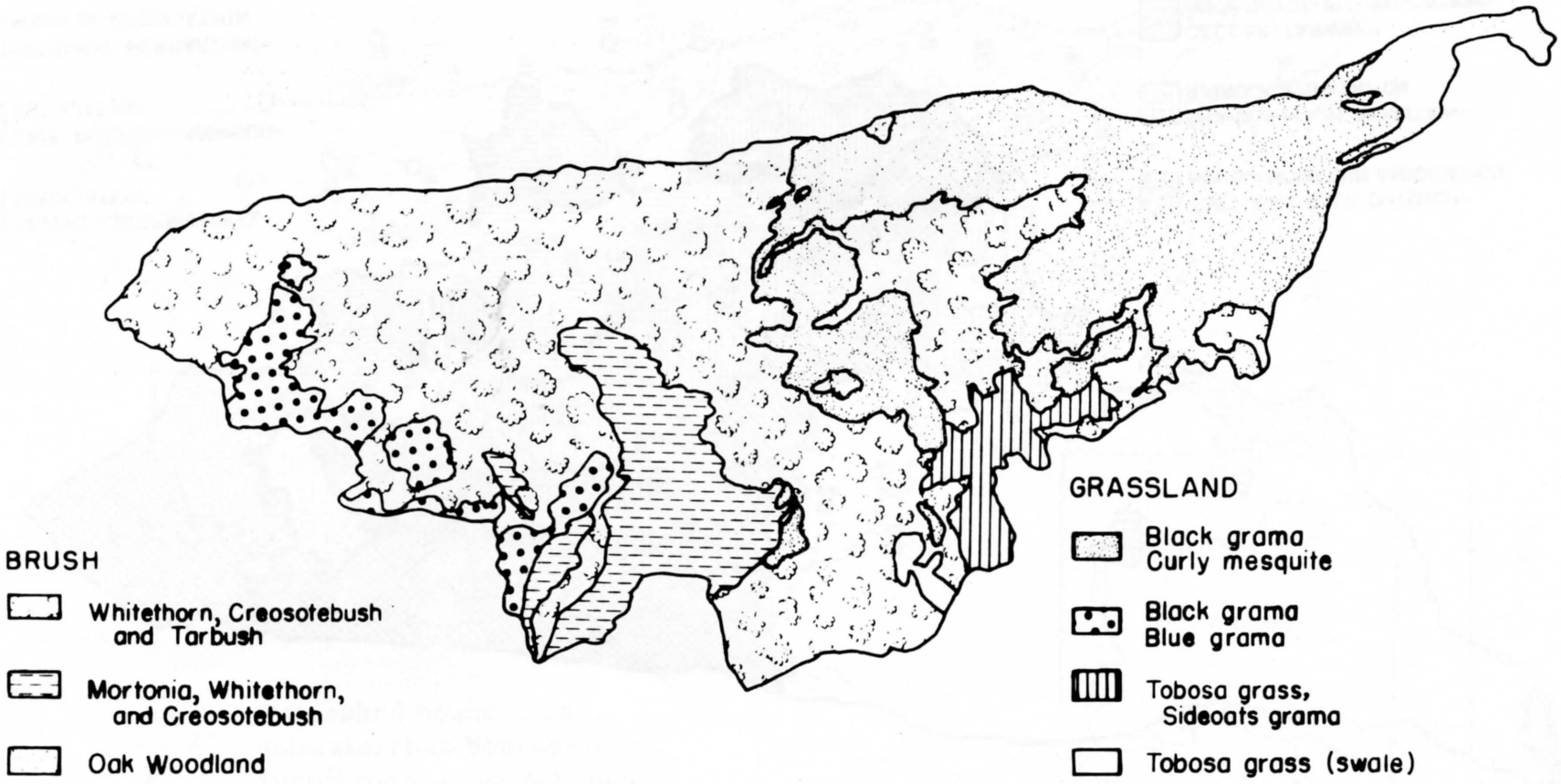

Figure 7.3. Vegetation map of the Walnut Gulch experimental watershed.

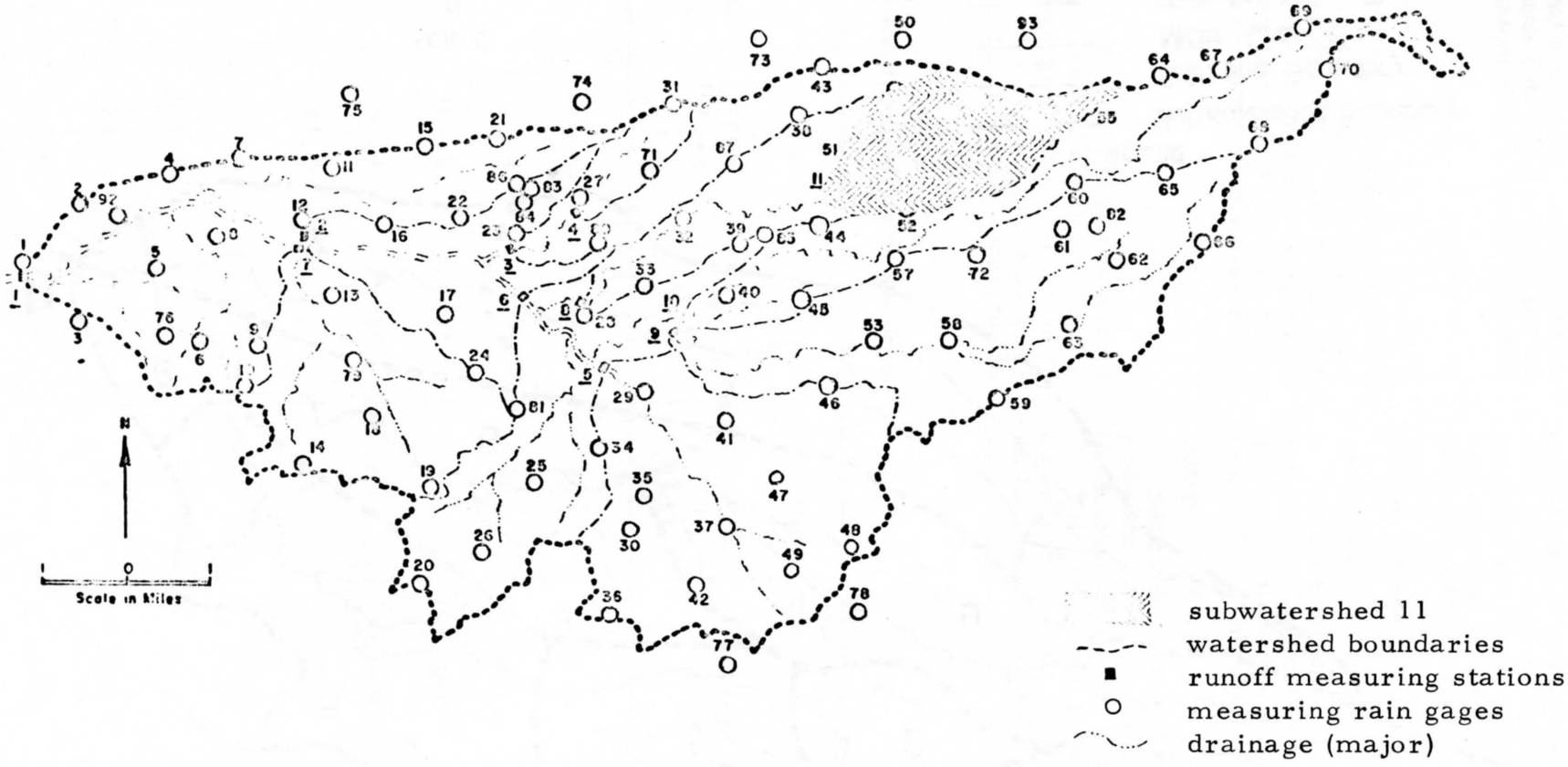

Figure 7.4. Map of the Walnut Gulch experimental watershed showing the location of subwatershed 11.

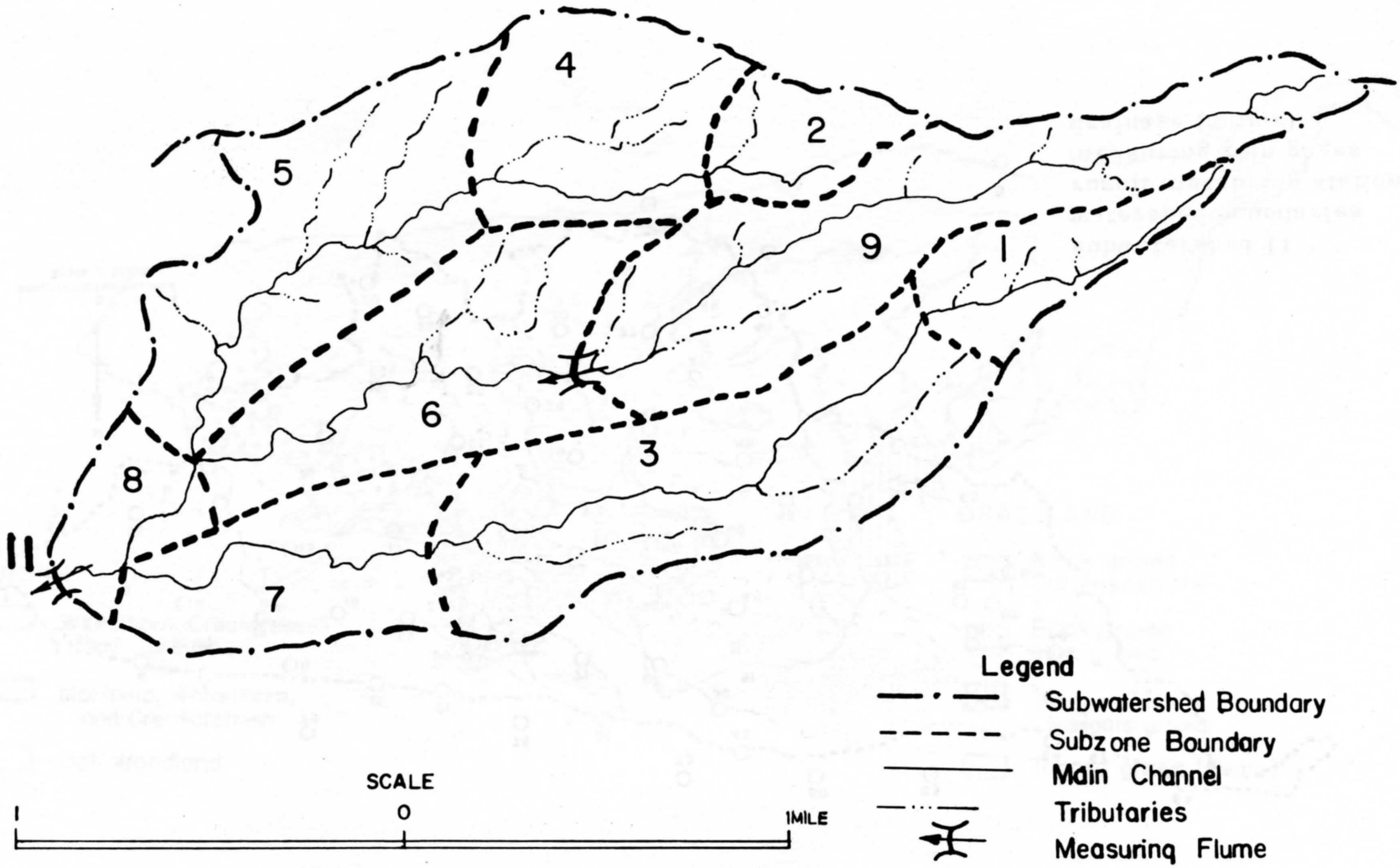

Figure 7.5. Subwatershed 11 of Walnut Gulch Experimental Watershed, as divided in 9 subzones.

the gravel range, that is, larger than 2 mm. The channels are dry about 99 percent of the time and have a potential to absorb large quantities of runoff (Renard et al. 1966).

Natural subzones

Subwatershed 11 has been divided into 9 subzones according to the watershed treatment procedure outlined in Chapter VI (see Figure 7.5). The physical characteristics of each subzone, measured from topographic maps and areal photographs of the Walnut Gulch, are listed in Table 7.1. The average depth of the channels is 6 feet.

Equivalent subzones

The equivalent subzone has the same drainage area as the natural subzone. Table 7.2 shows the physical characteristics of the rectangular sloping planes and of the portion of channel within each equivalent subzone. It is further assumed that the channel of the equivalent subzone is rectangular in cross-section and has a width equal to the average width of the natural channel. Under this assumption, the term G defined by Equation (2.26) is equal to zero, and the flow cross-sectional area is equal to the product of the channel width and the flow depth.

Boundary conditions

Overland flow

The upstream boundary conditions for the plane are those given by Equations (5.12). The condition of a continuing plane, as described in Chapter VI, is assumed to prevail at the downstream end of the plane.

Channel flow

Subwatershed 11 receives no water from the neighboring subbasins, and the conditions at the upstream end of each channel are expressed by Equations (5.19).

Flume 11 is located at the downstream end of the channel network. Figure 7.6 shows the cross-section of the flume measuring section. The conditions at the section are:

Table 7.1. Physical characteristics of the natural subzones.

Subzone No.	Area (acres)	Channel Dimensions			Average Land Slope
		Length (feet)	Average Width (feet)	Average Slope	
1	136.9	5,280	20	.025	0.040
2	75.4	2,640	25	.021	0.050
3	397.8	7,420	30	.022	0.038
4	189.7	1,980	20	.024	0.050
5	241.3	5,620	25	.018	0.051
6	252.7	7,260	20	.016	0.042
7	268.4	6,270	25	.015	0.045
8	73.9	3,000	20	.015	0.050
9	399.0	13,000	30	.023	0.048

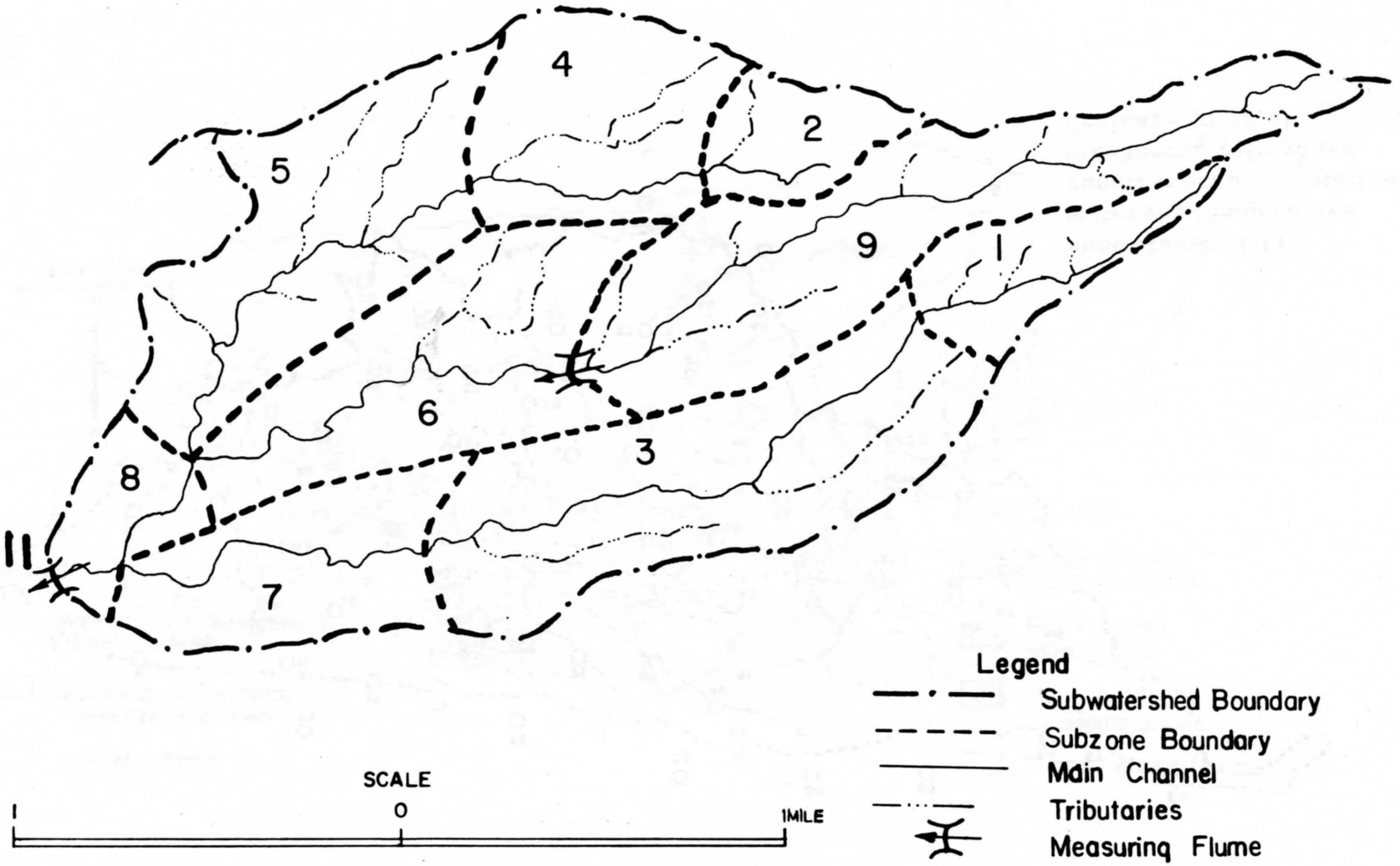

Figure 7.5. Subwatershed 11 of Walnut Gulch Experimental Watershed, as divided in 9 subzones.

the gravel range, that is, larger than 2 mm. The channels are dry about 99 percent of the time and have a potential to absorb large quantities of runoff (Renard et al. 1966).

Natural subzones

Subwatershed 11 has been divided into 9 subzones according to the watershed treatment procedure outlined in Chapter VI (see Figure 7.5). The physical characteristics of each subzone, measured from topographic maps and areal photographs of the Walnut Gulch, are listed in Table 7.1. The average depth of the channels is 6 feet.

Equivalent subzones

The equivalent subzone has the same drainage area as the natural subzone. Table 7.2 shows the physical characteristics of the rectangular sloping planes and of the portion of channel within each equivalent subzone. It is further assumed that the channel of the equivalent subzone is rectangular in cross-section and has a width equal to the average width of the natural channel. Under this assumption, the term G defined by Equation (2.26) is equal to zero, and the flow cross-sectional area is equal to the product of the channel width and the flow depth.

Boundary conditions

Overland flow

The upstream boundary conditions for the plane are those given by Equations (5.12). The condition of a continuing plane, as described in Chapter VI, is assumed to prevail at the downstream end of the plane.

Channel flow

Subwatershed 11 receives no water from the neighboring subbasins, and the conditions at the upstream end of each channel are expressed by Equations (5.19).

Flume 11 is located at the downstream end of the channel network. Figure 7.6 shows the cross-section of the flume measuring section. The conditions at the section are:

Table 7.1. Physical characteristics of the natural subzones.

Subzone No.	Area (acres)	Channel Dimensions			Average Land Slope
		Length (feet)	Average Width (feet)	Average Slope	
1	136.9	5,280	20	.025	0.040
2	75.4	2,640	25	.021	0.050
3	397.8	7,420	30	.022	0.038
4	189.7	1,980	20	.024	0.050
5	241.3	5,620	25	.018	0.051
6	252.7	7,260	20	.016	0.042
7	268.4	6,270	25	.015	0.045
8	73.9	3,000	20	.015	0.050
9	399.0	13,000	30	.023	0.048

Table 7.2. Physical characteristics of the equivalent subzones.

Subzone No.	Area (acres)	Channel Dimensions			Plane Dimensions		
		Length (feet)	Width (feet)	Slope	Length (feet)	Width (feet)	Slope
1	136.9	5,280	20	.025	565	5,280	0.040
2	75.4	2,640	25	.021	588	2,640	0.050
3	397.8	7,420	30	.022	1,167	7,420	0.038
4	189.7	1,980	20	.024	2,082	1,980	0.050
5	241.3	5,620	25	.018	940	5,620	0.051
6	252.7	7,260	20	.016	755	7,260	0.042
7	268.4	6,270	25	.015	932	6,270	0.045
8	73.9	3,000	20	.015	546	3,000	0.050
9	399.0	13,000	30	.023	774	13,000	0.048

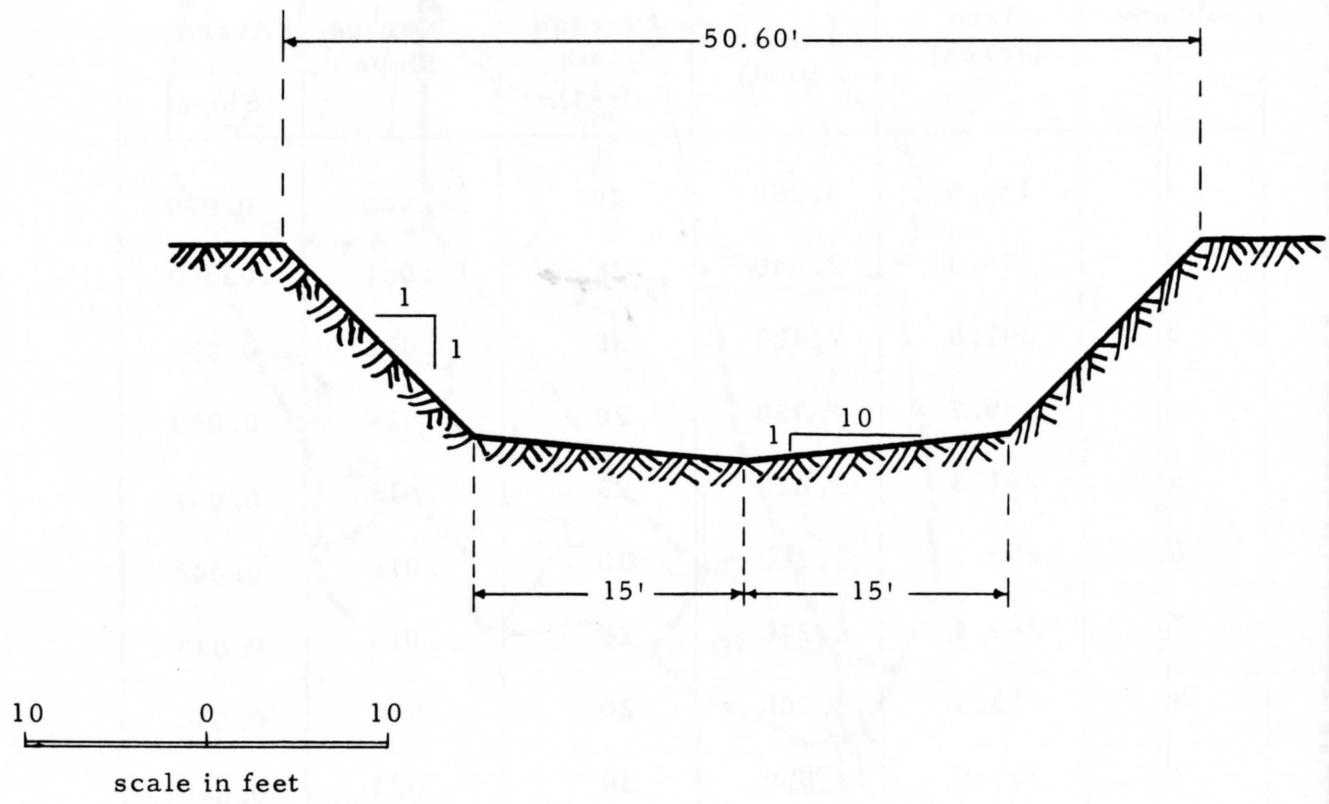

Figure 7.6. Measuring section of flume 11 located at the outlet of subwatershed 11.

$y \leq 1.5$ ft. , $A = 10y^2$ and $B = 20y$ . . . (7.1a)

$y > 1.5$ ft. , $A = y^2 + 27y - 20.25$

and $B = 2y + 27$ . . . (7.1b)

Flume 11 has a slope of 3 percent at the measuring section.

Runoff events

The runoff events selected for the purpose of this study were those of July 20 and July 29, 1966. A measured volume of 191.4 acre feet of precipitation fell on subwatershed 11 on July 20, 1966. The rainfall lasted one hour, with the major portion falling on the eastern part of the subwatershed. Table 7.3 gives the depth of rainfall for 5-minute intervals for each subzone. This rainfall event was the first runoff-producing storm of the year on subwatershed 11, and, consequently, infiltration and retention losses could be expected to be relatively high.

The rainfall of July 29, 1966, occurred on a watershed still wet from a rainfall event of the preceding day. On July 29 subwatershed 11 received 60.7 acre feet of rain in 40 minutes. The storm was concentrated mainly in the western subzones of the subwatershed. The rainfall for 5-minute intervals is given in Table 7.4 for each subzone.

Subzone 9 of subwatershed 11 contains 2 stock ponds, and did not contribute any flow on July 20 and July 29, according to records from the runoff-measuring station located at its outlet. Consequently, for these storms subzone 9 was treated as blind drainage, and excluded from hydrologic analysis in the simulation of the runoff.

Table 7.3. Precipitation data for event of July 20, 1966, on subwatershed 11 of the Walnut Gulch experimental watershed.

Subzone Number	Time from 1600 hours (minutes)[1]											
	5	10	15	20	25	30	35	40	45	50	55	60
1	0	.026	.123	.291	.306	.259	.199	.102	.034	.007	.007	.001
2	0	.012	.073	.225	.240	.264	.193	.105	.047	.009	.009	.003
3	0	.019	.081	.189	.225	.216	.152	.112	.047	.154	.109	.006
4	0	.013	.059	.193	.198	.232	.168	.103	.050	.010	.009	.005
5	.004	.013	.045	.136	.191	.215	.136	.085	.047	.018	.012	.004
6	.008	.022	.065	.174	.187	.204	.136	.098	.049	.023	.014	.005
7	.02	.012	.081	.170	.216	.189	.117	.078	.050	.018	.013	.005
8	.03	.006	.076	.166	.207	.200	.121	.072	.047	.017	.011	.003
9	.003	.019	.095	.250	.261	.240	.186	.104	.042	.011	.010	.003

[1] The tabulated values in the main body of the table are the precipitation depths computed by the isohyetal method during each five minute interval.

Table 7.4. Precipitation data for event of July 29, 1966, on subwatershed 11 of the Walnut Gulch experimental watershed.

Subzone Number	Time from 1820 hours (minutes)[1]							
	5	10	15	20	25	30	35	40
1	.037	.102	.097	.046	.026	.009	.001	.001
2	.015	.053	.095	.073	.038	.010	.001	.001
3	.023	.053	.074	.071	.061	.021	.007	.004
4	.019	.044	.091	.088	.050	.013	.003	.000
5	.016	.043	.119	.112	.075	.026	.011	.001
6	.017	.042	.096	.101	.074	.028	.01	.001
7	.034	.047	.104	.113	.090	.023	.01	.001
8	.035	.048	.131	.146	.108	.027	.013	.000
9	.024	.065	.090	.069	.039	.014	.003	.000

[1] The tabulated values in the main body of the table are the precipitation depths computed by the isohyetal method for each five minute interval.

CHAPTER VIII

RESULTS AND DISCUSSION

The mathematical model of surface runoff developed in the previous chapters was applied to subwatershed 11 of the Walnut Gulch experimental watershed. The model was fitted to the subbasin with the data from the runoff event of July 20, 1966, and then verified with the flow event of July 29, 1966. This chapter presents the results of that application.

Flow Hydrographs

Figures 8.1 and 8.2 show the computed and measured flow hydrographs at the outlet of subwatershed 11 for the events of July 20, and July 29, 1966, respectively. The selected criteria for goodness of fit are presented in Table 8.1 as the percent error which is permitted on each of the principal characteristics of the discharge hydrograph at the measuring flume 11. The measured and computed values of these characteristics are presented in Table 8.2 for the runoff event of July 20, and in Table 8.3 for that of July 29. Tables 8.2 and 8.3 also contain the percent errors or percent deviations of the computed values from the measured values. A comparison between these percent errors and the tolerance limits set for the errors in Table 8.1, indicates that, under the selected criteria, the fit is good for the two outflow hydrographs obtained from the mathematical model.

It will be observed from Figures 8.1 and 8.2 that the measured outflow hydrographs exhibit a "tail" which is not closely reproduced by the computed hydrographs. The exact origin of this "tail" is not yet known, although it is believed that part of it may have been caused by some traces of interflow or subsurface flow. In any case, the "tail" portions of the hydrographs are small and contribute less than 1 percent of the total volume of flow under the hydro- graphs.

As can be seen from Tables 8.2 and 8.3 or from Figures 8.1 and 8.2, the volume of runoff on July 20 was .279 acre-feet less than that of July 29, although the volume of rainfall on subwatershed 11 for July 20 exceeded that of July 29 by 130.7 acre-feet. Some light can be shed on that seemingly strange situation by the two following considerations. First of all, the runoff event of July 20, which was the first for 1966 on subwatershed 11, took place when the subbasin was dry, and, as a result, the retention and infiltration capacity rate functions (Equations (5.4) and (5.9) respectively) assumed the maximum values at the beginning of the storm. In contrast, on July 29 the subbasin was still wet from an event on July 28; the two runoff producing events were separated by only 7 hours. As a consequence of the wet initial condition on July 29, the infiltration capacity rate function assumed its minimum value throughout the event, and the actual retention rate was negligible since the retention storage was already essentially satisfied. In addition to the high loss rate values, the spatial distribution of the storm of July 20 permitted a large opportunity time for channel seepage. Because the rainfall was concentrated mainly on the upper part of the subwatershed, as depicted by Table 7.3, most of the outflowing water originated from the upper subzones. The routing process involved in the solution of the surface runoff reveals that the waters which contribute to the major part of the runoff, had to flow through almost the entire length of the main channels. This situation resulted in a long lag time, as evidenced by Figure 8.1, and a large amount of water was lost to channel infiltration and seepage. Only July 29, the storm was centered in the lower part of the basin, that is, in the subzones near the outlet. It was disclosed by the model that the flow from the upper subzones was negligible, and the lower subzones contributed the entire runoff. Therefore, in this instance the outflowing water had to travel a short distance, and only a small opportunity time for channel seepage existed. As a result, the time lag was relatively shorter, as illustrated in Figure 8.2, and the channel seepage losses were much less than those of July 20.

The model also yields the flow hydrographs at each section of the planes and of the channels. Flow hydrographs recorded at successive sections are presented in Figure 8.3 for the plane and in Figure 8.4 for the channel of subzone 2. Because every point on the plane of a particular subzone receives the same rainfall rate and shares the same loss functions, the flow starts at the same time at all the plane sections, but the time lag and time to peak increase with increasing distance from the upstream end. The picture can be different for the channel which re-

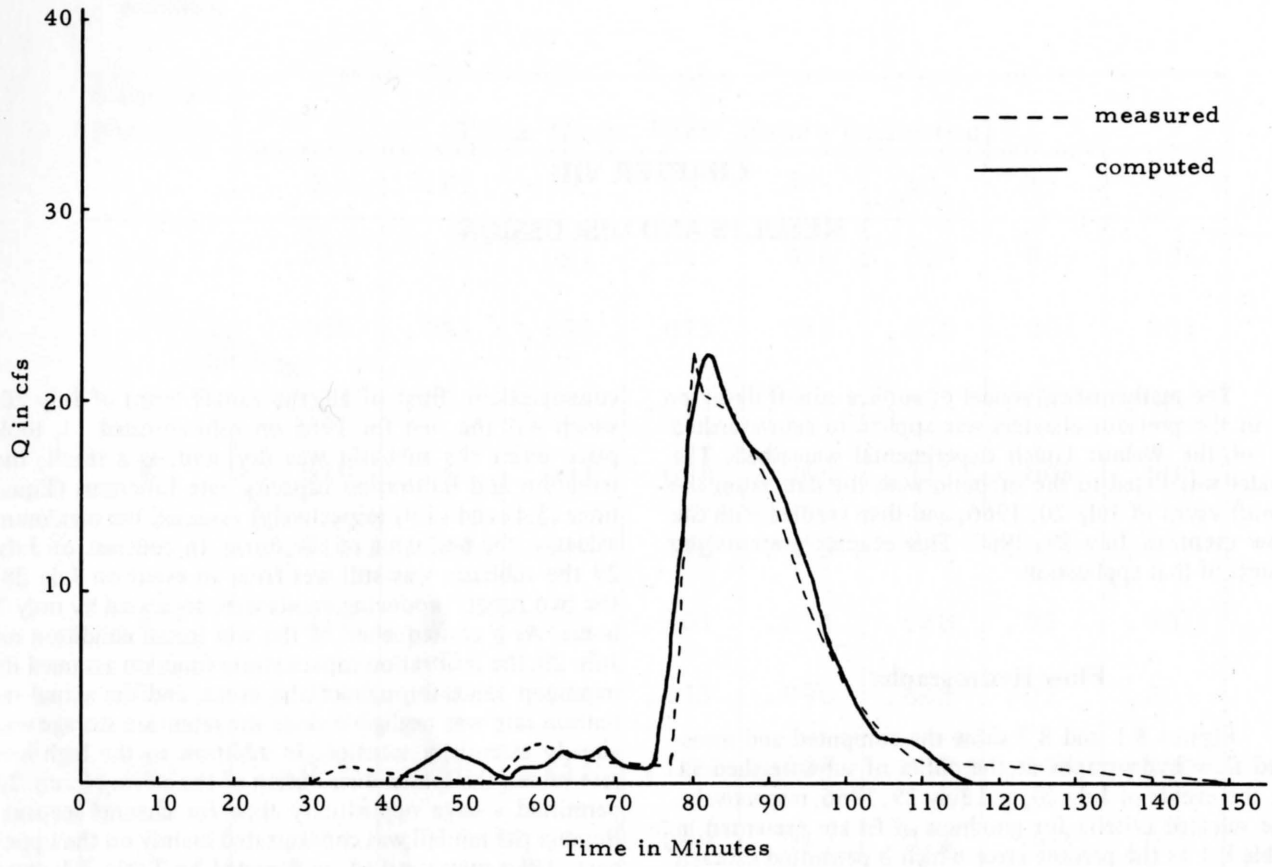

Figure 8.1. Outflow from subwatershed 11 for the event of July 20, 1966.

Table 8.1. Selected criteria for goodness of fit.

Principal outflow hydrograph characteristics	Maximum % error permitted
Peak flow rate	5%
Time to peak	5%
Total volume of flow	5%

Table 8.2. Principal outflow hydrograph characteristics and percent error for the event of July 20, 1966.

Hydrograph Characteristics	Measured	Computed	Discrepancy	% error
Peak flow rate (cfs)	22.20	22.24	.04	.17%
Time to peak (minutes)	80.00	81.66	1.66	2.1 %
Total volume of flow (acre-feet)	.573	.590	.019	3.05%

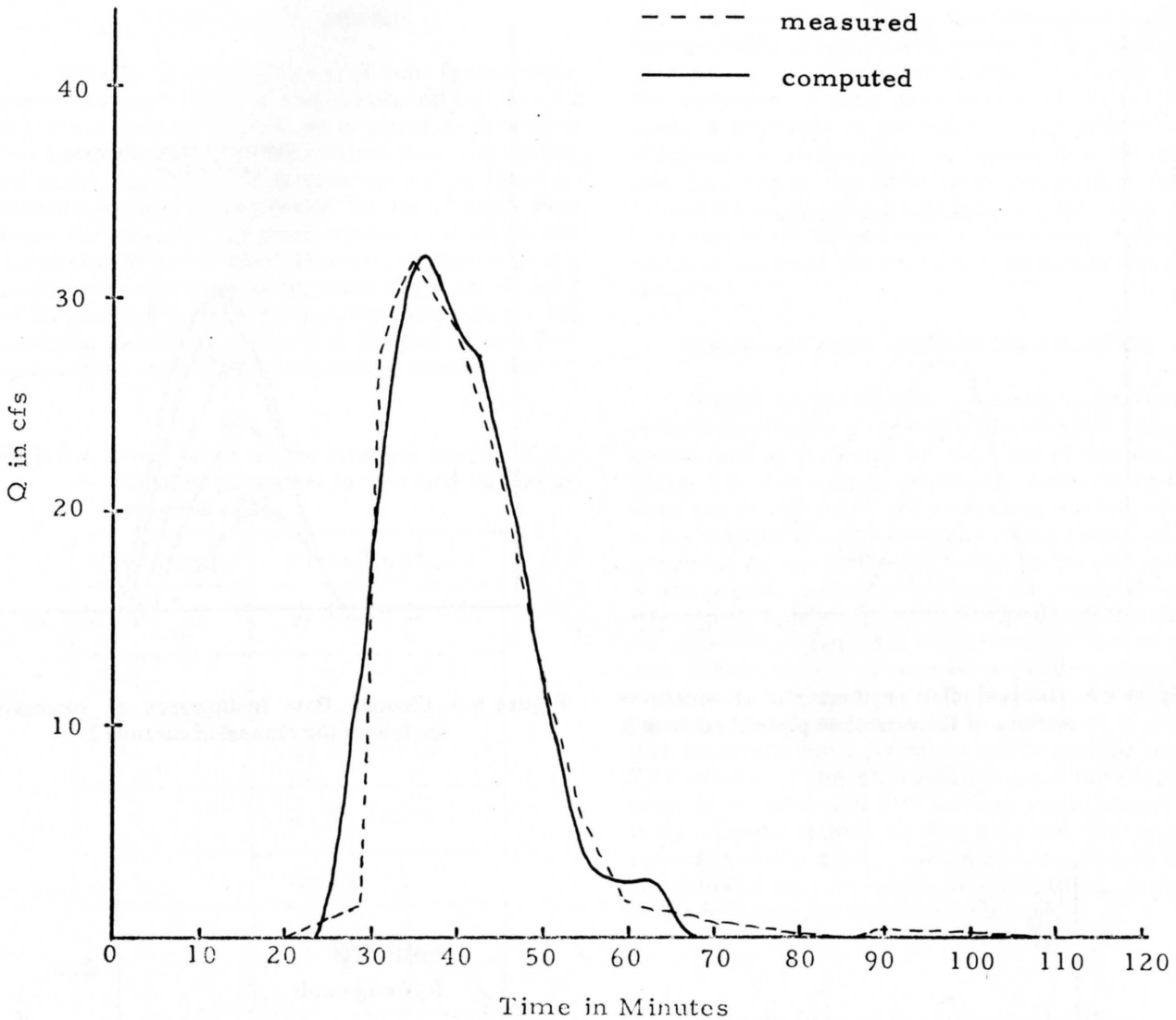

Figure 8.2. Outflow from subwatershed 11 for the event of July 29, 1966.

Table 8.3. Principal hydrograph characteristics and percent error for the event of July 29, 1966.

Hydrograph Characteristics	Measured	Computed	Discrepancy	% error
Peak flow rate (cfs)	32.05	32.40	.35	1.1%
Time to peak (minutes)	35.00	36.50	1.5	4.3%
Total volume of flow (acre-feet)	.852	.88	.028	3.5%

ceives at its upstream end section an additional input from the above subzones. However, since the channel of subzone 2 receives no water from adjacent subzones, the channel flow hydrographs shown in Figure 8.4 exhibit the same characteristics as those of the plane. The hydrographs of Figure 8.4 were obtained for channel seepage capacity rate values much less than those adopted for the subwatershed, and are presented here only for illustrative purposes. Actually there was not flow from subzone 2 as the water was lost to channel seepage.

Important flow characteristics which can be obtained from the model are the stage- and velocity-hydrographs at each channel and plane section. Typical stage- and velocity-hydrographs at a channel section are shown in Figure 8.5.

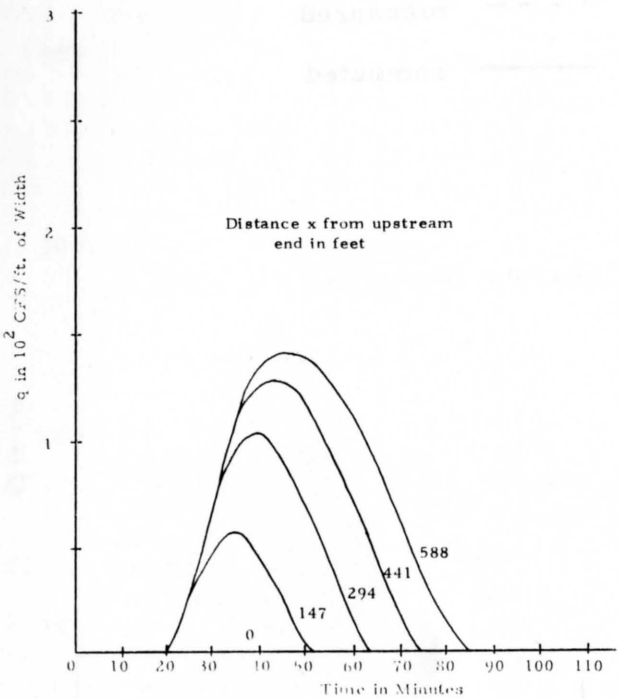

Figure 8.3. Overland flow hydrographs at successive sections of the equivalent plane of subzone 2.

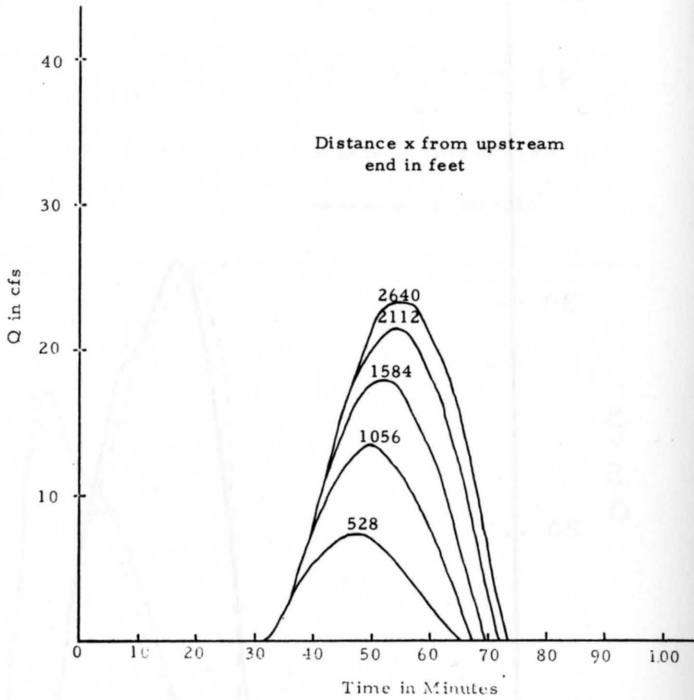

Figure 8.4. Channel flow hydrographs at successive sections of the channel of subzone 2.

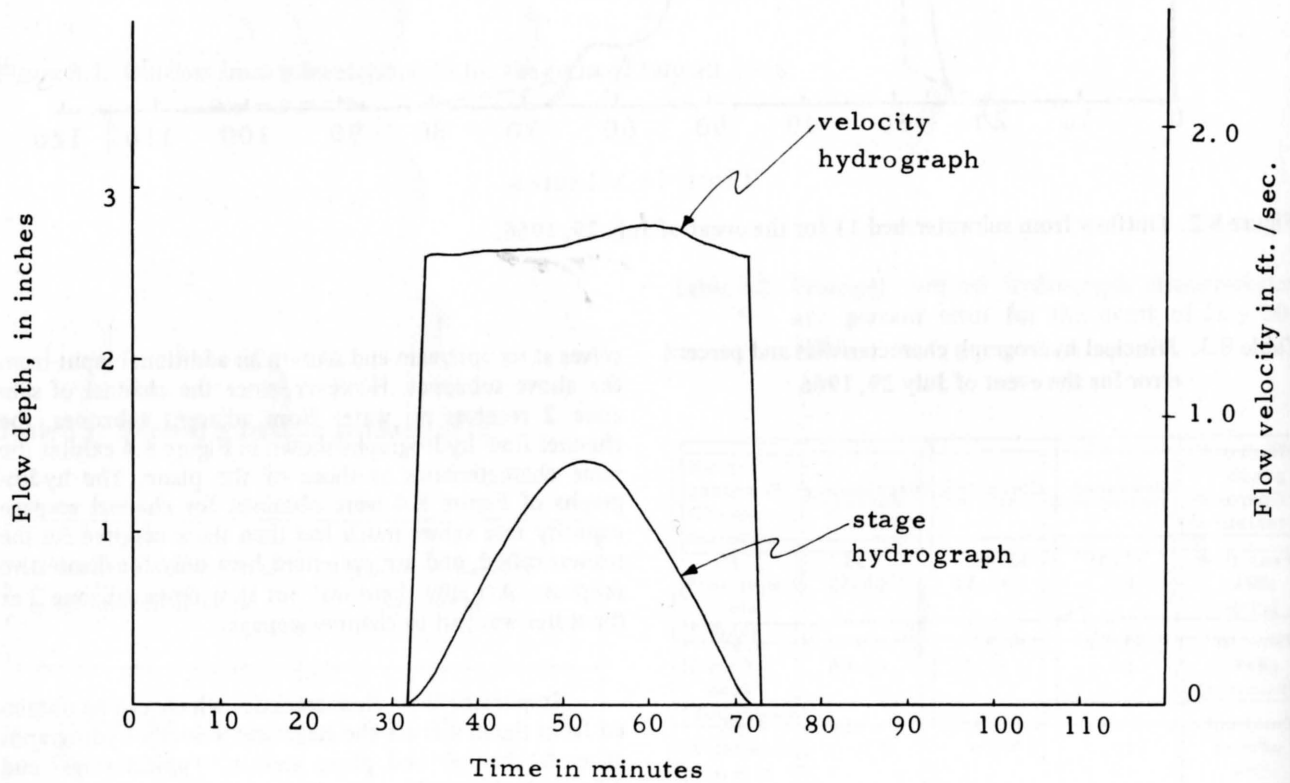

Figure 8.5. Stage and velocity hydrographs at a channel section of subzone 2.

Condition Parameters

Because of the uniformity of such factors as the vegetal cover, the soil type, and the channel bed material within subwatershed 11, one set of condition parameters was assumed to apply to the overland flow, and another set to the channel flow. The maximum and minimum infiltration capacity rates selected for the channels were larger than those of the planes because of the loose and coarse channel bed material. However, a higher roughness coefficient was assumed for the planes due to the presence of the grass and brush on the land. The fitted values of the condition parameters are listed in Tables 8.4 and 8.5 respectively for the planes and channels of subwatershed 11.

Table 8.4. Fitted values for the constants involved in the condition parameters for the land surfaces of subwatershed 11.

Constants	Fitted values
R_{cs}	0.15 in
k_r	1.0
f_m	0.18 in/hr
f_o	1.8 in/hr
k_f	0.60
K	0.093 $\frac{sec^2}{ft^2}$

Table 8.5. Fitted values for the constants involved in the condition parameters for the channels of subwatershed 11.

Constants	Fitted values
f_m	1.8 in/hr
f_o	4.2 in/hr
k_f	.04
c	.10 sec^{-1}
K	.03 $\frac{sec^2}{ft^2}$

They were obtained by fitting the mathematical model to the runoff data of July 20, and, therefore, they depend on the data used and the selected criteria for goodness of fit. The evaluation of these parameters would be more accurate if flow data at the outlet of each subzone, and additional information about the overland flow were available. Nevertheless, the fitted values presented in Tables 8.4 and 8.5 are considered reasonably accurate, since they were used in the model to predict the runoff of July 29 within errors which did not violate the criteria for goodness of fit.

Check on Conservation of Mass Principle

Besides the hydrographs, the analog model provides plots of the effective precipitation, the retention and infiltration rates as illustrated for the plane of subzone 2 in Figure 8.6. From those graphs, the actual amount of water lost to infiltration and to retention storage, as well as the volumes of water input and water output can be computed. By making a water budget for the subzones, it is thus possible to check how closely the principle of conservation of mass was satisfied. The results of this check are presented in Table 8.6 for the overland flow of subzone 2. Since there is no reservoir or pond on subzone 2, at the end of the flow event the total volume of water input, or rainfall, must be equal to the volume of runoff plus the volume lost to retention and infiltration. Of the 7.44 acre-feet of rain introduced as input in the computer program, an amount of 7.43 acre-feet was accounted for in the computer outputs, resulting in an error of only 0.18 percent. A similar check was carried for the overland flow of subzone 1 and the results are also reported in Table 8.6. In both cases the percent error is small.

Distribution of the Watershed Losses

From the histograms of rainfall input and the output hydrographs of overland the channel flows, the volumes of losses on the land surface on one hand and in the channel network on the other can be computed. Table 8.7 gives the respective amounts of water lost to infiltration and retention storage on the land surface and to seepage in the channel system of subwatershed 11 for the events on July 20 and July 29, 1966. Table 8.7 also shows that for those storms subzone 9 was treated as blind drainage for the reasons given in Chapter VII. It will be observed from Table 8.7 that the losses from the storm on July 20 were much larger than those on July 29 due to the different moisture conditions which prevailed on subwatershed 11 at the onset of each storm and to the different rainfall distribution as explained earlier in this chapter.

Solution Speed

The computer solution time was reduced by choosing a time scale factor h = 1/300, that is, one machine

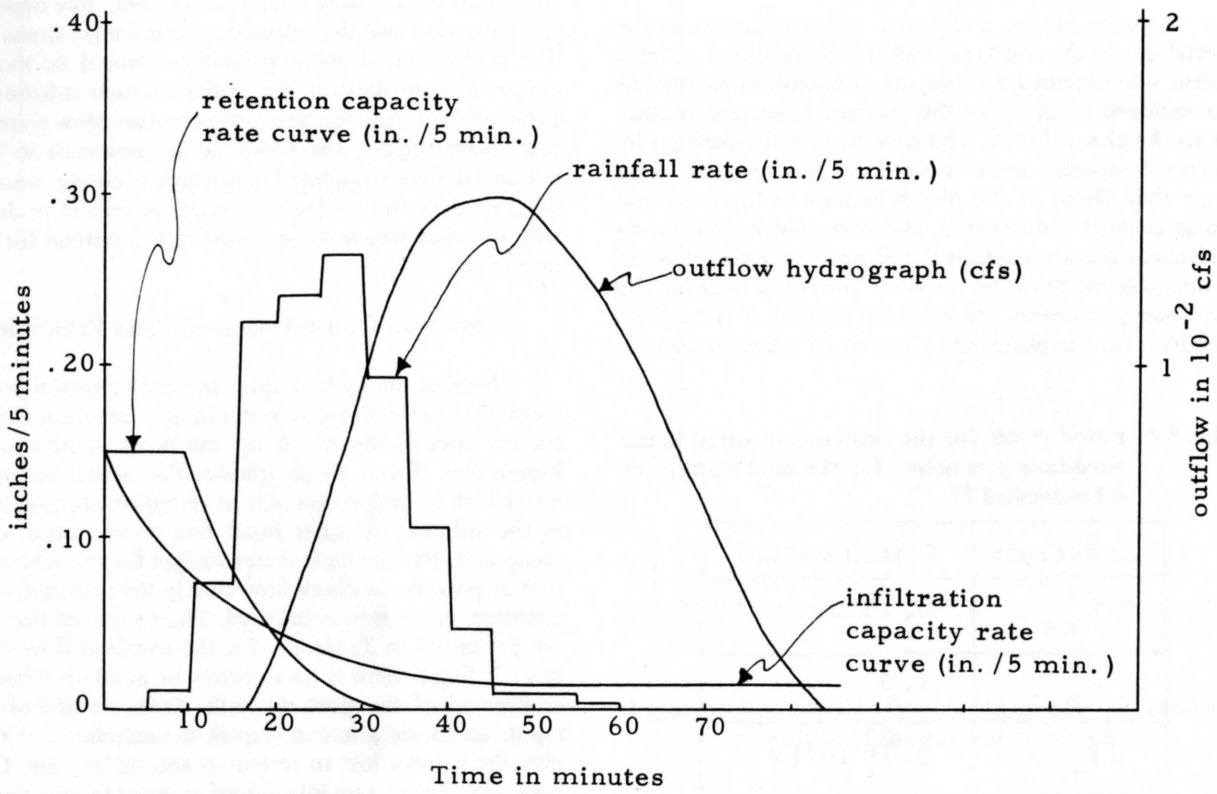

Figure 8.6. Input and output data for the plane of subzone 2 used in the check on the conservation of mass principle, July 20, 1966.

Table 8.6. Check on conservation of mass principle for subzones 1 and 2 for the event of July 20, 1966.

Subzone Number	Volume of rainfall input to program (acre-feet)	Volumes computed from program outputs				Error (acre-feet)	% error
		Retention (acre-feet)	Infiltration (acre-feet)	Outflow (acre-feet)	Total (acre-feet)		
1	13.00	1.92	5.99	5.20	13.11	0.11	0.85
2	7.44	1.04	2.19	4.20	7.43	0.01	0.13

Table 8.7. Distribution of watershed losses for the runoff events of July 20, and July 29, 1966, as computed from the model inputs and outputs.

Date of runoff event	Losses to infiltration and retention storage on land surface		Losses to channel seepage in channel system		Losses to blind drainage (all the rainfall on subzone 9)
	Total volume (acre-feet)	Volume per sq. mi. of land (acre-feet/mi^2)	Total volume (acre-feet)	Volume per mile of channel (acre-feet/mile)	Total volume (acre-feet)
July 20, 1966	114.18	42.80	36.14	4.84	40.47
July 29, 1966	37.06	13.90	9.86	1.32	12.9

second corresponded to 300 seconds of the physical system. Although the analog computer yielded the flow hydrographs at the downstream ends of the planes in only a few seconds, hardware limitations prevented the outlet of the watershed from being reached in a single programming operation. It was, therefore, necessary to record the simulated hydrographs at selected points, for example at the downstream end sections of the planes and at the outlets of the subzones. The computer was then programmed for the adjacent downstream parts of the model and the recorded hydrographs introduced as portions of the input quantities. The process of transforming the recorded hydrographs into an input form suitable to the analog computer is a tedious task which accounts for most of the delay experienced in solving the model. In addition, further delay was introduced because it was necessary to manually reset many of the potentiometers for each run.

The programming shortcomings discussed in the previous paragraph could be overcome by the use of a hybrid computer in which it is possible to set the potentiometers automatically, store the output hydrographs, and call for them when needed. With a sufficiently large storage capacity the hybrid computer would be capable of auomatic iterative processes and data fitting procedures according to a selected set of criteria for goodness of fit.

Models Based on Simplified Unsteady Flow Equations

An attempt was made to assess the validity of some simplifications usually made in the momentum equation. The simplifications considered here involved neglecting the convective acceleration $1/g\,\partial V^2/\partial x$ and the pressure term $\partial y/\partial x$.

In the case of the planes, flow depths and velocities were so small that the inertial term, $1/g\,\partial V^2/\partial x$, and the gradient of depth, $\partial y/\partial x$, were insignificant and had no effect on the overland flow hydrographs. The slopes of the channels of subwatershed 11 are very steep, as evidenced in Table 7.2. As a result, the slope and roughness terms were predominant to the extent that the convective acceleration was completely insignificant, and the gradient of depth had a negligible effect on the channel flow hydrograph. For the flow range involved in the two runoff events modeled here, the results did not change when the terms $\partial y/\partial x$ and $1/g\,\partial V^2/\partial x$ were dropped from the momentum equation.

Sensitivity Analysis

Subzone 2 of subwatershed 11 was selected for the study of the effect of condition parameter changes on the shape of the overland and channel flow hydrographs. The procedure used in this analysis consists in varying one parameter while keeping the others constant.

Overland flow hydrograph

The responses of the overland flow model for subzone 2 to changes in the plane condtions parameters are shown in Figures 8.7 to 8.12. Plots illustrating the variation of the flow hydrograph with changes in R_{cs} and k_r are given in Figures 8.7 and 8.8 respectively. For the

same retention storage capacity, and amount of water lost to retention storage increases with decreasing k_r values. The effect of the plane roughness coefficient K on the flow hydrograph is presented in Figure 8.9. Variation of K affects particularly the peak and the duration of flow, but does not change the time of rise. An increase in the K value results in a decrease in the flow volume because the flow velocity is reduced and infiltration opportunity time is thereby increased. Figure 8.10 and 8.11 indicate that, for k_f = 0.60, all the characteristics of the hydrograph are significantly affected by changes in f_m, while they experience little alteration when the value f_o is modified. However, this is not the case for low values of k_f, and whether or not variation of f_m affects the hydrograph more than variation of f_o, depends on the value of k_f. Figure 8.12 shows an increased amount of infiltration loss with decreasing values of k_f, and, therefore, suggests that the maximum infiltration capacity rate f_o plays an important role when the time constant k_f is small, while the minimum infiltration capacity rate f_m is predominant for large values of k_f.

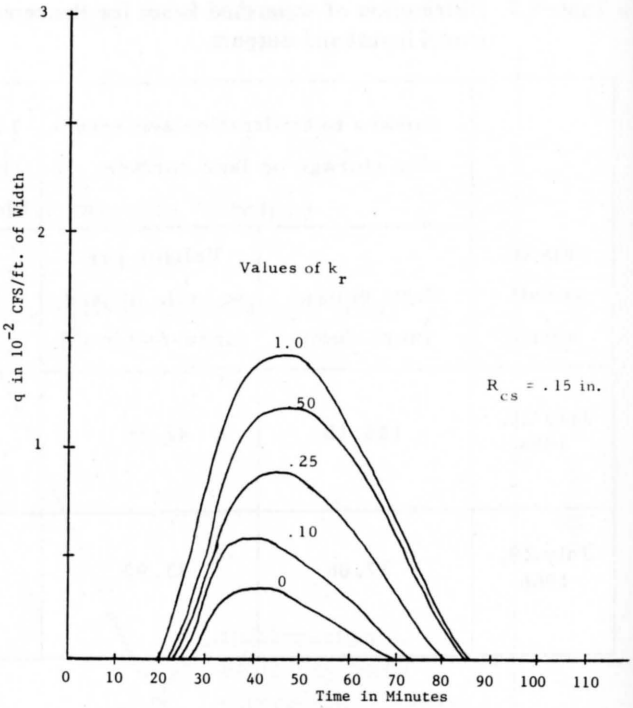

Figure 8.8. Overland flow hydrograph for subzone 2 as affected by changes in the time constant of the retention capacity rate function, k_r, July 20, 1966.

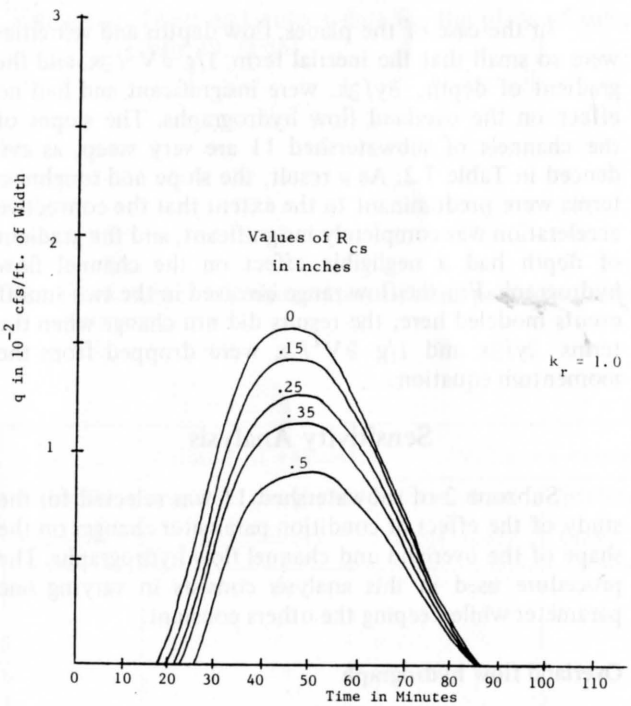

Figure 8.7. Overland flow hydrograph for the subzone 2 as affected by changes in the retention storage capacity, R_{cs}, July 20, 1966.

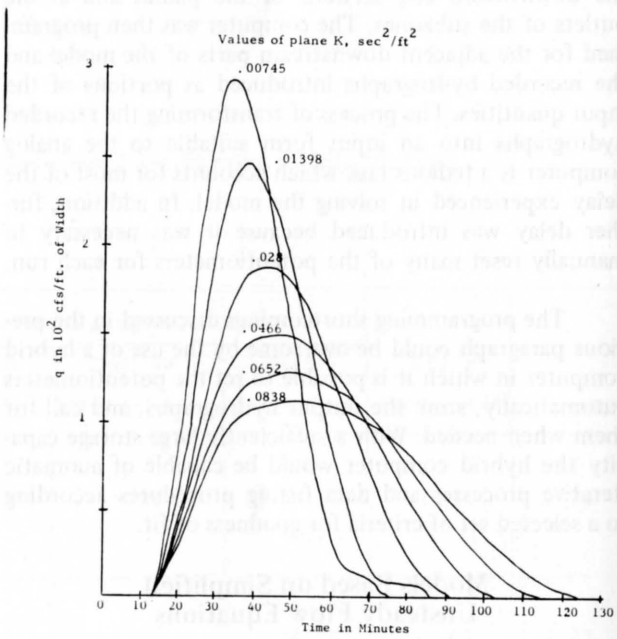

Figure 8.9. Overland flow hydrograph for subzone 2 as affected by changes in the plane roughness coefficient, K, July 20, 1966.

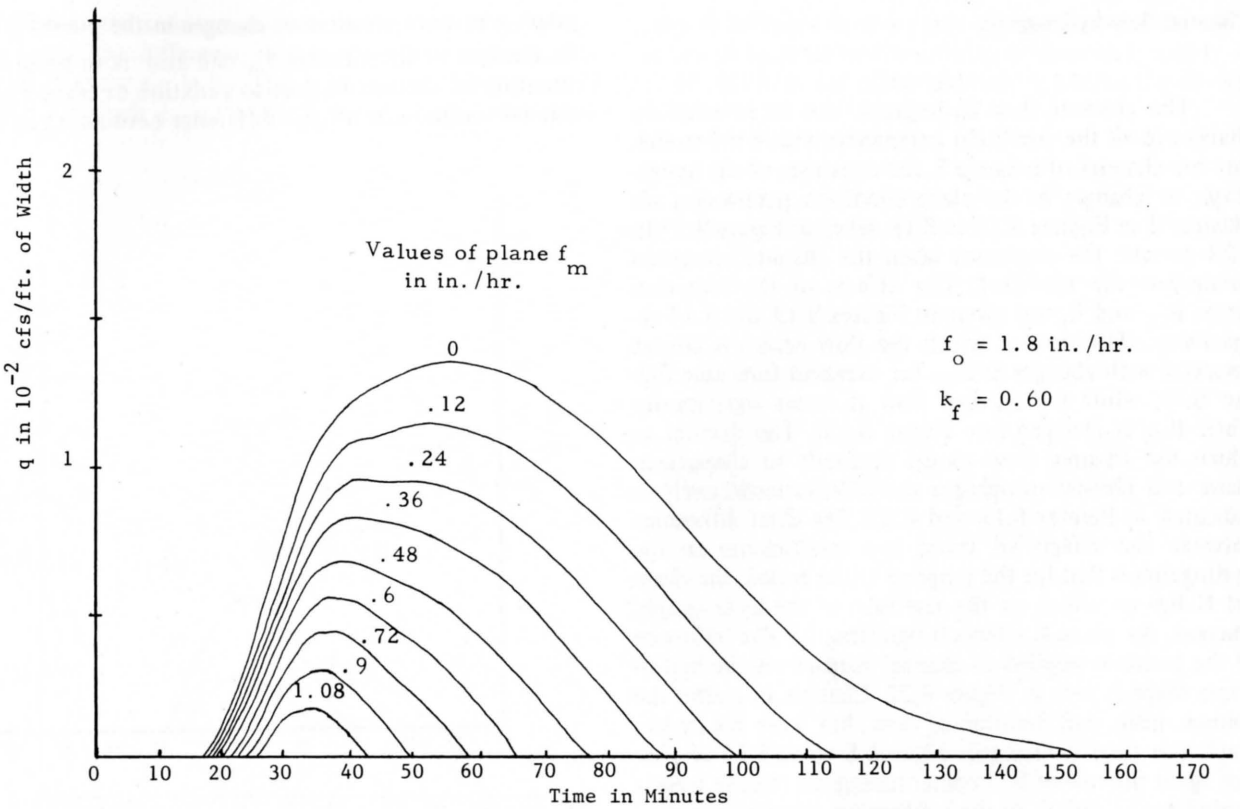

Figure 8.10. Overland flow hydrograph for subzone 2 as affected by changes in the plane minimum infiltration capacity rate, f_m, July 20, 1966.

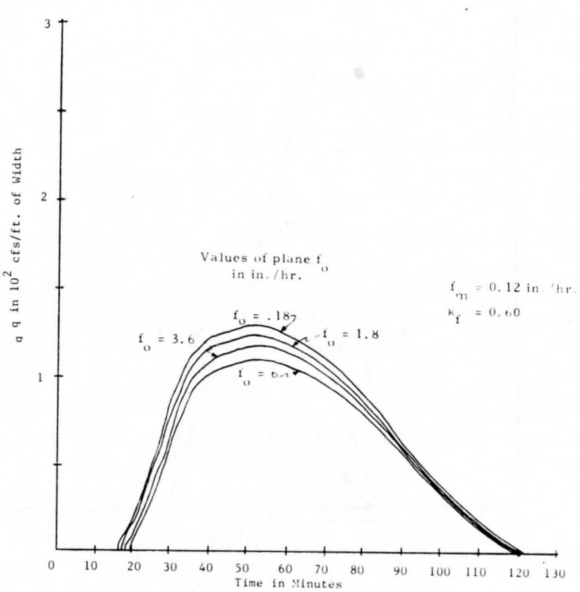

Figure 8.11. Overland flow hydrograph for subzone 2 as affected by changes in the plane maximum infiltration capacity rate, f_o, July 20, 1966.

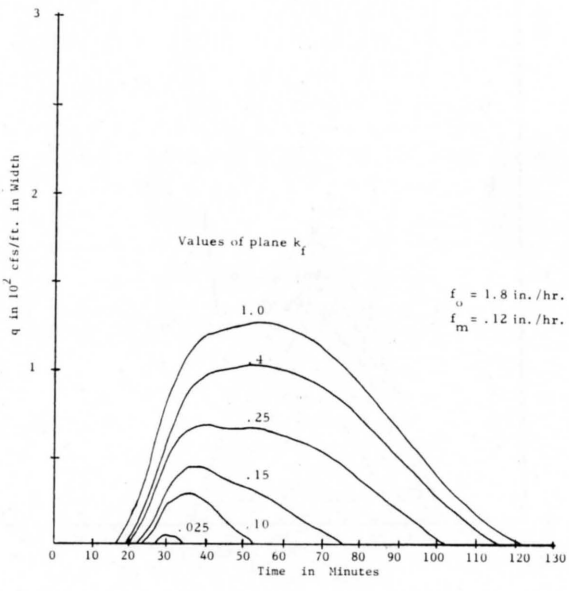

Figure 8.12. Overland flow hydrograph for subzone 2 as affected by changes in the plane time constant of the infiltration capacity rate function, k_f, July 20, 1966.

Channel flow hydrograph

The channel flow hydrograph can be affected by changes in all the condition parameters within the model. For the channel of subzone 2, the responses of the hydrograph to changes in the plane condition parameters are illustrated in Figures 8.13 to 8.18, whereas Figure 8.19 to 8.23 present the responses when the channel condition parameters are modified. The effects of the retention terms R_{cs} and k_r are given in Figures 8.13 and 8.14 respectively. The time at which the flow ceases is almost invariant with changes in R_{cs} for overland flow (see Figure 8.7), while for channel flow it varies significantly when R_{cs} is changed (see Figure 8.13). The manner in which the channel flow model responds to changes in plane and channel roughness coefficients respectively is indicated in Figures 8.15 and 8.23. The chief difference between the effects of those two coefficients on the hydrograph is that for the range of values tested, the channel K has no effect on the rise time of the hydrograph, whereas, the plane K affects it significantly. The influence of the constant applied to channel seepage on the hydrograph shape is seen in Figure 8.22. Changes in c alter the volume, peak, and duration of flow, but leave the hydrograph rise time unchanged. Figures 8.16 to 8.21 emphasize again the role of k_f in determining the relative weight carried by f_m and f_o in the infiltration capacity function and their influence on the flow hydrograph. The plots of Figures 8.16 and 8.17 were obtained for a plane k_f value of 0.60, while those of figures 8.19 and 8.20 had a channel k_f value of 0.10. These plots show that the hydrograph was more sensitive to changes in the plane f_m than to changes in the channel f_m, and also more sensitive to variation of channel f_o than to variation of plane f_o. The relative magnitude of the difference between f_o and f_m

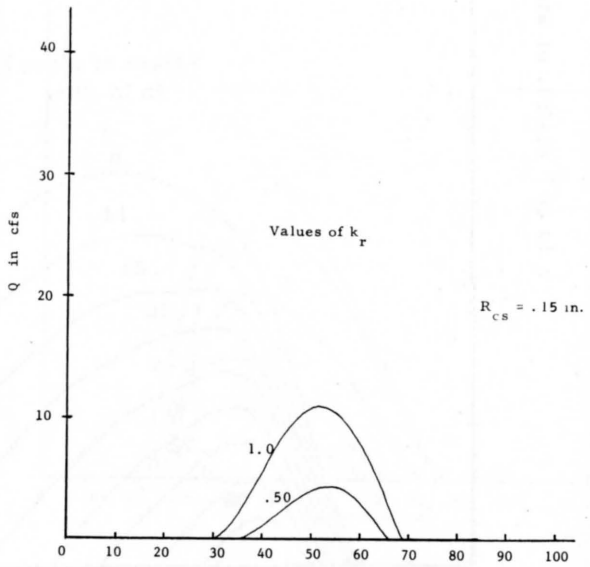

Figure 8.14. Channel flow hydrograph for subzone 2 as affected by changes in the time constant of the retention capacity rate function, k_r, July 20, 1966.

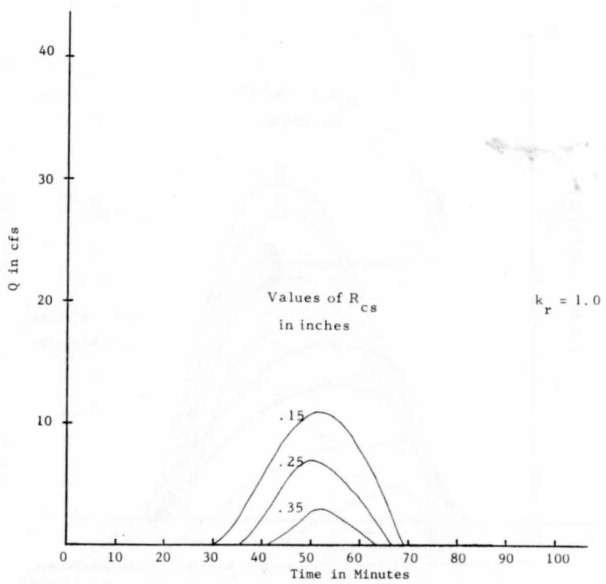

Figure 8.13. Channel flow hydrograph for subzone 2 as affected by changes in the retention storage capacity, R_{cs}, July 20, 1966.

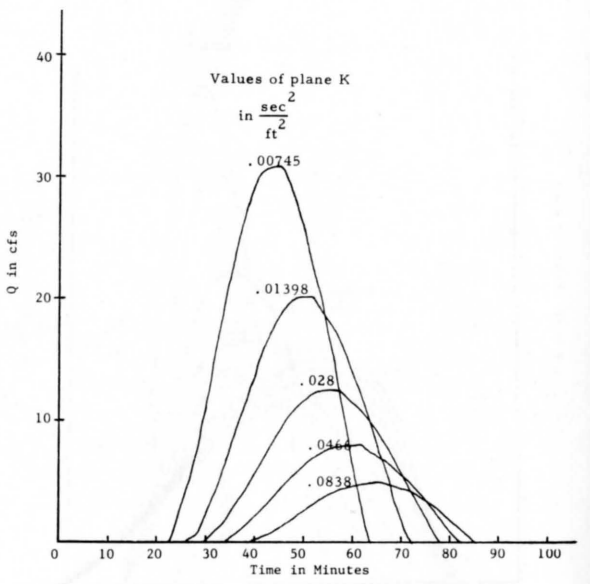

Figure 8.15. Channel flow hydrograph for subzone 2 as affected by changes in the plane roughness coefficient, K, July 20, 1966.

establishes the sensitivity of the model to changes in k_f: the larger the difference the more sensitive is the hydrograph to variation in k_f. This is illustrated in Figures 8.18 and 8.21 which show that the hydrograph was more sensitive to changes in the plane k_f than to variation in the channel k_f, because the difference between f_o and f_m was 1.68 in/hr for the plane and only 1.2 in/hr for the channel.

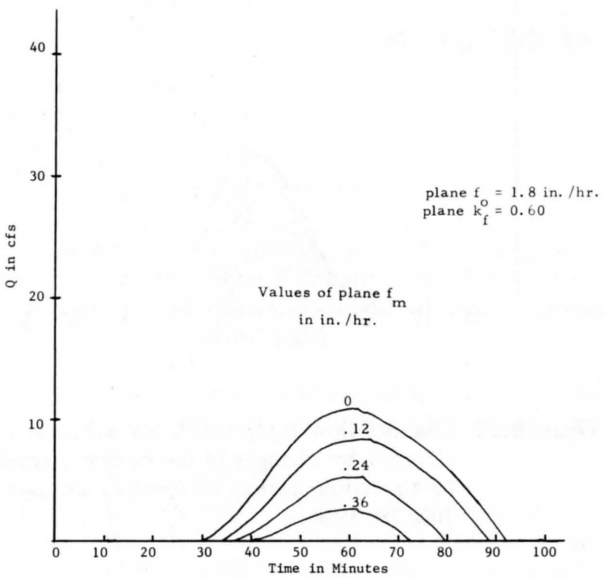

Figure 8.16. Channel flow hydrograph for subzone 2 as affected by changes in the plane minimum infiltration capacity rate, f_m, July 20, 1966.

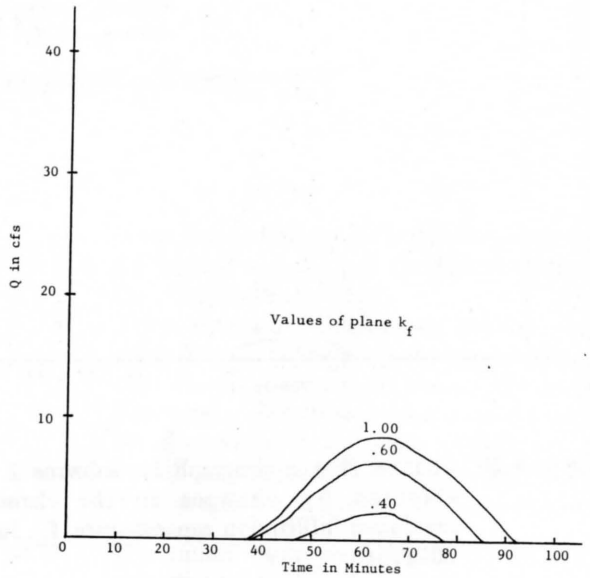

Figure 8.18. Channel flow hydrograph for subzone 2 as affected by changes in the plane infiltration time constant, k_f, July 20, 1966.

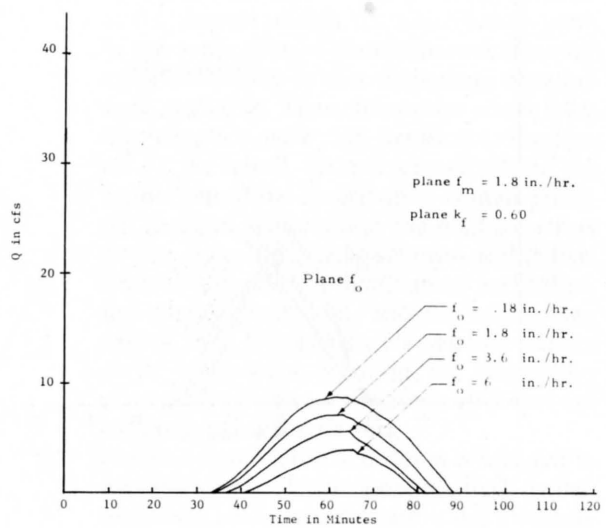

Figure 8.17. Channel flow hydrograph for subzone 2 as affected by changes in the plane maximum infiltration capacity rate, f_o, July 20, 1966.

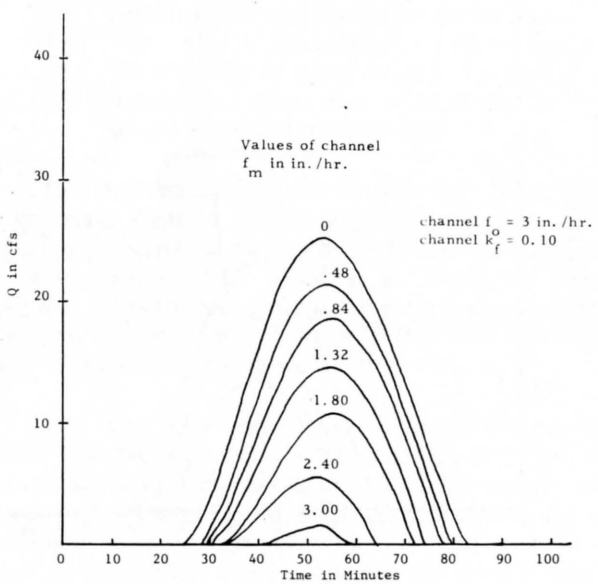

Figure 8.19. Channel flow hydrograph for subzone 2 as affected by changes in the channel minimum infiltration capacity rate, f_m, July 20, 1966.

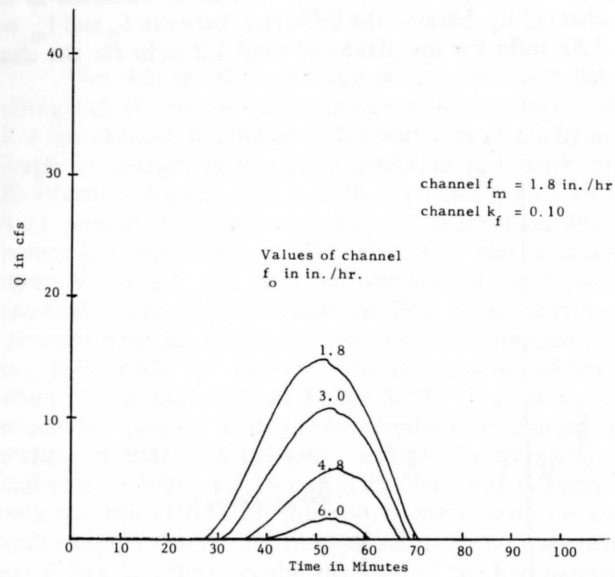

Figure 8.20. Channel flow hydrograph for subzone 2 as affected by changes in the channel maximum infiltration capacity rate, f_o, July 20, 1966.

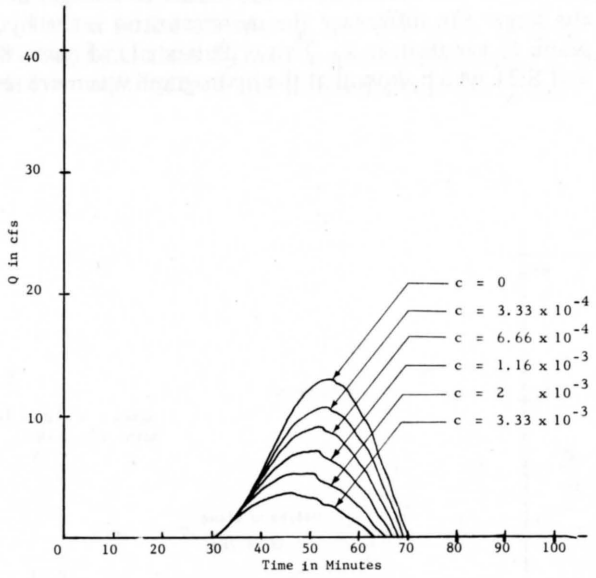

Figure 8.22. Channel flow hydrograph for subzone 2 as affected by changes in the constant applied to the computation of channel seepage, c, July 20, 1966.

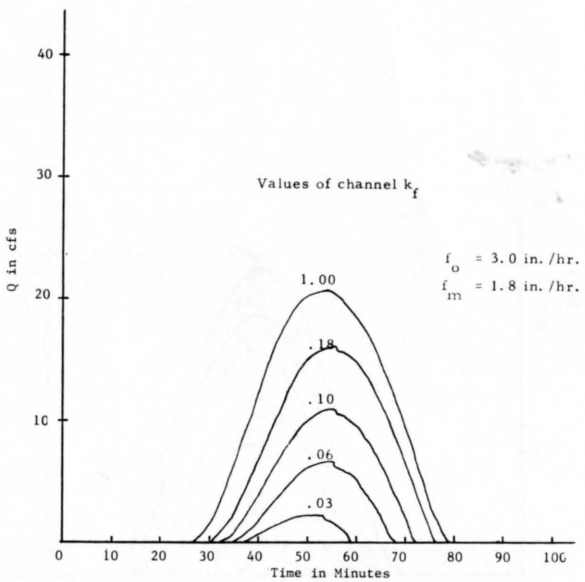

Figure 8.21. Channel flow hydrograph for subzone 2 as affected by changes in the channel infiltration time constant, k_f, July 20, 1966.

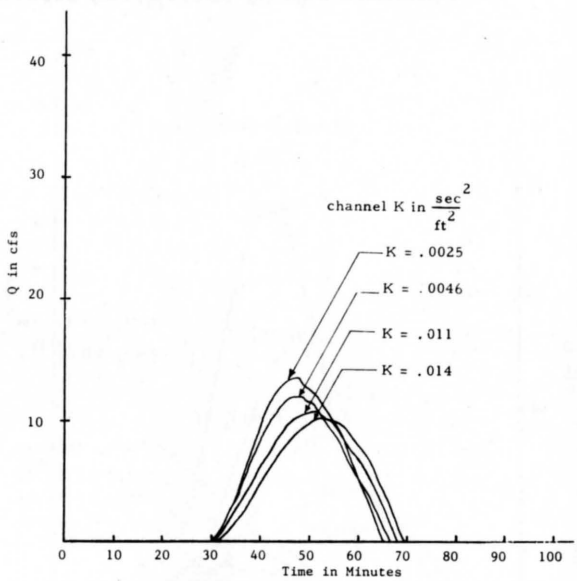

Figure 8.23. Channel flow hydrograph for subzone 2 as affected by changes in the channel roughness coefficient, K, July 20, 1966.

CHAPTER IX

CONCLUSIONS AND RECOMMENDATIONS

Conclusions

The numerical solution of the unsteady flow equations, together with the presentation and discussion of results from the mathematical model of surface runoff suggest the following conclusions:

1. The numerical solution of the full unsteady flow equations is feasible on the analog computer.
2. The perturbation method presented for the stability study of the differential-difference systems is adequate since the stability conditions derived from its application agree with the restrictions generally set on flow computations according to the flow regime. In addition, no instabilities appeared in the analog computer solution of the implicit differential-difference system as predicted by the perturbation method.
3. The solution of the implicit differential-difference system was found to be always stable, and there was no restriction on the size of the channel section, Δx, which can be used.
4. In the application of the mathematical model, space derivatives in the momentum equation were negligible. Thus, truncation errors from this equation were not significant. Furthermore, the small error encountered in the application of the conservation of mass principle tends to indicate that the machine errors do not make the analog solution prohibitive.
5. Because the pressure-distribution coefficient, the energy coefficient, and the momentum applied only to the negligible space derivatives in the momentum equation, the assumption of a value of unity for these coefficients did not introduce serious errors.
6. For the range of flow and slopes considered in the application of the mathematical model, neglecting the local acceleration and the gradient of depth does not change the results.
7. The consideration of both the overland and channel flow in the surface runoff model allows the computation of the volume of water loss to infiltration and retention storage on the land surfaces, and the determination of the channel seepage losses.
8. The subdivision of the drainage basin into subzones helps in reproducing the spatial distribution of the precipitation and of the model parameters. Subdivision also provides additional opportunity for improved fitting of the model to the watershed if measured flow hydrographs are available at the outlet of the subzones.
9. The runoff hydrograph predicted from the regulated model shows satisfactory agreement with the measured hydrograph under the selected set of criteria for goodness of fit.
10. The mathematical model of the surface runoff is flexible, and can be adapted to different flow conditions found on a watershed. It also presents the advantage of yielding directly such hydrograph characteristics as the time to peak and the rise time without resorting to empirical formulas for the time delay.
11. The results of the sensitivity analysis, that is, the responses of the hydrograph to changes in parameters, agree with what might be expected from field observations.

It is believed that the overall objective of the study which was to improve analog computer models of surface runoff with particular emphasis on the model developed by Riley (Riley, 1967, Riley et al. 1967) has been achieved. A brief comparison of the main features of the study with those of Riley's model will permit to assessment of improvement achieved by the study.

The chief difference between the surface runoff model described here and that developed by Riley lies in the mathematical expressions on which the models are based. In Riley's model the space derivatives were dropped from the continuity and momentum equations. As a result, Riley's model could not follow the flowing water en route to the basin outlet, and did not account for the time delay of the outflow hydrograph. Therefore, Riley found it necessary to introduce a mechanical time delay in order to reproduce such hydrograph characteristics as the

LITERATURE CITED

Agricultural Research Service, U.S. Department of Agriculture. 1964. Walnut Gulch experimental watershed. 15 p.

Agricultural Research Service, U.S. Department of Agriculture. 1967. Walnut Gulch experimental watershed. 28 p.

Amein, M. 1966. Streamflow routing on computer by characteristics. Water Resources Research, 2(1):123-130.

Amisial, Roger A., and J. Paul Riley. 1968. Adaptation of electronic computers for improved method of modeling surface runoff from rainfall for small watersheds. The use of analog and digital computers in hydrology. International Association of Scientific Hydrology, 2(81):392-404.

Baltzer, R. A., and C. Lai. 1968. Computer simulation of unsteady flows in waterways. Journal of the Hydraulics Division, Proceedings, American Society of Civil Engineers, 94(HY4): 1083-1117.

Brakensiek, D. L. 1967. A simulated watershed flow system for hydrograph prediction; A kinematic application. Proceedings, International Hydrology Symposium, September 6-8, 1967, Fort Collins, Colorado, 1:18-24.

Courant, R. K., K. O. Friedrichs, and H. Lewy. 1928. Uber die partiellen differenzengleichungen der mathematischen physik (On the partial difference equation of mathematical physics). Mathematische Annalen, 100:32-74.

Craya, A. 1946. Calcul graphique des regimes variables dans les canaux (Graphical computation of variable regimes of flows in channels). La Houille Blanche, No. 2:117-130.

Darcy, H. 1856. Les fontaines publiques de la ville de Dijon (The public fountains of the city of Dijon). Paris: Dijon. 100 p.

Daubert, A. P., P. Marvaud, L. Favre, and A. Margnac. 1967. Quelques applications de modeles mathematiques a l'etude des ecoulements non permanents dans un reseau ramifie de rivieres ou canaux (A few applications of mathematical models to the study of unsteady flows in a ramified river or canal network). La Houille Blanche, No. 7:735-746.

Deiters, R. M., and T. Namura. 1968. Improving the analog simulation of partial differential equations by hybrid computation. Simulation, 11(2):73-80.

DeSaint- Venant, Barre. 1871. Theorie du mouvement nonpermanent des eaus avec application aux crues des rivieres et a l'introduction des marees dans leur lit (Theory of unsteady water flow, with application to river floods and to propagation of tides in river channels). Comptes Rendus de l'Academie des Sciences de Paris 73:148-154 and 237-240.

Deymie, Ph. 1939. Propagation d'une intumescence allongee: problemeaval (Propagation of an elongated wave: tail-water problem). Proceedings of the Fifth International Congress for applied mechanics. John Wiley and Sons Inc., New York. p. 537-544.

Fisher, M. E. 1956. Higher order differences in the analog solution of partial differential equations. Proceedings of the International Analogy Computation Meeting, Brussels, 1955. Presses Academiques Europeennes, Brussels. p. 208-210.

Fletcher, A. G., and W. S. Hamilton. 1967. Flood routing in an irregular channel. Journal of the Engineering Mechanics Division, Proceedings, American Society of Civil Engineers, 93(EM3):45-62.

Harder, J. A., L Mockras, and R. Nishizaki. 1960. Flood control analogs. Water Resources Center Contribution No. 24, Hydraulic Laboratory, University of California, Berkeley, California. 52 p.

Hartree, Douglas R. 1949. Calculating instruments and machines. University of Illinois Press, Urbana, Illinois. 138 p.

Henderson, F. M., and R. A. Wooding. 1964. Overland flow and groundwater flow from a steady rainfall of finite duration. Journal of Geophysical Research, 69(8):1531-1540.

Isaacson, E., J. J. Stoker, and B. A. Troesch. 1956. Results of the numerical prediction of the 1945 and 1948 floods in the Ohio River, of the 1947 flood through the junction of the Ohio and Mississippi Rivers, and of the floods of 1950 and 1948 through Kentucky Reservoir. Institute of Mathematical Sciences, New York University, Report IMN-NYU-235. p. 1-70.

Isaacson, E., J. J. Stoker, and B. A. Troesch. 1965. Numerical solution of flood problems in simplified models of the Ohio River. Institute of Mathematical Sciences, New York University, Report IMN-NYU-205. p. 1-46.

Ishihara, T., and Y. Ishihara. 1955. On electronic analog computer for flood routing. Transactions, Japan Society of Civil Engineers, Tokyo, Japan. No. 24:44-57.

Iwagaki, Yuichi. 1951. Theory of flow on road surface. Eng. Fac. Mem. Kyoto University, Japan 13(3):139-147. (Original not seen; abstracted in Water Supply Paper 1690, U.S. Geological Survey. 1964. p. 144-145.

Jackson, Albert S. 1960. Analog computation. McGraw-Hill Book Company, Inc., New York. 652 p.

John, Fritz. 1952. On integration of parabolic equations by difference methods. Communications on Pure and Applied Mathematics, 5:155-211.

Johson, Clarence L. 1963. Analog computer techniques. Second edition, McGraw-Hill Book Company, New York. 315 p.

Keulegan, G. H. 1945. Spatially variable discharge over a sloping plane. Transactions, American Geophysical Union, 26(6):956-959.

Kwan, J. Y., J. P. Riley, and R. A. Amisial. 1968. A digital computer program to plot isohyetal maps and calculate volumes of precipitation. The use of analog and digital computers in hydrology. International Association of Scientific Hydrology, 1(80):240-248.

Liggett, J. A., and D. A. Woolhiser. 1967. Difference solutions of shallow-water equations. Journal of the Engineering Mechanics Division, Proceedings, American Society of Civil Engineers, 93(EM2):39-71.

Lighthill, M. J., and G. B. Whitham. 1955. On kinematic waves I, flood movements in long rivers. Proceedings, Royal Society of London, Series A 229:281-316.

Mackay, D. M., and M. E. Fisher. 1962. Analogue computing at ultra-high speed. John Wiley and Sons Inc., New York. 395 p.

Massau, Junius. 1889. Appendice au memoire sur l'integration graphique (Appendix to memoir on graphical integration). Annales de l'Association des Ingenieurs Sortis des Ecoles de Gand, Belgium, 12:185-444.

Masse, Pierre. 1939. Recherches sur la theorie des eaux courantes (Research on the theory of flowing water). Proceedings of the Fifth International Congress for applied mechanics. John Wiley and Sons, Inc., New York. p. 545-554.

Miura, Takeo, and Junzo Iwata. 1966. A consideration on the solution of partial differential equations by analog computer. Simulation, 6(2):105-108.

Morgali, J. R., and R. K. Linsley. 1965. Computer analysis of overland flow. Journal of the Hydraulics Division, Proceedings, American Society of Civil Engineers, 91(HY3): 81-100.

Nosek, T. M., and R. I. Dice. 1947. A theoretical study of flood waves resulting from sudden dam destruction. M.S. thesis, Massachusetts Institute of Technology. p. 1-28.

Preissman, A., and H. Lorgere. 1967. Experiences dans l'exploitation de modeles mathematiques de bassins fluviaux (Experience of the operation of mathematical river basin models). La Houille Blanche No. 7:747-749.

Renard, K. G., and K. V. Keppel. 1966. Hydrographs of ephemeral streams in the southwest. Journal of the Hydraulics Division, Proceedings, American Society of Civil Engineers, 92(HY2):33-52.

Riley, J. P. 1967. Application of an electronic analog computer to the problems of river basin hydrology. Ph.D. Dissertation, Utah State University, Logan, Utah. 200 p.

Riley, J. P., D. G. Chadwick, and E. K. Israelsen. 1967. Application of an electronc analog computer for the simulation of hydrologic events on a southwest watershed. Utah Water Research Laboratory, Utah State University, Logan, Utah, PR-WG 38-1. 53 p.

Ritchmyer, R. D. 1957. Difference methods for initial value problems. Interscience Tracts in Pure and Applied Mathematiques No. 4, Interscience Press, New York. 238 p.

Ritchmyer, R. D. 1962. A survey of difference methods for nonsteady fluid dynamics. NCAR Technical Notes 63-2, National Center for Atmospheric Research, Boulder, Colorado. 25 p.

Shen, John. 1965. Use of analog models in the analysis of flood runoff. Professional Paper 506-A, U.S. Geological Survey. 24 p.

Stocker, J. J. 1953. Numerical solution of flood prediction and river regulation problems; derivation of basic theory and formulation of numerical methods of attack. Institute of Mathematical Science, New York University, Report IMN-200. (Original not seen; abstracted in Water Supply Paper 1690, U.S. Geological Survey. 1964. p. 163.)

Thirriot, C., and H. Barthet. 1967. Possibilite et limite de la degenerescence en systeme differentiel du modele mathematique des intumescences (The possibility and limit of degeneration of a mathematical surge wave model into a differential system). La Houille Blanche No. 7:757-762.

Thomas, H. A. 1937. The hydraulics of flood movement in rivers. Carnegie Institute of Technology, Pittsburgh, Pennsylvania. 50 p.

Vichnevetsky, Robert. 1967. Error analysis in the computer simulation of dynamic systems: variational aspects of the problem. IEEE Transactions on Electronic Computers, EC-16 (4):403-411.

von Neumann, J., and R. D. Ritchmyer. 1950. A method for the numerical calculation of hydrodynamic shocks. Journal of Applied Physics, 21(3):232-237.

Watters, Gary Z. 1967. Lecture notes from "Advanced Fluid Mechanics," course no. CE 271 taught at Utah State University, Logan, Utah.

Wooding, R. A. 1965. A hydraulic model for the catchment-stream problem. Journal of Hydrology, 3:254-282.

Wooding, R. A. 1966. A hydraulic model for the catchment–stream problem: comparison with runoff observations. Journal of Hydrology, 4(1): 21-37.

Woolhiser, D. A., and J. A. Liggett. 1967. Unsteady, one-dimensional flow over a plane-the rising hydrograph. Water Resources Research, 3(3):753-771.

Yevjevich, V. M. 1964. Bibliography and discussion of flood-routing methods and unsteady flow in channels. Water Supply Paper 1960, U.S. Geological Survey. Washington, D.C. 235 p.